

**RAPIDLY-CONVERGENT, MIXED-PARTIAL
DERIVATIVE BOUNDARY CONDITION GREEN'S
FUNCTION FOR AN ANISOTROPIC HALF-SPACE:
PERFECT CONDUCTOR CASE**

J. M. Jarem

Electrical and Computer Engineering Department
University of Alabama in Huntsville
Huntsville, AL 35899, USA

Abstract—The problem of determining the Green's function of an electric line source located in a permeable, anisotropic ($\tilde{\mu}_{xx}, \tilde{\mu}_{xy}, \tilde{\mu}_{yx}, \tilde{\mu}_{yy}$ and $\tilde{\epsilon}_{zz}$ nonzero interacting parameters) half-space above a Perfect Magnetic Conductor (PMC) ground plane (called the TM^z case herein) for the case where image theory cannot be applied to find the Green's function of the PMC ground plane system has been studied. Monzon [2, 3] studied the Green's function TE^z problem dual to the present one for two cases; (1) when the system was unbounded, anisotropic space where $\tilde{\epsilon}_{xx}, \tilde{\epsilon}_{xy}, \tilde{\epsilon}_{yx}, \tilde{\epsilon}_{yy}$ and $\tilde{\mu}_{zz}$ were the nonzero interacting parameters; and (2) when the scattering system was an anisotropic half-space located above a Perfect Electric Conductor (PEC) ground plane and where $\tilde{\epsilon}_{xx}, \tilde{\epsilon}_{yy}$ and $\tilde{\mu}_{zz}$ were the nonzero interacting parameters and $\tilde{\epsilon}_{xy} = \tilde{\epsilon}_{yx} = 0$. Monzon [2] referred to the latter ground plane case as the case where “usual image” theory could be used to find the Green's function of the system. The Green's function for the TM^z -PMC case studied herein was derived by introducing and using a novel, linear coordinate transformation, namely $\tilde{x}' = (\sigma_P/\tau)\tilde{x} + \sigma_M\tilde{y}$, $\tilde{y}' = \tilde{y}$, (Eqs. (6c,d), herein). This transformation, a modification of that used by [2, 3], reduced Maxwell's anisotropic equations of the system to a non-homogeneous, Helmholtz wave equation from which the Green's function, G , meeting boundary conditions, could be determined. The coordinate transformation introduced was useful for the present PMC ground plane problem because it left the position of the PMC ground plane and all lines parallel to it, unchanged in position from the original coordinate system, thus facilitating imposition of EM boundary conditions at the PMC ground plane.

In transformed (or primed) coordinates, for the TM^z -PMC and TE^z -PEC ground plane problems, respectively, the boundary conditions for the Green's functions $G_{TM} \equiv E_z$ and $G_{TE} \equiv H_z$ were shown to be $\left[\alpha \frac{\partial G}{\partial \tilde{x}'} + \frac{\partial G}{\partial \tilde{y}'}\right]_{\tilde{y}'=0} = 0$, where $G = G_{TM}$ or G_{TE} , $\alpha = \alpha_{TM}$ or α_{TE} , where α_{TM} and α_{TE} are complex constants (dually related to each other by $\underline{\tilde{\mu}} \leftrightarrow \underline{\tilde{\epsilon}}$), and where $\tilde{y}' = 0$ is the position of the ground plane. An interesting result of the analysis was that the constant α_{TE} (as far as the author knows) coincidentally turned out to be the same as the first of two important constants, namely $S_1 \frac{d\ell_v}{d\ell}$ and $S_2 \frac{d\ell_v}{d\ell}$, which were used by Monzon [2, 3] to formulate integral equations (based on Green's second theorem) from which EM scattering from anisotropic objects could be studied.

Spatial Fourier transform (k -space) techniques were used to determine the Green's function of the Helmholtz wave equation expressed in transformed coordinates which satisfied the mixed-partial derivative boundary condition of the system. The Green's function G was expressed as a sum of a "free space" Green's function g_f (proportional to a Hankel function $H_0^{(2)}$ and assumed excited by the line source in unbounded space) and a homogeneous Green's function g whose spectral amplitude was chosen such that, when g was added to g_f , the sum $G = g_f + g$, satisfied boundary conditions. The k -space, Sommerfeld integrals making up g turned out to converge slowly, and so, using contour integration in the complex plane (Appendix B), g was expressed in a rapidly convergent form, and thus one leading to its practical numerical evaluation. Extensive numerical testing of how well the Green's functions $G = g_f + g$ satisfied boundary conditions and how well the homogeneous Green's function g satisfied Green's second theorem was performed. Excellent verification of the numerical and analytical procedures were found and displayed in the error tables of Tables 1–4 of the paper. Plots illustrating the novel coordinate transformation introduced were presented and several numerical plots of the Green's function developed herein were presented. The application of the present work to find the Green's function for the case when a negative-index, anisotropic metamaterial is adjacent to a conducting ground plane is discussed. Application of the Green's function theory developed herein to multi-layer anisotropic systems is discussed.

1. INTRODUCTION

An important problem in the area of electromagnetic (EM) scattering from objects, either composed of or embedded in anisotropic media, when determining the EM fields of the system by the Method of Moments (MoM), is the problem of determining the Green's function of the system meeting appropriate boundary conditions. This is an important problem because calculation of the Green's function itself is the key step from which an integral equation of the system may be formulated and from which a MoM matrix solution may be implemented. Because in anisotropic media, the different EM field components may be coupled together in a complicated way, the Green's function, meeting specific boundary conditions can be a difficult problem to solve [1–7].

To contribute to this field of study, this paper specifically will be concerned with the Two-Dimensional (2-D) problem of determining the Green's function meeting boundary conditions of an electric line source located in a magnetic, permeable, anisotropic homogeneous half-space ($\tilde{\mu}_{xx}, \tilde{\mu}_{xy}, \tilde{\mu}_{yx}, \tilde{\mu}_{yy}$ and $\tilde{\varepsilon}_{zz}$ are the nonzero interacting material parameters) which is located above a Perfect Magnetic Conductor (PMC) ground plane. The nonzero interacting field components of this system are E_z, H_x and H_y (Transverse Magnetic to z (TM^z) polarization) and the Green's function of this system is defined by $G \equiv G^{TM} \equiv E_z$. The Green's function problem dual to this one is defined by a magnetic line source located in a dielectric permittivity, anisotropic homogeneous half-space ($\tilde{\varepsilon}_{xx}, \tilde{\varepsilon}_{xy}, \tilde{\varepsilon}_{yx}, \tilde{\varepsilon}_{yy}$ and $\tilde{\mu}_{zz}$ are the nonzero interacting material parameters) which is located above a Perfect Electric Conductor (PEC) ground plane. The nonzero interacting field components of this system are H_z, E_x and E_y (Transverse Electric to z (TE^z) polarization) and the Green's function of this system is defined by $G \equiv G^{TE} \equiv H_z$. The two Green's functions problems are mathematically identical to one another.

Monzon and Damaskos [1] and Monzon [2, 3] have studied the 2-D problem of plane wave scattering from spatially homogeneous (or translationally invariant) anisotropic objects when the polarization of the system was TE^z (only nonzero interacting components, H_z, E_x and E_y) for two cases, namely; Case (1), when the only nonzero, interacting material parameters of the anisotropic object were $\tilde{\varepsilon}_{xx}, \tilde{\varepsilon}_{xy}, \tilde{\varepsilon}_{yx}, \tilde{\varepsilon}_{yy}$ and $\tilde{\mu}_{zz}$ and the scattering object was located in unbounded, free space [1–3]; and Case (2), when the only, nonzero, interacting material parameters of the anisotropic object were $\tilde{\varepsilon}_{xx}, \tilde{\varepsilon}_{yy}$ and $\tilde{\mu}_{zz}$ (therefore $\tilde{\varepsilon}_{xy} = \tilde{\varepsilon}_{yx} = 0$) and the scattering object was located just above a PEC ground plane [1, 2]. Monzon [2] has labeled the PEC case (with

$\tilde{\epsilon}_{xy} = \tilde{\epsilon}_{yx} = 0$) being the case when “usual image” theory applies because in this case an image line source aids in the specification of the Green’s function of the system meeting boundary conditions. Monzon [2, Eq. (2)] also specified how the TM^z scattering problem electromagnetically dual to the TE^z Case (1) and (2) problems analyzed in [2], could be obtained from the Case (1) and (2) solutions presented in [2].

This paper will be concerned with generalizing the Case (2) Green’s function analysis of [2] to the case when all of the material parameters, either $\tilde{\epsilon}_{xx}, \tilde{\epsilon}_{xy}, \tilde{\epsilon}_{yx}, \tilde{\epsilon}_{yy}$ and $\tilde{\mu}_{zz}$ (TE^z -PEC problem) or $\tilde{\mu}_{xx}, \tilde{\mu}_{xy}, \tilde{\mu}_{yx}, \tilde{\mu}_{yy}$ and $\tilde{\epsilon}_{zz}$ (TM^z -PMC problem), are nonzero. This Green’s function problem, as will be discussed, turns out to be more difficult than the one studied by Monzon [2] (Case (2)), when $\tilde{\epsilon}_{xy} = \tilde{\epsilon}_{yx} = 0$ (TE^z -PEC) or $\tilde{\mu}_{xy} = \tilde{\mu}_{yx} = 0$ (TM^z -PMC).

The TE^z 2-D scattering problem of [1–3] was studied by two independent methods, the first of which [1] was a plane wave expansion method and the second of which [2, 3] was a Green’s function method. The first method [1] which studied scattering from an anisotropic rod consisted of; (1) expanding the EM fields of the system inside the homogeneous region of the scattering object in a superposition (or spatial Fourier integral or k -space superposition) of plane waves of unknown spectral amplitude which satisfy Maxwell’s equations; (2) converting the plane wave expansion of the EM fields in the anisotropic region into a $[0, 2\pi]$ integral of unknown spectral amplitude $h(\zeta)$ (in the notation of [1]); (3) expressing the incident and scattered fields in the isotropic region of space outside the scattering rod in a Bessel function series; and (4) after matching EM boundary conditions, formulating an integral equation, from which the unknown spectral amplitude $h(\zeta)$ of the EM fields could be determined.

The second method used by Monzon [2, 3] to study the aforementioned 2-D scattering problem involved deriving a Green’s function for an infinite, homogeneous, anisotropic region of space, and then with this Green’s function, using Green’s second theorem to formulate an integral equation over the boundary of the anisotropic scattering object from which an integral equation could be formed and from which a solution by the MoM could be found. An important step in deriving the Green’s function of the system consisted of introducing a linear coordinate transformation, which when applied to Maxwell’s equations, reduced Maxwell’s equations in the anisotropic medium to a simple Helmholtz wave equation from which the Green’s function of the system could be found from well known techniques and known solutions. In the analysis of Monzon [2, 3], the Green’s function excitation used was a two-dimensional delta function (proportional to

a magnetic line source) and the Green's function that resulted from this delta function excitation was proportional to a Hankel function of the second kind.

A second important step and contribution made in [2, 3], using the second method, was the derivation of a set of interaction coefficients labeled $S_1 \frac{d\ell_v}{d\ell}$ and $S_2 \frac{d\ell_v}{d\ell}$ in [2, 3], which defined the Green's second theorem integral equation from which scattering in an anisotropic system could be studied. These coefficients were first derived in [2], and then later in [3], were shown to be actually constant in space. The fact that they were spatially constant was an important contribution because it allowed terms in the integral equation which contained tangential derivatives to be integrated by parts, and this in turn, led to a Green's second theorem integral equation form which specifically showed how the electric and magnetic fields which were tangential to the boundary of a scattering object when illuminated, might act as equivalent EM sources. This thus gave great physical insight into the scattering process associated with EM scattering from anisotropic material objects.

Returning to the TE^z -PEC ground plane, anisotropic, scattering object problem studied by Monzon [2], a natural question that arises is what values may the permittivity tensor components $\tilde{\epsilon}_{xx}$, $\tilde{\epsilon}_{xy}$, $\tilde{\epsilon}_{yx}$ and $\tilde{\epsilon}_{yy}$ assume in order that ordinary image theory may or may not be used to specify the Green's function of the system meeting proper boundary conditions when a PEC ground plane is present in the system. This is an important question because if image theory can be used to find the Green's function of the ground plane system, then the Green's function will be a simple sum of Hankel functions due to a line source and its image, whereas if image theory can't be used, then a much more complicated analysis may be needed to find the system Green's function.

In order to answer this question, for the first time (to the author's knowledge), a modification of the linear transformation of coordinates used by Monzon [2,3] has been introduced which clearly and simply defines, for the anisotropic-PEC ground plane problem under consideration, the values that $\tilde{\epsilon}_{xx}$, $\tilde{\epsilon}_{xy}$, $\tilde{\epsilon}_{yx}$ and $\tilde{\epsilon}_{yy}$ may assume in order that "usual image" theory [2] can or can't be used to determine the Green's function of the system meeting proper boundary conditions. Using the modified linear transformation coordinates (given herein by $\tilde{x}' = (\sigma_P^{TE}/\tau^{TE})\tilde{x} + \sigma_M^{TE}\tilde{y}$, $\tilde{y}' = \tilde{y}$, Eqs. (6c,d)), it will be shown for the present TE^z case, that this Green's function, G_{TE} ($G_{TE} \equiv H_z$ is assumed excited by a magnetic line source located above a PEC ground plane); (1) satisfies a Helmholtz wave equation (the same Helmholtz wave equation as in [2, 3]); and (2) satisfies the mixed-

partial derivative boundary condition $\left[\alpha_{TE} \frac{\partial G_{TE}}{\partial x'} + \frac{\partial G_{TE}}{\partial y'}\right] \Big|_{\tilde{y}'=0} = 0$ ($\tilde{y}' = 0$ is the location of the PEC boundary) where the quantity α_{TE} (Eq. (12) herein) is a complex constant which is zero when $\tilde{\epsilon}_{xy} = \tilde{\epsilon}_{yx}$ and nonzero when $\tilde{\epsilon}_{xy} \neq \tilde{\epsilon}_{yx}$. Thus the image theory question at a PEC ground plane is answered simply by asking if $\tilde{\epsilon}_{xy}$ and $\tilde{\epsilon}_{yx}$ are equal to each other or not. If they are equal then $\alpha_{TE} = 0$ and G_{TE} satisfies a Neumann boundary condition (in x' and y') and thus the Green's function for this case may be derived by simply using the image theory corresponding to a magnetic line source which is located above a PEC ground plane. When $\tilde{\epsilon}_{xy}$ and $\tilde{\epsilon}_{yx}$ are unequal, then α_{TE} is nonzero, and then G_{TE} must satisfy a mixed-partial partial derivative boundary condition, and thus a much more complicated problem has arisen, a problem where ordinary image theory can't be applied to find the Green's function of the system. The mixed-partial derivative boundary condition for the TM^z case is $\alpha \frac{\partial G}{\partial x} + \frac{\partial G}{\partial y} = 0$ where α ($\alpha \equiv \alpha_{TM}$, Eq. (11) herein) may be obtained from α_{TE} (and vice versa) by using duality, $\underline{\tilde{\mu}} \leftrightarrow \underline{\tilde{\epsilon}}$, [2, Eq. (2)]. The present author believes that the mixed-partial derivative boundary conditions, just described, have been derived herein for the first time.

An interesting fact is that the constant α_{TE} defining the mixed-partial derivative boundary condition described earlier, also just happens to be the same as the first of two important constants, namely $S_1 \frac{d\ell_x}{d\ell}$ and $S_2 \frac{d\ell_y}{d\ell}$ (discussed earlier), which were used by Monzon [2], [3, Eq. (6)] to formulate integral equations (based on Green's second theorem) from which EM scattering from anisotropic objects could be studied. The present author is not sure at the present time if this is an interesting coincidence or if there is a more fundamental underlying analytical reason why the constant α_{TE} (defined in Eq. (12) herein) should equal the constant $S_1 \frac{d\ell_x}{d\ell}$ derived by Monzon [3, Eq. (6)], keeping in mind that the two constants were derived here and in [3] for two entirely different applications and reasons.

Several papers have been concerned with the problem of determining Green's functions and in studying solutions of Maxwell's equations in anisotropic, multi-layer material systems. Refs. [4, 5] derived the anisotropic Green's functions for the case when the upper half-space is free space and the lower half-space is a homogeneous anisotropic material. In Refs. [4, 5] the Green's functions were used to study scattering from an anisotropic inclusion (embedded in the anisotropic lower half-space) when a plane wave was incident on the lower half-space [4] and when a Gaussian beam was incident on the lower half-space [5]. Ref. [6] derived the anisotropic Green's function for the complicated case when an anisotropic layer was bounded by

free space above the layer and bounded by a dielectric substrate below the layer. The Green's function for this system in [6] was used to study plane wave scattering from an anisotropic inclusion when the inclusion was embedded in the anisotropic layer. In Refs. [4–6], the Green's function was derived by using a k -space or plane wave spectral approach and the Green's function were derived directly from Maxwell's anisotropic equations without using the simplifying linear transformation as was introduced by Monzon [2]. In Ref. [7] (an earlier work than Refs. [4–6]), the mathematical techniques (such as integration of Sommerfeld integrals in the complex plane) used to derive the Green's functions in [4–6] were described. Ref. [8] used k -space techniques to study scattering and reflection of a Gaussian beam from a composite, anisotropic absorbing layer mounted on a perfect conducting metal cladding. Ref. [9] studied scattering and reflection of a Gaussian beam when it was incident on an anisotropic, chiral layer and Ref. [10] studied layered bianisotropic media. In a very recent article [11], June 2006, the Green's function of a two dimensional (2-D), isotropic material, multi-layer planar system was derived using a spectral domain, transmission line approach. In [11] through the use of a boundary integral equation formulation, scattering from a PEC object and a smooth dielectric object located inside the isotropic, multi-layer system was studied.

In Refs. [4–9] the anisotropic media was spatially homogeneous and translationally invariant. In references [12–14] Monzon used the same principles as he had developed in Refs [2, 3] to derive Green's functions and study EM scattering from anisotropic systems in the much more difficult and complicated case when the anisotropic system was cylindrically, rotationally invariant with respect to the z -axis rather than translationally invariant. (The permittivity tensor $\underline{\underline{\tilde{\epsilon}}}$ (assuming $\tilde{\epsilon}_{\rho\rho}, \tilde{\epsilon}_{\rho\phi}, \tilde{\epsilon}_{\phi\rho}, \tilde{\epsilon}_{\phi\phi}$, and $\tilde{\epsilon}_{zz}$ are the only nonzero tensor elements) is, for example, rotationally invariant with respect to the z -axis, if the permittivity tensor elements $\tilde{\epsilon}_{\rho\rho}, \tilde{\epsilon}_{\rho\phi}, \tilde{\epsilon}_{\phi\rho}$ and $\tilde{\epsilon}_{\phi\phi}$ are constant in value or homogeneous in value in the cylindrical coordinate system centered on the z -axis for which the rotational invariance is referenced to.) The rotationally case is much more difficult than the translationally invariant case because an anisotropic material which is rotationally invariant is spatially inhomogeneous, in general, and is thus not amenable to a plane wave, spectral analysis. The analysis of rotationally invariant anisotropic systems is very useful for studying EM scattering from cylindrical, anisotropic, layer-coatings which are (in Ref. [13]'s words) "conformal with a locally, cylindrical surface." In Ref. [12] Monzon develops a Sommerfeld representation and introduces spatial transformations for simplifying Maxwell's equations for a

rotationally invariant anisotropic system. In Ref. [13] Monzon uses the spatial transformations developed in [12] and the methodology used in [2] to derive Green's functions for rotationally invariant anisotropic systems. Finally in Ref. [14], mirroring the analysis in Refs. [2, 3], Monzon uses the Green's function theory developed in Ref. [13] and Green's second theorem to derive an integral equation formulation which can be used to study EM scattering in rotationally invariant anisotropic systems.

Additional research work concerning the derivation of Green's functions in homogeneous, anisotropic and bianisotropic materials, and EM scattering in anisotropic media may be found in Refs. [15–19].

The purpose of the present paper will be to extend the Green's function work of Monzon [2, 3, 12–16] and Refs. [4–11, 17]. This will be accomplished by the analysis of the TM^z -PMC half-space anisotropic Green's function problem discussed earlier. Section 2 of the paper will be concerned with introducing a modification of the linear transformation of coordinates that was presented by Monzon [2], and will derive, for the first time using these coordinates, a mixed-partial derivative, boundary condition equation from which the anisotropic Green's function of the system may be determined. Section 3 will derive the k -space Green's function of the anisotropic PMC system and Sections 4 and 5, using integration techniques in the complex plane, will express the k -space Sommerfeld integrals associated with the Green's function in a rapidly convergent form, which thus may be accurately evaluated. An interesting and useful fact concerning the Green's function when expressed in a rapidly convergent form is the fact that the functions and integrals making up this form (called Green's sub-functions herein) are themselves, individually, solutions of the Helmholtz wave equation. This is useful because one may then study how well each of these Green's sub-functions individually satisfy the wave equation, and thus if error occurs in the Green's function solution overall, one can possibly get a sense of which sub-functions are leading to that error.

In Sections 6–8, a study of the accuracy of the Green's function developed herein has been made and presented. This study has been made for the following reasons. If the Green's function derived in this paper were to be used to determine EM scattering from an anisotropic object above a PMC ground plane, using the Green's second theorem integral equation formulation developed by Monzon [2, 3], an important question that arises is how accurate are these Green's functions, and how accurate are they when integrated around a closed loop representing the shape of a scattering object that might be under consideration. When integrating over a portion

of the closed loop testing path or when a Green's function source point is relatively far from the PMC boundary, the invisible integrals (containing evanescent terms, that is, exponential terms with real, negative arguments) converge very rapidly and there is little trouble in numerically calculating and integrating over the Green's function for these conditions. However, if a segment of the contour and the Green's function source point are close to or on the PMC boundary, special integration techniques (involving; asymptotic evaluation of k -space integrals over infinite, highly oscillatory spectral ranges; approximation of some spatial integrals by Dirac delta functions; and principal value integration of some divergent spatial integrals) must be employed to properly evaluate the integrals of Green's second theorem, and thus careful numerical testing of these integration techniques is needed to see how accurately the integrations are performed.

Sections 6–8 address the testing of Green's second theorem integrals by substituting a known homogeneous solution of the Helmholtz wave equation (namely a sum of an incident and reflected plane wave which meets boundary conditions at the PMC boundary) and substituting the Green's functions developed herein into the integrals of Green's second theorem taken over a closed testing path (in this paper a rectangular and semicircular loop were chosen as testing paths, see Figs. 2a,b) and seeing numerically how well Green's second theorem was satisfied. If a known plane wave solution and the Green's function's developed herein satisfy Green's second theorem to a high degree of accuracy, then probably the Green's functions developed herein can be used to solve more complicated problems involving unknown EM fields as was done by Monzon [2, 3, 14]. Section 6 presents the Green's second theorem integrals used to test the Green's functions of the system and Sections 7 and 8 present error data showing how well the Green's functions and Green's sub-function terms developed herein satisfy Green's second theorem integral equations. In addition to the testing of Green's second theorem, an error table indicating how closely the Green's function satisfies the mixed-partial derivative boundary condition of the system is also provided in Section 8. Plots of the Green's function are presented in Section 9 and summary and conclusions are presented in Section 10. Concerning the Green's second theorem testing and discussion presented in Sections 6–8, we note that other authors than Monzon [2, 3] have used Green's second theorem to study scattering in EM systems. Ref. [20] has recently used Green's second theorem to study EM scattering from a PEC object located in a waveguide T-junction and Ref. [11] and has used a Green's second theorem integral equation form to study EM scattering in a multi-layer isotropic system.

The Green's function developed and studied in Sections 3–9 is a sum of a “free space” Green's function g_f (proportional to a Hankel function of the second kind and assumed excited by the line source in unbounded space) and a homogeneous Green's function g whose spectral amplitude was chosen such that, when g was added to g_f , the sum $G = g_f + g$, satisfies boundary conditions. The function g is called a “homogeneous” Green's function because it satisfies a homogeneous Helmholtz wave equation. The function may also be termed an “imperfect image” Green's function because in k -space as will be shown in Section 2, all of its spectral components, propagating and evanescent, are traveling away from the PMC boundary and thus appear to, or may thought of, as arising from an imperfect, image source located below the PMC boundary. Felson and Marcuvitz [21, pp. 506] have used the EM fields of an image source point to describe the scattered or reflected EM fields which arise from an electric current element, point source which is located above a mismatched, dielectric half-space.

Concerning the testing of Green's function $G = g_f + g$ in Green's second theorem in Sections 6–8, the following simplification has been made. Because the “free space” Green's function g_f is proportional to a Hankel function of the second kind (expressed in primed or transformed coordinates) and is well known to satisfy Green's second theorem exactly for a closed loop enclosing homogeneous material, Green's second theorem testing of only the homogeneous Green's function g and the individual Green's sub-function terms making up was performed in Sections 6–8.

An application of the present anisotropic, Green's function work would be to determine the Green's function for a negative-index, anisotropic metamaterial [22–24] when forming a “superresolution” optical system which might be in the presence of a mirror (PEC ground plane) or some other bounding planar surface. (A negative-index metamaterial behaves in a given frequency range, as if as if it possesses a negative index of refraction [22] and “superresolution” as detailed in a recent issue of Scientific American [22, pp. 67] means obtaining resolution much better and sharper than was possible by conventional positive index optics.) Super imaging has already been demonstrated in principal by illuminating a very thin silver layer at resonance (relative permittivity, $\varepsilon = -1$) and from this system, forming a superresolution image from the near field radiation of the silver layer [22, pp. 67].

An interesting question which concerns the Green's function work to be presented herein for metamaterials is what type of near field radiation (therefore what type of near field Green's function)

is produced when a source point is placed in a negative-index, anisotropic metamaterial when the source point is very close to a perfectly conducting boundary. The perfectly conducting boundary causes a strong interaction with the source point for positive index, anisotropic materials as will be discussed in the present paper. A similar type of strong interaction can also be expected in a negative-index, anisotropic metamaterial when the Green's function source point is very close to a perfectly conducting boundary plane. Specific questions concerning this matter are: (1) What is the mathematical form of the near field interaction that might occur? and (2) Do the EM fields of the interaction possess superresolution characteristics? The present paper is concerned with the near field Green's function of anisotropic materials in the presence of a perfecting conducting layer, thus the theory presented in this paper could be very useful towards answering the last two questions. Knowledge of the Green's function of an anisotropic negative index metamaterial in the presence of a perfect conductor ground plane could also be very useful as one could use this Green's function to study scattering from objects (such as device imperfections, material imperfections in the metamaterial, etc.) which might be embedded in the metamaterial of the imaging system.

2. TRANSFORMATION OF COORDINATES AND MIXED-PARTIAL DERIVATIVE BOUNDARY CONDITIONS

We are interested in determining the Green's function for a homogeneous, anisotropic half-space which is bounded by a perfect magnetic conductor at $\tilde{y} = 0$ (Fig. 1a) that results when; (1) an electric line source $\vec{J} = I_S \delta(\tilde{x} - \tilde{x}_s) \delta(\tilde{y} - \tilde{y}_s)$, $\tilde{y}_s > 0$ (\tilde{x} , \tilde{y} , \tilde{x}_s , etc. are in units of *meters*) excites the system; (2) when the dielectric permittivity $\tilde{\epsilon} \equiv \tilde{\epsilon}_{zz} \equiv \epsilon \tilde{\epsilon}_f$ ($\tilde{\epsilon}_f$ is the permittivity in a vacuum or free space and ϵ is the relative permittivity) is assumed to be isotropic in the half-space; and (3) when the magnetic permeability is anisotropic and characterized

$$\underline{\underline{\tilde{\mu}}} = \begin{bmatrix} \tilde{\mu}_{xx} & \tilde{\mu}_{xy} & 0 \\ \tilde{\mu}_{yx} & \tilde{\mu}_{yy} & 0 \\ 0 & 0 & \tilde{\mu}_{zz} \end{bmatrix} = \underline{\underline{\mu}} \tilde{\mu}_f \quad (1)$$

($\tilde{\mu}_f$ is the permeability in a vacuum and $\underline{\underline{\mu}}$ is the relative permeability tensor). The just described polarization case is termed TM^z . The polarization case dual to this one is termed TE^z and the dielectric permittivity tensor $\underline{\underline{\tilde{\epsilon}}}$ associated with this case is given in [2, Eq. (1)]

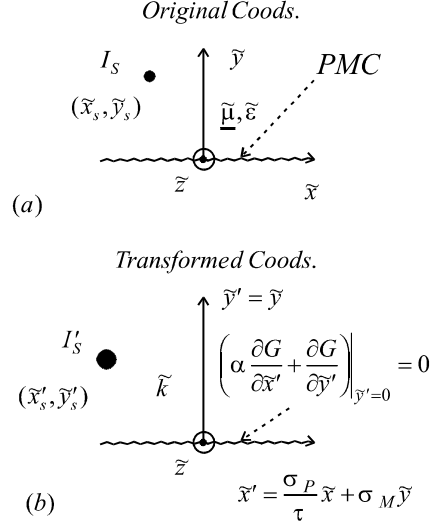


Figure 1. (a) The basic problem geometry (TM^z case) in the \tilde{x}, \tilde{y} original (or untransformed) coordinates including the location of the electric line source I_S and the perfect magnetic conductor (PMC) is shown. (b) The basic geometry in the transformed \tilde{x}', \tilde{y}' coordinate coordinate including the location of the location of the electric line source I'_S and the mixed-partial derivative boundary condition that the system Green's G satisfies is shown.

and is found from $\tilde{\underline{\mu}}$ of Eq. (1) by replacing $\tilde{\mu}_{xx}$ by $\tilde{\epsilon}_{xx}$, $\tilde{\mu}_{xy}$ by $\tilde{\epsilon}_{xy}$, etc. The EM fields of the electric line source (which define the Green's function G of the system) are \tilde{z} independent, and the only nonzero field components of the system are the longitudinal electric field E_z , where $G \equiv G_{TM} \equiv E_z$, and the transverse magnetic field components are H_x and H_y . The nonzero Maxwell equations of the system (assuming time harmonic $e^{j\omega t}$) are

$$\frac{\partial H_y}{\partial \tilde{x}} - \frac{\partial H_x}{\partial \tilde{y}} = J_z + j\omega \tilde{\epsilon} E_z \quad (2a)$$

$$\frac{\partial E_z}{\partial \tilde{y}} = -j\omega [\tilde{\mu}_{xx} H_x + \tilde{\mu}_{xy} H_y] \quad (2b)$$

$$-\frac{\partial E_z}{\partial \tilde{x}} = -j\omega [\tilde{\mu}_{yx} H_x + \tilde{\mu}_{yy} H_y] \quad (2c)$$

Following the analysis and general notation of Monzon [2, 3] and letting $\tilde{\gamma} \equiv \tilde{\gamma}_{TM} = \tilde{\mu}_{xx}\tilde{\mu}_{yy} - \tilde{\mu}_{xy}\tilde{\mu}_{yx} \neq 0$, we find

$$H_x = -\frac{\tilde{\mu}_{xy}}{j\omega\tilde{\gamma}} \frac{\partial E_z}{\partial \tilde{x}} - \frac{\tilde{\mu}_{yy}}{j\omega\tilde{\gamma}} \frac{\partial E_z}{\partial \tilde{y}} \quad (3a)$$

$$H_y = \frac{\tilde{\mu}_{xx}}{j\omega\tilde{\gamma}} \frac{\partial E_z}{\partial \tilde{x}} + \frac{\tilde{\mu}_{yx}}{j\omega\tilde{\gamma}} \frac{\partial E_z}{\partial \tilde{y}} \quad (3b)$$

Substitution of H_x and H_y of Eqs. (3a,b) into the left hand side of Eq. (2a) gives the equation

$$\tilde{\mu}_{xx} \frac{\partial^2 E_z}{\partial \tilde{x}^2} + \tilde{\mu}_{yy} \frac{\partial^2 E_z}{\partial \tilde{y}^2} + [\tilde{\mu}_{xy} + \tilde{\mu}_{yx}] \frac{\partial^2 E_z}{\partial \tilde{x} \partial \tilde{y}} + \omega^2 \tilde{\gamma} \tilde{\epsilon} E_z = j\omega\tilde{\gamma} J_z \quad (4)$$

An important step in the analysis is to make a linear change of coordinates in order to reduce the mixed derivative PDE of Eq. (4) to a standard Helmholtz wave equation, a form to which well known, analysis techniques may be applied and wave equation solutions may be found. The linear change of coordinates to reduce Eq. (4) to a Helmholtz wave equation has been presented by Monzon [2, Eqs. (4),(5)] for the TE^z polarization case, and when applied to the present TM^z case using duality [2, Eq. (2)], is given by

$$\tilde{x} = (\sigma_1 \tilde{\zeta} + \sigma_2 \tilde{\xi}) / 2 \quad (5a)$$

$$\tilde{y} = (\sigma_1 \tilde{\zeta} - \sigma_2 \tilde{\xi}) / (2\tau) \quad (5b)$$

where $\tau \equiv \tau^{TM} = \sqrt{\tilde{\mu}_{xx}/\tilde{\mu}_{yy}}$ and $\sigma_{1,2} \equiv \sigma_{1,2}^{TM} = [2 \pm (\tilde{\mu}_{xy} + \tilde{\mu}_{yx}) / \sqrt{\tilde{\mu}_{xx}\tilde{\mu}_{yy}}]^{1/2}$ where the upper plus sign refers to σ_1 and the lower minus sign refers to σ_2 .

In the present work because of the need to impose the perfect magnetic conductor boundary condition in as simple a way as possible at $\tilde{y} = 0$, a modified linear coordinate transformation will be used to reduce Eq. (4) to a standard Helmholtz wave equation, rather than that used by Monzon [2, 3] (listed in Eqs. (5a,b) herein). The modified linear transformation of coordinates to be used is given by

$$\tilde{x} = (\tau/\sigma_P) [\tilde{x}' - \sigma_M \tilde{y}'] \quad (6a)$$

$$\tilde{y} = \tilde{y}' \quad (6b)$$

or

$$\tilde{x}' = (\sigma_P/\tau) \tilde{x} + \sigma_M \tilde{y} \quad (6c)$$

$$\tilde{y}' = \tilde{y} \quad (6d)$$

where $\sigma_P \equiv \sigma_P^{TM} = \frac{2}{\sigma_1\sigma_2} = \frac{1}{2}[\frac{\sigma_2}{\sigma_1} + \frac{\sigma_1}{\sigma_2}]$ and $\sigma_M \equiv \sigma_M^{TM} = \frac{\sigma_2^2 - \sigma_1^2}{2\sigma_1\sigma_2} = \frac{1}{2}[\frac{\sigma_2}{\sigma_1} - \frac{\sigma_1}{\sigma_2}]$ or also $\sigma_M \equiv \sigma_M^{TM} = \frac{-(\tilde{\mu}_{xy} + \tilde{\mu}_{yx})}{\sigma_1\sigma_2\sqrt{\tilde{\mu}_{xx}\tilde{\mu}_{yy}}}$. The parameters $\sigma_P^{TE}, \sigma_M^{TE}$ and τ^{TE} referred to in the Introduction for the TE^z -PEC ground plane problem dual to the present TM^z one are found by replacing $\tilde{\mu}_{xx}$ by $\tilde{\varepsilon}_{xx}, \tilde{\mu}_{xy}$ by $\tilde{\varepsilon}_{xy}, \tilde{\mu}_{yx}$ by $\tilde{\varepsilon}_{yx}$, and $\tilde{\mu}_{yy}$ by $\tilde{\varepsilon}_{yy}$ in $\sigma_P^{TM}, \sigma_M^{TM}$ and τ^{TM} in Eqs. (5), (6).

The transformation given by Eqs. (6a–d) is simpler than that of Monzon [2, 3] for the present PMC application because the linear transformed coordinate \tilde{y}' equals the original untransformed coordinate \tilde{y} , and thus the magnetic boundary condition in the transformed and in the untransformed coordinate systems occurs for the same coordinate value, namely $\tilde{y} = \tilde{y}' = 0$. Applying the Monzon [2, 3] coordinate transformation system to the TM^z case (Eqs. (5a,b)), the magnetic perfect conductor location expressed in $\tilde{\zeta}, \tilde{\xi}$ transformed coordinates is found to be located at $\tilde{y} = 0 = (\sigma_1\tilde{\zeta} - \sigma_2\tilde{\xi})/(2\tau)$ or $\tilde{\xi} = (\sigma_1/\sigma_2)\tilde{\zeta}$, which is the equation of a slanted line. Thus when imposing boundary conditions at the PMC, it is more difficult to impose boundary conditions at a slanted boundary line, as occurs using the Monzon coordinate transformation [2, 3] (defined herein by Eq. (5)), than it would be at the $\tilde{y} = \tilde{y}' = 0$ horizontal line, as occurs using the modified linear transformation of Eq. (6). We also mention that imposing boundary conditions at $\tilde{y} = \tilde{y}' = 0$ horizontal line using Eq. (6) will allow a simpler interpretation of numerical results than would result from using the transformation of Eq. (5).

The mixed-derivative TM^z PDE of Eq. (4), after transformation to the coordinates of Eq. (6) as derived in the Appendix A, is given by the Helmholtz wave equation

$$\frac{\partial^2 E_z}{\partial \tilde{x}'^2} + \frac{\partial^2 E_z}{\partial \tilde{y}'^2} + \tilde{k}^2 E_z = \frac{j\omega\tilde{\gamma}}{\tilde{\mu}_{yy}} J_z \equiv I'_S \delta(\tilde{x}' - \tilde{x}'_s) \delta(\tilde{y}' - \tilde{y}'_s) \quad (7)$$

where $\tilde{k}^2 \equiv \tilde{k}_{TM}^2 = \frac{\omega^2 \tilde{\varepsilon} \tilde{\gamma}}{\tilde{\mu}_{yy}}$ and where (Fig. 1b) $I'_S = \frac{j\omega\tilde{\gamma}}{\tilde{\mu}_{yy}} |\frac{\sigma_P}{\tau}| I_S$, assuming σ_P and τ are real (which is the case to be studied herein). The parameter \tilde{k} may be called the effective, wavenumber (units of $1/meters$) of the system when expressed in the transformed coordinates of Eqs. (6a,b) for the TM^z case under consideration.

It is interesting to note that the TE^z Helmholtz wave equation for a source free region, using the transformed coordinates [2, Eqs. (4)–(7)] is given by $\frac{\partial^2 H_z}{\partial \tilde{\xi}^2} + \frac{\partial^2 H_z}{\partial \tilde{\zeta}^2} + \tilde{v}_{TE}^2 H_z = 0$, $\tilde{v}_{TE}^2 = \frac{\omega^2 \tilde{\mu}_{zz} \tilde{\gamma}_{TE}}{\tilde{\varepsilon}_{xx}}$, $\tilde{\gamma}_{TE} = \tilde{\varepsilon}_{xx} \tilde{\varepsilon}_{yy} - \tilde{\varepsilon}_{xy} \tilde{\varepsilon}_{yx}$. The TM^z Helmholtz equation for a source free region using Monzon [2] transformed coordinates $(\tilde{\xi}, \tilde{\zeta})$ (Eqs. (5a,b)) is

$\frac{\partial^2 E_z}{\partial \xi^2} + \frac{\partial^2 E_z}{\partial \tilde{\xi}^2} + \tilde{v}_{TM}^2 E_z = 0$, $\tilde{v}_{TM}^2 = \frac{\omega^2 \tilde{\varepsilon}_{zz} \tilde{\gamma}_{TM}}{\tilde{\mu}_{xx}}$, $\tilde{\gamma} \equiv \tilde{\gamma}_{TM} = \tilde{\mu}_{xx} \tilde{\mu}_{yy} - \tilde{\mu}_{xy} \tilde{\mu}_{yx}$, $\tilde{\varepsilon} \equiv \tilde{\varepsilon}_{zz}$. The TM^z Helmholtz equation for a source free region (Eq. (7), when $J_z = 0$) using the modified transformed coordinates (\tilde{x}', \tilde{y}') (Eqs. (6c,d)) introduced in this paper is $\frac{\partial^2 E_z}{\partial \tilde{x}'^2} + \frac{\partial^2 E_z}{\partial \tilde{y}'^2} + \tilde{k}^2 E_z = 0$, $\tilde{k}^2 \equiv \tilde{k}_{TM}^2 = \frac{\omega^2 \tilde{\varepsilon}_{zz} \tilde{\gamma}_{TM}}{\tilde{\mu}_{yy}} \equiv \frac{\omega^2 \tilde{\varepsilon} \tilde{\gamma}}{\tilde{\mu}_{yy}}$. Thus use of the modified coordinate transformation of Eqs. (6a-d) introduced in this paper leads to a different wavenumber, namely $\tilde{k} \equiv \tilde{k}_{TM} = \left(\frac{\omega^2 \tilde{\varepsilon}_{zz} \tilde{\gamma}_{TM}}{\tilde{\mu}_{yy}} \right)^{1/2}$, than the wavenumber, namely $\tilde{v}_{TM} = \left(\frac{\omega^2 \tilde{\varepsilon}_{zz} \tilde{\gamma}_{TM}}{\tilde{\mu}_{xx}} \right)^{1/2}$, that would result if the Monzon [2] transformed coordinates $(\tilde{\xi}, \tilde{\zeta})$ of Eqs. (5a,b) were used to define the Helmholtz wave equation of the system. The two wave numbers differ by the reversal of the two $\tilde{\mu}_{xx}$ and $\tilde{\mu}_{yy}$ permeability tensor components in the in the denominator of the wavenumber formulas.

At this point it is useful to use relative permittivity and permeability material values and to introduce dimensionless coordinates defined by $x = \tilde{k}_f \tilde{x}$, $y = \tilde{k}_f \tilde{y}$, $x' = \tilde{k}_f \tilde{x}'$, $y' = \tilde{k}_f \tilde{y}'$ etc. where $\tilde{k}_f = 2\pi/\tilde{\lambda}_f = \omega\sqrt{\tilde{\mu}_f \tilde{\varepsilon}_f}$, where $\tilde{\lambda}_f$ is the free space wavelength (in meters). Using the above dimensionless coordinates and relative material parameters, Eq. (7) becomes

$$\frac{\partial^2 E_z}{\partial x'^2} + \frac{\partial^2 E_z}{\partial y'^2} + k^2 E_z = \frac{j\gamma}{\mu_{yy}} \left[\frac{\tilde{\eta}_f}{\tilde{k}_f} \right] J_z \quad (8)$$

where $\tilde{\eta}_f = \sqrt{\tilde{\mu}_f/\tilde{\varepsilon}_f} = 377\Omega$, $\gamma \equiv \gamma_{TM} \equiv \tilde{\gamma}/\tilde{\mu}_f^2 = [\tilde{\mu}_{xx}\tilde{\mu}_{yy} - \tilde{\mu}_{xy}\tilde{\mu}_{yx}]/\tilde{\mu}_f^2$, and $k^2 \equiv k_{TM}^2 \equiv \varepsilon\gamma/\mu_{yy}$. The parameter k may be thought of as the effective, normalized, wavenumber of the wave equation as expressed in transformed, normalized coordinates x' and y' of Eq. (6).

The magnetic field in the anisotropic medium in terms of the normalized, transformed coordinates x' and y' of Eq. (6), is given by

$$H_x = \left[\frac{j\mu_{yy}}{\tilde{\eta}_f \gamma} \right] \left[\alpha \frac{\partial E_z}{\partial x'} + \frac{\partial E_z}{\partial y'} \right] \quad (9a)$$

$$H_y = \left[\frac{-j\mu_{yy}}{\tilde{\eta}_f \gamma} \right] \left[\left(\tau \sigma_P + \frac{\mu_{yx}}{\mu_{yy}} \sigma_M \right) \frac{\partial E_z}{\partial x'} + \frac{\mu_{yx}}{\mu_{yy}} \frac{\partial E_z}{\partial y'} \right] \quad (9b)$$

where

$$\alpha \equiv \alpha_{TM} = \left(\frac{\mu_{xy}}{\mu_{yy}} \right) \left(\frac{\sigma_P}{\tau} \right) + \sigma_M \quad (9c)$$

is the mixed-partial derivative boundary condition constant discussed in the Introduction. It's clear from Eq. (9a) that to meet boundary conditions at the PMC, that the tangential magnetic field H_x must vanish at $y = y' = 0$, and thus the electric field E_z ($G \equiv E_z$) must satisfy the mixed-partial derivative boundary condition

$$\left[\alpha_{TM} \frac{\partial E_z}{\partial x'} + \frac{\partial E_z}{\partial y'} \right] \Big|_{y=y'=0} = 0 \quad (10)$$

For this reason the constant $\alpha \equiv \alpha_{TM}$, has been termed the mixed-partial derivative boundary condition constant in this paper.

The parameter $\alpha \equiv \alpha_{TM}$ after algebra may also be expressed in terms of the relative permeability tensor parameters as

$$\alpha \equiv \alpha_{TM} = \frac{\mu_{xy} - \mu_{yx}}{[4\mu_{xx}\mu_{yy} - (\mu_{xy} + \mu_{yx})^2]^{1/2}} = \frac{\mu_{xy} - \mu_{yx}}{2 \left[\gamma - \left(\frac{\mu_{xy} - \mu_{yx}}{2} \right)^2 \right]^{1/2}} \quad (11)$$

where $\gamma \equiv \gamma_{TM} = \mu_{xx}\mu_{yy} - \mu_{xy}\mu_{yx}$ and as in [2] γ is assumed to be nonzero $\gamma \neq 0$. The parameter $\alpha \equiv \alpha_{TM}$ is an important one and clearly defines the cases and conditions for which a mixed-partial derivative boundary condition will occur for the TM^z case under consideration. For the perfect electric conductor, ground plane- TE^z polarization case, dual to the present one, the mixed-partial derivative boundary condition is given by

$$\left[\alpha_{TE} \frac{\partial H_z}{\partial x'} + \frac{\partial H_z}{\partial y'} \right] \Big|_{y=y'=0} = 0 \quad (12)$$

where the parameter α_{TE} is given by Eq. (11) after using the duality of the two cases and thus replacing $\tilde{\mu}_{xx}$ by $\tilde{\epsilon}_{xx}$, $\tilde{\mu}_{xy}$ by $\tilde{\epsilon}_{xy}$, $\tilde{\mu}_{yx}$ by $\tilde{\epsilon}_{yx}$, and $\tilde{\mu}_{yy}$ by $\tilde{\epsilon}_{yy}$. An interesting feature of the constant $\alpha = \alpha_{TE}$ defined by (12) is the fact that this constant is identical to the constant $S_1 \frac{d\ell_y}{d\ell}$ (in the notation of [2, 3]) derived by Monzon [3, Eq. (6)] for the TE^z case he considered. The constants $S_1 \frac{d\ell_x}{d\ell}$ and $S_2 \frac{d\ell_y}{d\ell}$ (a constant closely related to $S_1 \frac{d\ell_y}{d\ell}$) were very important constants used in Refs. [2, 3] to formulate a Green's second theorem integral equation from which scattering from an anisotropic object might be studied. The constants $S_1 \frac{d\ell_x}{d\ell}$ and $S_2 \frac{d\ell_y}{d\ell}$ were used to express the normal, linear-transformed coordinate derivative of the axial EM field (H_z in [2, 3] and $(\tilde{\xi}, \tilde{\zeta})$ were the linear transformed coordinates used in [2, 3]) in terms of the untransformed (\tilde{x}, \tilde{y}) -coordinate, tangential derivative of the axial

EM field (H_z in [2, 3]) of the system and in terms of the tangential EM field (E_t in [2, 3]) of the system. In [2, 3] the linear-transformed, (ξ, ζ) -normal derivative of the axial EM field (H_z in [2, 3]) were needed to be expressed in terms of the tangential derivative and the tangential EM fields (using the constants $S_1 \frac{d\ell_x}{d\ell}$ and $S_2 \frac{d\ell_y}{d\ell}$) because only these tangential EM field components were continuous at a boundary, and thus only these quantities could be used to boundary match the EM fields exterior to an anisotropic scattering object when formulating a Green's second theorem integral equation from which the unknowns of the system could be determined. Please refer to [2, 3] for a detailed description of the $S_1 \frac{d\ell_x}{d\ell}$, $S_2 \frac{d\ell_y}{d\ell}$ constants, their derivation, and their role in defining system integral equations for anisotropic systems.

The present author is not sure why analytically, the important constant $S_1 \frac{d\ell_x}{d\ell}$ used to express the (ξ, ζ) -normal derivative of the axial EM field in terms of tangential field and tangential derivative field quantities in [2, 3], should just happen to equal the constant $\alpha \equiv \alpha_{TE}$ in Eq. (12) which is used to define the mixed-partial derivative boundary condition for the PEC ground plane- TE^z case of Eq. (12). Is it a coincidence that these two constants are equal, or is there a more fundamental underlying reason why the two should be equal?

In this paper we will be interested in determining the Green's function for the perfect magnetic conductor-ground plane- TM^z case when μ_{xy} and μ_{yx} are unequal and thus the Green's function of the system must satisfy the mixed-partial derivative boundary condition of Eq. (10), since for this case $\alpha_{TM} \neq 0$, as seen from Eq. (11). For the PEC ground plane- TE^z problem dual to the present one (which has not been studied by [2, 3] when ε_{xy} and ε_{yx} are unequal (thus α_{TE} is nonzero as shown by Eqs. (10)–(12)), the Green's function for this case must satisfy the mixed-partial derivative boundary condition as specified in Eq. (12). The TM^z, TE^z ground plane problems are dual to each other, and are completely equivalent to one another.

In this paper for computational simplicity, the numerical case when the effective wavenumber k is real and positive will be treated. To give an example which meets this condition, we choose the case when μ_{xx}, μ_{yy} , $\varepsilon \equiv \varepsilon_{zz}$ are real and positive and we choose $\mu_{xy} = (\mu_{yx})^* = \mu_R + j\mu_I$. For this case $\gamma \equiv \gamma_{TM} = \mu_{xx}\mu_{yy} - \mu_{xy}\mu_{yx} = \mu_{xx}\mu_{yy} - \mu_R^2 - \mu_I^2$ and since $k = (\gamma\varepsilon/\mu_{yy})^{1/2} \equiv (\gamma_{TM}\varepsilon_{zz}/\mu_{yy})^{1/2}$, to meet the condition that k be real and positive, we further require $\gamma = \mu_{xx}\mu_{yy} - \mu_R^2 - \mu_I^2 > 0$ or require that the choice of permeability parameters satisfy $\mu_{xx}\mu_{yy} > \mu_R^2 + \mu_I^2$. For the case under consideration we have $\mu_{xy} - \mu_{yx} = 2j\mu_I$, $\mu_{xy} + \mu_{yx} = 2\mu_R$ and thus for this case we

find

$$\alpha \equiv \alpha_{TM} = \frac{j\mu_I}{[\mu_{xx}\mu_{yy} - \mu_R^2]^{1/2}} = \frac{j\mu_I}{[\gamma + \mu_I^2]^{1/2}} \quad (13)$$

Thus in this paper we will be concerned with numerical computations for which mixed-partial derivative boundary condition constant is purely imaginary. We also note for the case under consideration that $|\alpha| < 1$.

As a specific example, we will study extensively the TM^z numerical case corresponding to the following parameters; $\varepsilon \equiv \varepsilon_{zz} = 2.2321428$, $\mu_{xx} = 4.4$, $\mu_{xy} = (\mu_{yx})^* = \mu_R + j\mu_I = 0.6 + j0.2116601$ and $\mu_{yy} = 1.1$. With these choices we find $k = (\gamma\varepsilon/\mu_{yy})^{1/2} = 3.0$, $\tau = \sqrt{\mu_{xx}/\mu_{yy}} = 2.0$, $\sigma_1 = 1.5954480$, $\sigma_2 = 1.2066045$, $\sigma_P = 1.0394023$, $\sigma_M = -0.2834733$, $\gamma = 4.4352000$ and $\alpha = 0.0 + j0.1$ (or $\alpha = j\alpha_I$, $\alpha_I = 0.1$). In Eq. (9c) for the present numerical case σ_P, σ_M, τ and μ_{yy} are all real, but α is still purely imaginary because $\text{Real}(\alpha) = \left(\frac{\text{Real}(\mu_{xy})}{\mu_{yy}}\right) \left(\frac{\sigma_P}{\tau}\right) + \sigma_M = 0$, ($\text{Real}(\mu_{xy}) = \mu_R = 0.6$) as may be verified by direct numerical substitution. Eq. (13) also verifies for the present numerical case that α is purely imaginary. Figs. 2a and 2b show examples of two original and transformed, closed paths that result when using the numerical values of the case just presented and when using transformed normalized coordinates defined in Eqs. (6a–d), (8) are used. The transformed closed path shown in Figs. 2a,b will be used extensively to validate the Green's functions to be presented in later sections of the paper.

3. K-SPACE GREEN'S FUNCTION FORMULATION

In the previous section a linear coordinate transformation was introduced which reduced Maxwell's equations for the anisotropic TM^z half space case under consideration (E_z, H_x , and H_y nonzero) to a Helmholtz wave equation for the longitudinal electric field E_z . It was further shown that the vanishing of the tangential magnetic field H_x as given by Eq. (9a) at the surface of the PMC (Fig. 1a) led to the mixed-partial derivative boundary condition on E_z which was given by Eq. (10). This section will be concerned with determining the Green's function of the Helmholtz wave equation Eq. (8), expressed in transformed, normalized coordinates (x', y') (Eqs. (6a,6b), (8)) which meets the boundary condition as specified by Eq. (10). This will be accomplished in the standard way by choosing the electric line current source strength I_S ($\vec{J} = I_S\delta(\tilde{x} - \tilde{x}_s)\delta(\tilde{y} - \tilde{y}_s)$, Fig. 1a) such that the right hand side of Eq. (8) equals a unity delta source, to give (now

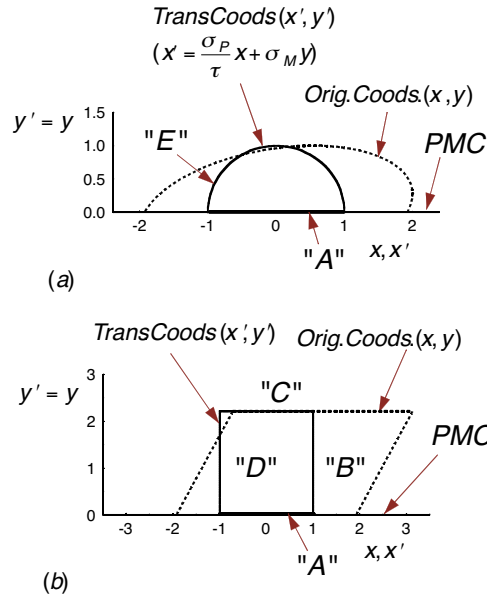


Figure 2. Two closed paths (Figs. 2a,b) as expressed in the normalized original coordinates x, y (dotted line) and normalized, transformed coordinates $x' = \frac{\sigma_P}{\tau} x + \sigma_M y$, $y' = y$ (solid line) ($x = \tilde{k}_f \tilde{x}$, $x' = \tilde{k}_f \tilde{x}'$, etc. ($\tilde{k}_f = 2\pi/\tilde{\lambda}_f$)) are shown (TM^z case) when; $\varepsilon \equiv \varepsilon_{zz} = 2.2321428$, $\mu_{xx} = 4.4$, $\mu_{xy} = (\mu_{yx})^* = 0.6 + j0.2116601$ and $\mu_{yy} = 1.1$. For these values $\tau = \sqrt{\tilde{\mu}_{xx}/\tilde{\mu}_{yy}} = 2.0$, $\sigma_P = 1.0394023$, $\sigma_M = -0.2834733$, $\gamma = 4.4352000$ and $\alpha = 0.0 + j0.1$ as defined in Section 2.

letting $G \equiv G^{TM} \equiv E_z$)

$$\frac{\partial^2 G}{\partial x'^2} + \frac{\partial^2 G}{\partial y'^2} + k^2 G = \delta(x' - x'_s) \delta(y' - y'_s) \equiv \delta(\vec{\rho}' - \vec{\rho}'_s) \quad (14)$$

and then solving Eq. (14) with the mixed-partial derivative boundary condition

$$\left[\alpha \frac{\partial G}{\partial x'} + \frac{\partial G}{\partial y'} \right] \Big|_{y'=0} = 0 \quad (15)$$

($\alpha \equiv \alpha_{TM}$) as defined by Eq. (10) (Fig. 1b). In Eq. (14) it is assumed that $y'_s > 0$.

The Green's function of Eq. (14) is found by decomposing G into two terms $G = g_f + g$ where the first term is $g_f = \frac{j}{4} H_0^{(2)}(k|\vec{\rho}' - \vec{\rho}'_s|)$

which is, as is well known, a particular solution of Eq. (14) in infinite, unbounded space (the “ f ” subscript is for “free space” solution corresponding to wavenumber k) in the transformed coordinates (x', y') [2, Eq. (10)]. The second term g is chosen to satisfy the homogeneous wave equation

$$\frac{\partial^2 g}{\partial x'^2} + \frac{\partial^2 g}{\partial y'^2} + k^2 g = 0 \quad (16)$$

in the region $y' \geq 0$ and is also chosen so, that it, when added to g_f to form G , satisfies the boundary condition of Eq. (15), namely ($\alpha \equiv \alpha_{TM}$, Eq. (9c))

$$\left[\alpha \frac{\partial(g_f + g)}{\partial x'} + \frac{\partial(g_f + g)}{\partial y'} \right] \Big|_{y'=0} = 0 \quad (17)$$

A large amount of the analysis now will be devoted to determining the homogeneous function g of Eqs. (16), (17). The basic procedure will be to expand the known function g_f and the unknown homogeneous Green’s function g in a plane wave k -space spectrum, and after imposing the boundary condition of Eq. (17), determining the unknown spectral amplitude of the homogeneous g function. The g_f function is given by [21, pp. 487]

$$g_f = \frac{j}{4} H_0^{(2)}(k|\bar{\rho}' - \bar{\rho}'_s|) = \int_{-\infty}^{\infty} F_f(k_x) \exp[-jk_x(x' - x'_s) - jk_y|y' - y'_s|] dk_x \quad (18)$$

where

$$F_f(k_x) = \frac{j}{4\pi k_y} \quad (19)$$

where

$$k_y = \begin{cases} (k^2 - k_x^2)^{1/2}, & |k_x| \leq k \\ -j(k_x^2 - k^2)^{1/2}, & |k_x| \geq k \end{cases} \quad (20)$$

The choice of $-j$ (as opposed to $+j$) in the lower line of Eq. (20) ensures, as is well known, that the exponential in Eq. (18) approaches zero for $|y' - y'_s| > 0$ as $k_x \rightarrow \pm\infty$.

Since the source point is above the PMC boundary ($y'_s > 0$), the g_f function of Eq. (18) may be regarded as a k -space superposition of propagating waves ($|k_x| < k$, also called the visible, k -space range) and evanescent waves ($|k_x| > k$, also called the invisible k -space range) incident on the PMC ground plane boundary located at $y' = 0$. For

$y' < y'_s$, the g_f function is given by

$$g_f = \int_{-\infty}^{\infty} F_f(k_x) \exp[-jk_x(x' - x'_s) + jk_y(y' - y'_s)] dk_x \quad (21)$$

since in Eq. (18), $-|y' - y'_s| = y' - y'_s < 0$.

The homogeneous Green's function g may be regarded as a superposition of propagating and evanescent plane waves reflected, scattered and traveling away from the PMC located at $y' = 0$. Thus in the region $y' > 0$, g must be written as

$$g = \int_{-\infty}^{\infty} F(k_x) \exp[-jk_x(x' - x'_s) - jk_y(y' + y'_s)] dk_x \quad (22)$$

The minus sign on the $-jk_y y'$ term in the exponential of Eq. (22) guarantees that only outgoing plane waves are reflected or scattered away from the PMC located at $y' = 0$. Substitution of Eqs. (21), (22) into the boundary condition of Eq. (17), and after differentiation and a small amount of algebra, it is found

$$F(k_x) = \left(\frac{k_y - \alpha k_x}{k_y + \alpha k_x} \right) \frac{j}{4\pi k_y} \quad (23)$$

In addition to calculating the Green's function $G = g_f + g$, any use of the Green's function in a practical application requires knowledge and numerical computation of the partial derivatives of the Green's function $G = g_f + g$. The x' and y' partial derivatives of the Green's function $G = g_f + g$, namely $\frac{\partial G}{\partial x'} = \frac{\partial g_f}{\partial x'} + \frac{\partial g}{\partial x'}$ and $\frac{\partial G}{\partial y'} = \frac{\partial g_f}{\partial y'} + \frac{\partial g}{\partial y'}$ are given by

$$\frac{\partial g_f}{\partial x'} = \frac{j}{4} H_0^{(2)'}(k|\bar{\rho}' - \bar{\rho}'_s|) \frac{k(x' - x'_s)}{|\bar{\rho}' - \bar{\rho}'_s|} \quad (24)$$

$$\frac{\partial g_f}{\partial y'} = \frac{j}{4} H_0^{(2)'}(k|\bar{\rho}' - \bar{\rho}'_s|) \frac{k(y' - y'_s)}{|\bar{\rho}' - \bar{\rho}'_s|} \quad (25)$$

$$\frac{\partial g}{\partial x'} = \int_{-\infty}^{\infty} (-jk_x) F(k_x) \exp[-jk_x(x' - x'_s) - jk_y(y' + y'_s)] dk_x \quad (26)$$

$$\frac{\partial g}{\partial y'} = \int_{-\infty}^{\infty} (-jk_y) F(k_x) \exp[-jk_x(x' - x'_s) - jk_y(y' + y'_s)] dk_x \quad (27)$$

The k -space integrals defined by Eqs. (26), (27) are actually three separate integrals defined on the intervals; $-\infty < k_x < -k$ (called the negative invisible range), $-k < k_x < k$ called the visible range) and $k < k_x < \infty$ (called the positive invisible range). A useful change of variables is; in the negative invisible range, to let $k_x = -k \cosh(u)$, $0 \leq u < \infty$ (k_y becomes $k_y = -jk \sinh(u)$); in the visible range to let $k_x = k \cos(u)$, $-1 \leq u < 1$ (k_y becomes $k_y = k \sin(u)$); and in the positive invisible range to let $k_x = k \cosh(u)$, $0 \leq u < \infty$ (k_y becomes $k_y = -jk \sinh(u)$). This overall change of variable is useful as it removes the square root singularity due to the k_y factor in the denominator of Eq. (23) at the k -space integration points $k_x = \pm k$. The positive and negative invisible integrals making up Eqs. (22), (26), (27) after making the just described change of variables are given by

$$g_I^\pm \equiv \int_0^\infty \Gamma^\pm(u) \exp[\mp jk \cosh(u)X - k \sinh(u)Y] du \quad (28)$$

$$\frac{\partial g_I^\pm}{\partial x'} = \int_0^\infty \mp jk \cosh(u) \Gamma^\pm(u) \exp[\mp jk \cosh(u)X - k \sinh(u)Y] du \quad (29)$$

$$\frac{\partial g_I^\pm}{\partial y'} = \int_0^\infty -k \sinh(u) \Gamma^\pm(u) \exp[\mp jk \cosh(u)X - k \sinh(u)Y] du \quad (30)$$

where

$$\Gamma^\pm(u) = \frac{1}{4\pi} \frac{\alpha \pm j \tanh(u)}{\alpha \mp j \tanh(u)} \quad (31)$$

where $X = x' - x'_s$, $Y = y' + y'_s$. In the above equations, the plus sign corresponds to the positive invisible integral and the negative sign corresponds to the negative, invisible integral. The visible integrals making up Eqs. (22), (26), (27) after making the just described change of variables is given by

$$g_{VIS} \equiv \int_0^\pi \Gamma_{VIS}(u) \exp[-jk \cos(u)X - jk \sin(u)Y] du \quad (32)$$

$$\frac{\partial g_{VIS}}{\partial x'} = \int_0^\pi -jk \cos(u) \Gamma_{VIS}(u) \exp[-jk \cos(u)X - jk \sin(u)Y] du \quad (33)$$

$$\frac{\partial g_{VIS}}{\partial y'} = \int_0^\pi -jk \sin(u) \Gamma_{VIS}(u) \exp[-jk \cos(u)X - jk \sin(u)Y] du \quad (34)$$

where

$$\Gamma_{VIS}(u) = \frac{j \sin(u) - \alpha \cos(u)}{4\pi \sin(u) + \alpha \cos(u)} \quad (35)$$

where X and Y have been defined previously.

4. RAPID CONVERGENCE GREEN'S FUNCTION'S FORMULAS

As can be seen from Eqs. (22)–(27), the accurate calculation of G , $\frac{\partial G}{\partial x'}$ and $\frac{\partial G}{\partial y'}$ requires the accurate numerical calculation of the Hankel function $H_0^{(2)}(k|\bar{\rho}' - \bar{\rho}'_s|)$ and its derivative $H_0^{(2)'}(k|\bar{\rho}' - \bar{\rho}'_s|)$ and the accurate calculation of the Fourier integrals specified in Eqs. (22)–(27). The numerical and analytic properties of the Hankel function and its derivative are very well known and described in Abramowitz and Stegun [25] and many other references. The numerical calculation of the k -space integrals in Eqs. (22), (23), (26), (27) involves the following complications. The first complication is due to the fact that a first order pole exists in the integrals of Eqs. (22), (26), (27) (occurs when $\alpha k_x + k_y = 0$, Eq. (23)) and thus a principal value integral must be carried out in order to ensure the proper numerical evaluation of the integral. Two additional complications occur when $Y = y' + y'_s$ is small or very close to zero (as occurs when y'_s is small and when y' is evaluated at the PMC boundary $y' = 0$), and the exponential factor $\exp[-jk_x(x' - x'_s) - k_y(y' + y'_s)]$ in the integrands of these integrals is close to unity in magnitude. In this case the integrals of Eqs. (22), (26), (27) converge slowly and they are also highly oscillatory when $|k_x(x' - x'_s)| = |k \cosh(u)(x' - x'_s)|$ is large. These two complications when $Y = y' + y'_s$ is small make the accurate calculation of Eqs. (22), (26), (27) difficult.

Because the k -space invisible integrals for $\frac{\partial g_I^\pm}{\partial x'}$ and $\frac{\partial g_I^\pm}{\partial y'}$ in Eqs. (29), (30) are slowly convergent when Y is small, it is useful to change the form of these invisible integrals in order that accurate computations can be made. A numerically efficient form for $\frac{\partial g_I^\pm}{\partial x'}$ and $\frac{\partial g_I^\pm}{\partial y'}$ may be found by expressing the integral of Eq. (28) as a sum of two convergent integrals and subsequently differentiating this sum to find the desired partial derivatives. The two convergent integrals are found by adding and subtracting from the integrand of the integral of Eq. (28) the constant $\Gamma_{asm}^\pm = \frac{1}{4\pi} \frac{\alpha \pm j}{\alpha \mp j} = \lim_{u \rightarrow \infty} \Gamma^\pm(u)$ where $\Gamma^\pm(u)$ is defined in Eq. (31). After carrying out this operation it is found that

Eq. (28) may be rewritten as the sum of the following two integrals

$$g_I^\pm = \int_0^\infty [\Gamma^\pm(u) - \Gamma_{asm}^\pm] \exp[k\rho\psi^\pm] du + \Gamma_{asm}^\pm \int_0^\infty \exp[k\rho\psi^\pm] du \quad (36)$$

where

$$k\rho\psi^\pm = \mp jk \cosh(u)X - k \sinh(u)Y \quad (37)$$

$$\psi^\pm = \mp j \cosh(u) \sin \phi - \sinh(u) \cos \phi = -j \cos(\pi/2 \mp \phi + ju) \quad (38)$$

$\rho = [X^2 + Y^2]^{1/2}$, $X = \rho \sin \phi$, $Y = \rho \cos \phi$ and $-\pi/2 < \phi < \pi/2$. The addition and subtraction of the asymptotic constant Γ_{asm}^\pm produces tractable integrals for numerical calculations because the first integral and its x' and y' partial derivatives can be shown to have exponential convergence and the second integral and its x' and y' partial derivatives, as will be shown, can be expressed as a sum of a Hankel function and an integral over a finite k -space range, both quantities which are also amenable to numerical computation.

The $\Gamma^\pm(u) - \Gamma_{asm}^\pm$ factor in the integrand of the first integral of Eq. (36) after algebra and simplification equals

$$\Gamma_{conv}^\pm(u) \equiv \Gamma^\pm(u) - \Gamma_{asm}^\pm = \frac{1}{4\pi} \frac{\mp 4j\alpha \exp(-2u)}{[\alpha \mp j] [\alpha \mp j \tanh(u)] [1 + \exp(-2u)]} \quad (39)$$

Thus, for $u \rightarrow \infty$, the integrand of first integral of Eq. (36) approaches zero exponentially as $\exp(-2u)$. We also note that the integrand of the x' partial derivative of the first integral in Eq. (36) has the factor $\mp jk \cosh(u) \Gamma_{conv}^\pm(u)$ and that the y' partial derivative of the first integral has the factor $-k \sinh(u) \Gamma_{conv}^\pm(u)$. Thus as $u \rightarrow \infty$, the integrands corresponding to the partial derivatives of the first integral in Eq. (36), approach zero exponentially as $\exp(-u)$. Thus the first integral of Eq. (36) and its x' and y' partial derivatives possess exponential convergence and thus can be numerically calculated accurately as mentioned earlier.

An important part of the analysis now is the evaluation of the second integral in Eq. (36), namely

$$I^\pm \equiv \int_0^\infty \exp[k\rho\psi^\pm] du \quad (40)$$

Following Felson and Marcuvitz [21, pp. 459–464, 487–488] it is useful to make a change of variables in Eq. (40) and use complex integration to deform the path of integration in Eq. (40) to a numerically more

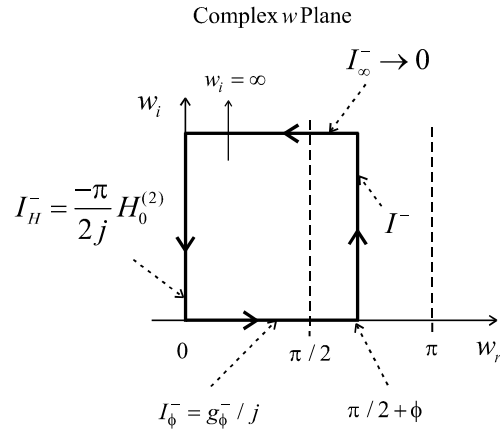


Figure 3. The closed contour, rectangular path C used to transform the negative, invisible integral I^- of Eq. (41) in the complex w plane as detailed in Appendix B is shown. The Green's sub-function g_ϕ^- is defined by integration over the lower leg of contour C (labeled I_ϕ^-) as specified in Eq. (B15) of Appendix B.

convenient form. In Appendix B, the specific steps used to evaluate the I^- integral of Eq. (40), namely,

$$I^- = \int_0^\infty \exp[k\rho\psi^-] du = \int_0^\infty \exp[-jk\rho \cos(\pi/2 + \phi + ju)] du \quad (41)$$

are given, and Fig. 3 shows the complex integration path that is used to make this evaluation. The evaluation of the I^+ integral of Eq. (40) is identical to the I^- analysis except for sign changes in different terms and the final evaluation result is also given in Appendix B.

Using the results of Appendix B we are now in a position to write the negative and positive invisible integrals g_I^\pm of Eqs. (28), (36) and their associated x' and y' partial derivatives as occurs in Eqs. (29), (30). We have after straightforward algebra and differentiation

$$g_I^\pm = g_c^\pm + \frac{\pi}{2j} \Gamma_{asm}^\pm H_0^{(2)}(k\rho) - \frac{1}{j} \Gamma_{asm}^\pm g_\phi^\pm \quad (42)$$

$$\frac{\partial g_I^\pm}{\partial x'} = \frac{\partial g_I^\pm}{\partial X} = \frac{\partial g_c^\pm}{\partial X} + \frac{\pi}{2j} \Gamma_{asm}^\pm H_0^{(2)'}(k\rho) \left(\frac{kX}{\rho} \right) - \frac{1}{j} \Gamma_{asm}^\pm \frac{\partial g_\phi^\pm}{\partial X} \quad (43)$$

$$\frac{\partial g_I^\pm}{\partial y'} = \frac{\partial g_I^\pm}{\partial Y} = \frac{\partial g_c^\pm}{\partial Y} + \frac{\pi}{2j} \Gamma_{asm}^\pm H_0^{(2)'}(k\rho) \left(\frac{kY}{\rho} \right) - \frac{1}{j} \Gamma_{asm}^\pm \frac{\partial g_\phi^\pm}{\partial Y} \quad (44)$$

where

$$g_c^\pm \equiv \int_0^\infty \Gamma_{conv}^\pm(u) \exp[\mp jk \cosh(u)X - k \sinh(u)Y] du \quad (45)$$

$$\frac{\partial g_c^\pm}{\partial X} = \int_0^\infty [\mp jk \cosh(u)] \Gamma_{conv}^\pm(u) \exp[\mp jk \cosh(u)X - k \sinh(u)Y] du \quad (46)$$

$$\frac{\partial g_c^\pm}{\partial Y} = \int_0^\infty [-k \sinh(u)] \Gamma_{conv}^\pm(u) \exp[\mp jk \cosh(u)X - k \sinh(u)Y] du \quad (47)$$

$$g_\phi^\pm \equiv \int_0^{\pi/2 \mp \phi} \exp[-jk\rho \cos u] du \quad (48)$$

$$\frac{\partial g_\phi^\pm}{\partial X} = \frac{X}{\rho} \frac{\partial g_\phi^\pm}{\partial \rho} \mp \frac{Y}{\rho^2} \exp[\mp jkX] \quad (49)$$

$$\frac{\partial g_\phi^\pm}{\partial Y} = \frac{Y}{\rho} \frac{\partial g_\phi^\pm}{\partial \rho} \pm \frac{X}{\rho^2} \exp[\mp jkX] \quad (50)$$

where $\frac{\partial g_\phi^\pm}{\partial \rho} = \int_0^{\pi/2 \mp \phi} (-jk \cos u) \exp[-jk\rho \cos u] du$. The Hankel function $H_0^{(2)}(k\rho)$ with $\rho = [X^2 + Y^2]^{1/2} = [(x' - x'_s)^2 + (y - (-y'_s))^2]^{1/2}$ can be referred as an ‘‘image’’ Hankel function because it appears to emanate from the ‘‘image’’ source point $(x' = x'_s, y' = -y'_s)$ located below the $y' = 0$ PMC boundary.

One notices in these formulas that when calculating $\frac{\partial g_\phi^\pm}{\partial y'}$ at $y' = 0$ with $y'_s \rightarrow 0$, (therefore $Y = y' + y'_s \rightarrow 0$) that the second term of Eq. (50), namely

$$\pm \frac{X}{\rho^2} \exp[\mp jkX] = \pm \frac{X}{X^2 + Y^2} \exp[\mp jkX] \rightarrow \pm \frac{1}{X} \exp[\mp jkX], \quad Y \rightarrow 0 \quad (51)$$

is divergent at $X = x - x'_s = 0$. In applications where one must integrate over this term and $y'_s \rightarrow 0$, the integration over this term must be carried out as a principal value integral.

Concerning the g_ϕ^\pm function defined in Eq. (48), it is interesting to note that g_ϕ^\pm is a solution of the homogeneous wave equation for $y'_s > 0$.

This follows because the terms g_I^\pm, g_c^\pm and $H_0^{(2)}(k\rho)$ in Eq. (42) satisfy the homogeneous wave equation (g_I^\pm and g_c^\pm for $y'_s > 0$ satisfy the wave equation because they are convergent k -space integrals) and g_ϕ^\pm in Eq. (42) is a linear combination of these terms. One may also verify that g_ϕ^\pm is a solution of the wave equation by calculating $\nabla'^2 g_\phi^\pm$ directly in cylindrical coordinates (using the fact that g_ϕ^\pm is z independent) to find

$$\nabla'^2 g_\phi^\pm = \frac{\partial^2 g_\phi^\pm}{\partial x'^2} + \frac{\partial^2 g_\phi^\pm}{\partial y'^2} = \frac{\partial^2 g_\phi^\pm}{\partial X^2} + \frac{\partial^2 g_\phi^\pm}{\partial Y^2} = \frac{1}{\rho} \frac{\partial}{\partial \rho} \rho \frac{\partial g_\phi^\pm}{\partial \rho} + \frac{1}{\rho^2} \frac{\partial^2 g_\phi^\pm}{\partial \phi^2} \quad (52a)$$

$$\begin{aligned} \nabla'^2 g_\phi^\pm &= \frac{jk}{\rho} \cos \phi \exp[\mp jk\rho \sin \phi] \\ &+ \int_0^{\pi/2 \mp \phi} [-k^2 \cos^2 u - \frac{jk}{\rho} \cos u] \exp[-jk\rho \cos u] du \quad (52b) \end{aligned}$$

and then comparing this term, $\nabla'^2 g_\phi^\pm$ in Eq. (52b), to $-k^2 g_\phi^\pm$ for numerically specific values of ρ, ϕ , and k . Several numerical checks of equality of the left and right sides of $\nabla'^2 g_\phi^\pm = -k^2 g_\phi^\pm$ have been made and excellent agreement of the left and right sides have been found.

The summation of g_f and $g = g_{VIS} + g_I^- + g_I^+$ to form $G = g_f + g$ as defined in Eqs. (32)–(35), (42)–(50) specifies the rapidly convergent Green's function of the system and it's associated (x', y') partial derivatives.

5. INTEGRATION OF THE INVISIBLE, K -SPACE, CONVERGENT GREEN'S FUNCTIONS

Despite the fact that k -space invisible integrals $g_c^\pm, \frac{\partial g_c^\pm}{\partial X}$ and $\frac{\partial g_c^\pm}{\partial Y}$ of Eqs. (45)–(47) are exponentially convergent, the numerical integration of these integrals must still account for the facts that; (1) the denominator of the factor $\Gamma_{conv}^\pm(u)$, Eq. (39), in the integrands of these equations vanishes whenever $\alpha \mp j \tanh(u) = 0$ ($\alpha \equiv \alpha_{TM} = j\alpha_I$) and thus a principal value integral must be carried over this pole; and (2) that the factor $\pm jk \cosh(u)X$ in the exponent of Eqs. (45)–(47) makes the integrand of these equations highly oscillatory and thus difficult to evaluate numerically, even when taking into account presence of the exponential factors $\exp(-2u)$ and $\exp(-u)$ in the integrands. It is

useful in these integrals to make the change of variable $z = \exp(-u)$. The denominator factor of $\Gamma_{conv}^{\pm}(u)$ in Eq. (39) is given by

$$[\alpha + jr_i \tanh(u)][1 + \exp(-2u)] = [\alpha + jr_i][1 + s_i z^2] \quad (53)$$

where $r_1 = 1$, $r_2 = -1$ and where the constant $s_i = \frac{\alpha - jr_i}{\alpha + jr_i}$ for $i = 1, 2$. After algebra it also turns out that the spatial expression in the argument of the exponential in Eqs. (45)–(47) may be written

$$\begin{aligned} jr_i kX \cosh(u) - kY \sinh(u) &= \frac{1}{2}[jr_i kX(z^{-1} + z) - kY(z^{-1} - z)] \\ &= \beta_i^* z - \beta_i z^{-1} \end{aligned} \quad (54)$$

where $\beta_i = \frac{k}{2}[Y - jr_i X]$ for $i = 1, 2$. Thus with the substitution $z = \exp(-u)$, letting

$$g^{(i,q)} \equiv \int_0^{\infty} \frac{z^q}{1 + s_i z^2} \exp[\beta_i^* z - \beta_i z^{-1}] du \quad (55)$$

where $i = 1, 2$, we find that the total contribution of the infinite, positive and negative, invisible, k -space integrals in Eq. (45), namely $g_c^- + g_c^+$, is given by

$$g_c \equiv g_c^- + g_c^+ = \frac{j\alpha}{\pi(\alpha + j)^2} g^{(1,2)} - \frac{j\alpha}{\pi(\alpha - j)^2} g^{(2,2)} \quad (56)$$

The x' and y' partial derivatives of the g_c invisible Green's function may also be calculated in terms of sums of the $g^{(i,q)}$ integral of Eq. (55) as was g_c . After algebra we have

$$\begin{aligned} \frac{\partial g_c}{\partial X} &\equiv \frac{\partial g_c^-}{\partial X} + \frac{\partial g_c^+}{\partial X} \\ &= \frac{-k\alpha}{2\pi(\alpha + j)^2} [g^{(1,1)} + g^{(1,3)}] + \frac{-k\alpha}{2\pi(\alpha - j)^2} [g^{(2,1)} + g^{(2,3)}] \end{aligned} \quad (57)$$

$$\begin{aligned} \frac{\partial g_c}{\partial Y} &\equiv \frac{\partial g_c^-}{\partial Y} + \frac{\partial g_c^+}{\partial Y} \\ &= \frac{-jk\alpha}{2\pi(\alpha + j)^2} [g^{(1,1)} - g^{(1,3)}] + \frac{-jk\alpha}{2\pi(\alpha - j)^2} [-g^{(2,1)} + g^{(2,3)}] \end{aligned} \quad (58)$$

To compute $g^{(i,q)}$ of Eq. (55) as it occurs in Eqs. (56)–(58), there are two important integral ranges that must be evaluated by different and separate integration methods. The first integration range, which may

be called the pole integration range, is near the pole value of z where the denominator factor (Eq. (53)) $1 + s_i z^2$ ($z = \exp(-u)$) vanishes. In this range principal value integration is required in order to evaluate the $g^{(i,q)}$ integral. The second integration range is the range where the value of u is large, and series approximations of the integral in Eq. (55) can be made which take advantage of the large values of u used in the integration.

Concerning the pole integration range, when $\alpha_I < 0$ the factor $1 + s_1 z^2$ (corresponding to a negative, invisible integral) vanishes at the value of $z = z_P \equiv [(1 - |\alpha_I|)/(1 + |\alpha_I|)]^{1/2}$ and when $\alpha_I > 0$ the factor $1 + s_2 z^2$ (corresponding to a positive, invisible integral) vanishes at the same value of $z = z_P$. In this paper the pole integration range of Eq. (55) has been taken to be $2z_P - 1 \leq z \leq 1$, where for simplicity, we are assuming numerical cases where $0 \leq 2z_P - 1$.

The integral over this range using the integrand of Eq. (55) after algebra has been found to be

$$g_{Pole}^{(i,q)} \equiv \int_{z_L=2z_P-1}^{z_H=1} \frac{h^{(i,q)}(z)}{z - z_P} dz \quad (59)$$

where $i = 1, 2$ and where

$$h^{(i,q)}(z) \equiv \frac{-z_P^2 z^{q-1}}{z + z_P} \exp[\beta_i^* z - \beta_i z^{-1}] \quad (60)$$

The limits of the integration range used in Eq. (59) $z_L = 2z_P - 1 \leq z \leq z_H = 1$ have been chosen to place the pole location z_P midpoint in the range $z_L \leq z \leq z_H$, in order to facilitate carrying out a principal value integral of Eq. (59). It is useful to change variables in Eq. (59). If we let $z' = z - z_P$, then we find

$$g_{Pole}^{(i,q)} = \int_{-(1-z_P)}^{1-z_P} \frac{\tilde{h}^{(i,q)}(z')}{z'} dz' \quad (61)$$

where $\tilde{h}^{(i,q)}(z') \equiv h^{(i,q)}(z' + z_P)$. The quantity $\tilde{h}^{(i,q)}(z')$ may be written as a sum of an odd and even function around the point $z' = 0$. We find $\tilde{h}^{(i,q)}(z') = \tilde{h}_{ODD}^{(i,q)}(z') + \tilde{h}_{EVEN}^{(i,q)}(z')$ where

$$\tilde{h}_{ODD}^{(i,q)}(z') = \frac{1}{2} [\tilde{h}^{(i,q)}(z') - \tilde{h}^{(i,q)}(-z')] \quad (62)$$

$$\tilde{h}_{EVEN}^{(i,q)}(z') = \frac{1}{2} [\tilde{h}^{(i,q)}(z') + \tilde{h}^{(i,q)}(-z')] \quad (63)$$

Substituting the above equation into Eq. (61) we find after taking advantage of symmetry that

$$\begin{aligned}
g_{Pole}^{(i,q)} &= \int_{-(1-z_P)}^{1-z_P} \frac{\tilde{h}_{EVEN}^{(i,q)}(z')}{z'} dz' + \int_{-(1-z_P)}^{1-z_P} \frac{\tilde{h}_{ODD}^{(i,q)}(z')}{z'} dz' \\
&= 0 + 2 \int_0^{1-z_P} \frac{\tilde{h}_{ODD}^{(i,q)}(z')}{z'} dz' \tag{64}
\end{aligned}$$

The integrals over $\tilde{h}_{EVEN}^{(i,q)}(z')/z'$ over the intervals $-(1-z_P) \leq z' \leq 0$ and $0 \leq z' \leq 1-z_P$ are divergent, but because of symmetry, are opposite in sign to one another, and thus the integral over $\tilde{h}_{EVEN}^{(i,q)}(z')/z'$ in Eq. (64) is zero. The integrand $\tilde{h}_{ODD}^{(i,q)}(z')/z'$ is even about $z' = 0$ and thus the last part of Eq. (64) results. We also notice that $\tilde{h}_{ODD}^{(i,q)}(z') \rightarrow 0$ as $z' \rightarrow 0$ and since $\tilde{h}(z')$ approaches a finite value as $z' \rightarrow 0$, we find $\tilde{h}_{ODD}^{(i,q)}(z')/z'$ approaches a finite value as $z' \rightarrow 0$, and thus we find that the last integral in Eq. (64) is convergent. Eq. (64) represents a principal value integration of the original integral defined in Eq. (59).

The portion of the g_c function of Eq. (56), which has been integrated over the pole integration range $u_{L,Pole} \equiv 0 \leq u \leq u_{H,Pole} \equiv -\ln z_L = -\ln(2z_P - 1) > 0$, has been named the function $g_{c,Pole}$ and is given by $g_{c,Pole} \equiv \frac{j\alpha}{\pi(\alpha+j)^2} g_{Pole}^{(1,2)}$ when the pole occurs in the negative invisible integral of g_c^- (Eq. (45)), and is given by $g_{c,Pole} \equiv \frac{-j\alpha}{\pi(\alpha-j)^2} g_{Pole}^{(2,2)}$ when the pole occurs in the positive invisible integral of g_c^+ (Eq. (45)). (In the present analysis only one pole can occur in either the positive or negative invisible integration ranges.) The function $g_{c,Pole}$ satisfies the homogeneous, Helmholtz wave equation and thus satisfies Green's second theorem over a closed loop or path. The degree to which $g_{c,Pole}$ satisfies Green's second theorem will be studied in a later section. For the numerical case studied in this paper (Section 2) for $\alpha_I = 0.1$ ($\alpha = j\alpha_I$) using the substitution $z = \exp(-u)$; we find that $z_P = 0.9045340$ which corresponds to a u pole value of $u_P \equiv -\ln(z_P) = 0.1003353$; we find that the upper z upper limit of Eq. (59), $z_H = 1$, corresponds to the u lower limit value of $u = u_{L,Pole} \equiv 0$; and we find that the lower z limit $z_L = 2z_P - 1 = 0.8090680$ corresponds to the u upper limit value point $u = u_{H,Pole} \equiv -\ln z_L = -\ln(2z_P - 1) = 0.2118722$.

We will now be concerned in carrying out the numerical integration of Eq. (55) over the integration range, call it $u_E \leq u < \infty$, where the constant u_E is assumed to be large enough so that the

integral defined by

$$g_E^{(i,q)} \equiv \int_{u_E}^{\infty} \frac{z^q}{1 + s_i z^2} \exp[\beta_i^* z - \beta_i z^{-1}] du \quad (65)$$

($z = \exp(-u)$) may be approximated by an infinite sum of exponential integrals which individually may be evaluated quickly and very accurately. To carry out this calculation, we write the factor $\exp(\beta_i^* z)/[1 + s_i z^2]$ in Eq. (65) in the infinite power series

$$\exp(\beta_i^* z) / [1 + s_i z^2] = \sum_{p=0}^{\infty} f_{i,p} z^p \quad (66)$$

($f_{i,p}$ resulted from the product series formula of [25, Eq. (3.6.21), pg. 15] after expressing $\exp(\beta_i^* z)$ and $[1 + s_i z^2]^{-1}$ each in a power series), and after substituting this factor into Eq. (65) and interchanging integration and summation, we find

$$g_E^{(i,q)} = \sum_{p=0}^{\infty} f_{i,p} \int_{u_E}^{\infty} z^{p+q} \exp[-\beta_i z^{-1}] du \quad (67)$$

If we define the integral

$$I_\ell(u_E, \beta) \equiv \int_{u_E}^{\infty} \exp[-\ell u - \beta \exp(u)] du \quad (68)$$

using $z = \exp(-u)$, $\ell = 0, 1, 2, \dots$, we find after algebra, that Eq. (65) becomes

$$g_E^{(i,q)} \equiv \sum_{p=0}^{\infty} f_{i,p} I_{p+q}(u_E, \beta_i) \quad (69)$$

It is further useful to change variables in Eq. (68) and let $t = \exp[u - u_E]$. With this change of variables, we find; when $u = u_E$, $t = 1$ and when $u = \infty$, $t = \infty$, and thus after algebra, we have

$$I_\ell(u_E, \beta) = \exp[-\ell u_E] E_{\ell+1}[\beta \exp(u_E)] \quad (70)$$

where $E_\ell[Z] \equiv \int_1^\infty \frac{\exp[-Zt]}{t^\ell} dt$, $\ell = 0, 1, 2, \dots$, $\text{Real}(Z) > 0$, is the well known exponential integral in standard form as defined by Abramowitz and Stegun [25, pg. 228, Eq. (5.1.4)]. Altogether in terms

of exponential integrals we find that Eqs. (65), (69) may be expressed as

$$g_E^{(i,q)} = \sum_{p=0}^{\infty} f_{i,p} \exp[-(p+q)u_E] E_{p+q+1}[\beta_i \exp(u_E)] \quad (71)$$

Since $\beta_i = \frac{k}{2}[Y - jr_i X]$, $i = 1, 2$ and $Y > 0$, we see that $\text{Real}[\beta_i \exp(u_E)] > 0$. In using Eq. (71) to calculate $g^{(i,q)}$ of Eq. (55) over the range $u_E \leq u < \infty$, care was used when making numerical calculations to ensure that both the infinite power series in Eq. (66) converged correctly and that a sufficiently large value of u_E was used to ensure that the infinite series of exponential functions in Eq. (71) also converged correctly.

In this paper we have only treated numerical cases where $u_{H,Pole}$ (upper limit of the pole integration range) is assumed less than or equal to u_E , used to define $g_E^{(i,q)}$ given in Eqs. (65), (69), (71). In this paper in the intermediate range $u_{H,Pole} \leq u \leq u_E$ (assuming $u_{H,Pole} < u_E$) sufficiently small integration steps have been used to ensure that the oscillatory nature of the integrand in Eq. (55) was correctly accounted for when carrying out the numerical integration of $g^{(i,q)}$ in this range.

6. VALIDATION USING GREEN'S SECOND THEOREM

In the developing the Green's function solution of the previous sections, several important interrelated questions concerning the validity and accuracy of these solutions arises. These questions are: (1) How well and over what parameter range does the Green's function satisfy the mixed-partial derivative boundary condition of Eq. (15)? (2) How well do the Green's function, k -space integrals converge to the correct solution? (3) How well does the Green's function satisfy the delta-source driven Helmholtz wave equation specified by Eq. (14)? (4) How well and over what parameter range does the Green's function and its partial derivatives satisfy Green's second theorem when tested with a known electric field solution? (We assume the known electric field solution meets the boundary condition of Eq. (15).)

The first and second questions are interrelated because the degree to which the overall Green's function $G = g_f + g$, $g_f \equiv \frac{j}{4} H_0^{(2)}(k|\vec{\rho}' - \vec{\rho}'_s|)$ meets the mixed-partial derivative boundary condition of Eq. (15) is an indication of how well g , the homogeneous Green's function solution and its partial derivatives converge. This follows because g_f and its partial derivatives may be calculated very accurately since g_f is proportional to a Hankel function, a function which can be calculated very accurately by standard mathematical packages and techniques

[25–27]. In other words, if the partial derivatives of the Green's functions integrals of the homogeneous Green's function solution and the partial derivatives of the free space Green's function $g_f \equiv \frac{j}{4} H_0^{(2)}(k|\vec{\rho}' - \vec{\rho}'_s|)$ add to zero to satisfy the mixed-partial derivative boundary condition of Eq. (15), and since the partial derivatives of $H_0^{(2)}(k|\vec{\rho}' - \vec{\rho}'_s|)$ may be accurately computed, this then shows excellent convergence of the k -space integrals and the mathematical functions that make up the homogeneous Green's function g and its partial derivatives.

The third and fourth questions are interrelated because it is well known that solutions that satisfy the wave equation must also satisfy Green's second theorem. The fourth question concerning how well the Green's function satisfy Green's second theorem when tested with a known electric field solution is very important because Green's second theorem, itself, is the basis of the integral equation from which unknown EM fields of the system may be determined as demonstrated by Monzon in [2, 3, 13, 14, 16] and [11, 20]. Testing of Green's second theorem is important because if Green's second theorem can't be verified accurately using the Green's functions developed herein when tested with a known electric field solution, then there is little hope that these Green's functions can be used to formulate a useful EM boundary value integral equation to study EM scattering as was done by [2, 3, 11, 13, 14, 16, 20]. The degree to which Green's second theorem can be verified using a known electric field test solution gives a good indication of how accurately these Green's functions can be used to solve EM field problems where the EM field solution is unknown.

Testing of Green's second theorem in this paper is further important because it turns out that when integrating over different partial derivative terms making up the Green's function when $Y = y' + y'_s$ is very small (which occurs when $Y = y' + y'_s > 0$, $y' = 0$, $y'_s > 0$, (for example, y'_s very small and near path "A" ($y' = 0$) of Figs. 2a,b)), that some of the normal derivative terms of $\left. \frac{\partial G}{\partial y'} \right|_{y'=0}$ are very nearly proportional to Dirac delta functions as $y'_s \rightarrow 0$. Thus attempts to integrate this type of term without approximation by the use of a Dirac delta function can lead to totally erroneous results. Testing of Green's second theorem is therefore required to know, numerically, how large or small $Y = y' + y'_s$ should be before approximation by Dirac delta functions is required. The normal derivative term of the g_ϕ^\pm function (part of the total Green's function G) is divergent as $y'_s \rightarrow 0$, (as discussed in Section 4, Eq. (51)) and thus testing of Green's second theorem is necessary to ensure that proper principal value integration over this term has been performed. Thus the testing of Green's second

theorem is required to know how accurately both the Dirac delta-like integrations and the principal value integrations just discussed are being evaluated. Numerical results for illustrating how well the Green's functions satisfy the mixed-partial derivative boundary condition will be given in the next section.

We will now give the mathematical details for testing Green's second theorem with a known electric field solution. The electric field E_{zT} which will be used to test Green's second theorem and which meets the mixed-partial derivative boundary condition of Eq. (15), is given by

$$E_{zT} = E_z + RE_{z1} \quad (72)$$

where

$$E_z = E_0 \exp(-jk_x x' - jk_y y') \quad (73)$$

$$E_{z1} = E_0 \exp(-jk_x x' + jk_y y') \quad (74)$$

where $E_0 = 1.0$ (V/m), $R = \frac{\alpha k_x + k_y}{-\alpha k_x + k_y}$, $\alpha = j\alpha_I$, $-1 < \alpha_I < 1$, $k_x^2 + k_y^2 = k^2$, k_x and k_y are real numbers. The paths that will be used to test Green's second theorem are the rectangular and semicircular paths shown in Figs. 2a,b. The paths have been chosen so that they share a common face at $y' = 0$ namely, path segment "A" in Figs. 2a,b.

The Green's $G = g_f + g$ developed in earlier sections and given by Eqs. (21), (22) and the electric field E_{zT} given in Eq. (72), both satisfy the boundary condition as specified by Eqs. (15), (10), respectively, and also satisfy for $y' \geq 0$, the Helmholtz wave equations

$$\begin{aligned} \frac{\partial^2 G}{\partial x'^2} + \frac{\partial^2 G}{\partial y'^2} + k^2 G &= \frac{\partial^2 (g_f + g)}{\partial x'^2} + \frac{\partial^2 (g_f + g)}{\partial y'^2} + k^2 (g_f + g) \\ &= \delta(x' - x'_s) \delta(y' - y'_s) \end{aligned} \quad (75)$$

$$\frac{\partial^2 E_{zT}}{\partial x'^2} + \frac{\partial^2 E_{zT}}{\partial y'^2} + k^2 E_{zT} = 0 \quad (76)$$

where we have assumed that $y'_s > 0$. Since $g_f = \frac{j}{4} H_0^{(2)} [k|\bar{\rho}' - \bar{\rho}'_s|]$ and since g_f satisfies for all values x' and y' , the equation $\frac{\partial^2 g_f}{\partial x'^2} + \frac{\partial^2 g_f}{\partial y'^2} + k^2 g_f = \delta(x' - x'_s) \delta(y' - y'_s)$ ([2, Eq. (8)]), it then follows, from Eq. (75), that g satisfies the homogeneous wave equation

$$\frac{\partial^2 g}{\partial x'^2} + \frac{\partial^2 g}{\partial y'^2} + k^2 g = 0 \quad (77)$$

for $y' \geq 0$.

If we apply Green's second theorem [26, Eq. (4A-6), pg. 566] using G and E_{zT} of Eqs. (75), (76), and assuming that $y'_s > 0$, we find

$$\oint_{P'} [E_{zT} \nabla' G - G \nabla' E_{zT}] \cdot \hat{a}_{n'} d\ell' = \iint_{S'} \delta[\vec{\rho}' - \vec{\rho}'_s] E_{zT} dS' \quad (78)$$

where S' represents the cross sectional area which is enclosed by the closed path P' (semicircular and rectangular solid line paths of Figs. 2a,b respectively) and where $\hat{a}_{n'}$ is the outward normal of path P' . Substituting $G = g_f + g$ in Eq. (78) and performing algebra we further have

$$\begin{aligned} \oint_{P'} [E_{zT} \nabla' g_f - g_f \nabla' E_{zT}] \cdot \hat{a}_{n'} d\ell' + \oint_{P'} [E_{zT} \nabla' g - g \nabla' E_{zT}] \cdot \hat{a}_{n'} d\ell' \\ = \iint_{S'} \delta[\vec{\rho}' - \vec{\rho}'_s] E_{zT} dS' \end{aligned} \quad (79)$$

In observing this equation, we see that because $g_f = \frac{j}{4} H_0^{(2)} [k|\vec{\rho}' - \vec{\rho}'_s|]$ is the free space Green's function of infinite, unbounded, homogenous space ($-\infty < x' < \infty, -\infty < y' < \infty$) and because the Path P' is in homogenous x', y' space (see Figs. 2a,b), it follows from Green's second theorem, as is well known, that g_f must satisfy the equation

$$\oint_{P'} [E_{zT} \nabla' g_f - g_f \nabla' E_{zT}] \cdot \hat{a}_{n'} d\ell' = \iint_{S'} \delta[\vec{\rho}' - \vec{\rho}'_s] E_{zT} dS' \quad (80)$$

Using this relation in Eq. (79) we thus see that the homogeneous Green's function g in Eq. (79) must then satisfy the equation

$$\begin{aligned} I(g, E_{zT}) &\equiv \oint_{P'} [E_{zT} \nabla' g - g \nabla' E_{zT}] \cdot \hat{a}_{n'} d\ell' \\ &= \oint_{P'} \left[E_{zT} \frac{\partial g}{\partial n'} - g \frac{\partial E_{zT}}{\partial n'} \right] d\ell' = 0 \end{aligned} \quad (81)$$

In Eq. (81) in the region $y' \geq 0$, $\frac{\partial}{\partial n'}$ represents the outward normal on the path P' and $d\ell' = [dx'^2 + dy'^2]^{1/2}$. The evaluation of the delta function term in Eqs. (79), (80) is given by

$$\iint_{S'} \delta[\vec{\rho}' - \vec{\rho}'_s] E_{zT} dS' = \begin{cases} 0, & \text{outside Path } P' \\ E_{zT}(x'_s, y'_s)/2, & \text{exactly on Path } P' \\ E_{zT}(x'_s, y'_s), & \text{inside Path } P' \end{cases} \quad (82)$$

Eq. (78), derived from Green's second theorem, is an important equation, because it represents the fundamental integral equation

relation that can be used to determine E_{zT} when it is treated as an unknown when analyzing an EM scattering problem above a perfect magnetic conductor system.

The calculation of $g_f = \frac{i}{4}H_0^{(2)}[k|\vec{\rho}' - \vec{\rho}'_s|]$ and its integration in Eqs. (78)–(80) is well understood and has been extensively studied in the literature for many different free space scattering problems. Therefore in this paper we are most interested in studying $I(g, E_{zT})$ in Eq. (81) because it represents a way to test how well the homogeneous Green's function has been calculated and how well it satisfies the homogeneous Helmholtz wave equation of Eq. (77) when using a known testing electric field E_{zT} . The closer that $I(g, E_{zT})$ in Eq. (81) numerically integrates to zero, the more accurate is the homogeneous Green's function solution g that has been found. Concerning the testing function E_{zT} , we further note, that because both of the terms E_z and E_{z1} which make up E_{zT} satisfy Eq. (76), that the quantities $I(g, E_z)$ and $I(g, E_{z1})$ are zero ($I(g, E_z)$ and $I(g, E_{z1})$ are formed, respectively, when E_z and E_{z1} replace E_{zT} in Eq. (81)) and thus $I(g, E_{zT}) = I(g, E_z) + RI(g, E_{z1}) = 0$.

The numerical calculations of $I(g, E_z)$, $I(g, E_{z1})$ and $I(g, E_{zT})$ are approximate and all these quantities will be small, but nonzero numbers if a good numerical job of calculating the homogeneous Green's function g is being carried out. In performing an error analysis of Green's second theorem as specified in Eq. (81), because the functions E_z and E_{z1} differ from each other only by the factor $\exp(\pm jk_y y')$, it is felt that a very good understanding of the error induced in the system can be found by simply studying just the numerical error that results from $I(g, E_z)$ or $I(g, E_{z1})$ alone, instead of their more complicated linear combination. In other words, if the homogeneous Green's function converges well and is calculated accurately, then $I(g, E_z)$ and $I(g, E_{z1})$ will be small numbers and so will the linear combination $I(g, E_{zT}) = I(g, E_z) + RI(g, E_{z1})$. Thus a sense of the error of the system is gained by studying the error of either $I(g, E_z)$ or $I(g, E_{z1})$ alone. For this reason to simplify the error analysis in this paper we will base the error analysis on the closeness that $I(g, E_z)$ alone integrates to zero, rather than the more complicated quantity function $I(g, E_{zT})$ of Eq. (81). In performing the error analysis using $I(g, E_z)$ we will base this analysis on the semicircular and rectangular paths shown in Figs. 2a,b.

We now specify the $I(g, E_z)$ Green's second theorem integrals of Eq. (81) for the rectangular and semicircular paths shown in Figs. 2a,b. The integral over the horizontal flat section of the semicircular loop (labeled "A" in Fig. 2a) and the flat sections of the rectangular

loop (labeled “A” or “C” in Fig. 2b) is given by

$$I^{A,C}(g, E_z) \equiv \int_{x'_1=-r'=-1}^{x'_2=r'=1} \left[E_z \left(\frac{\partial g}{\partial y'} \right) - g \left(\frac{\partial E_z}{\partial y'} \right) \right]_{y'=y'_1=0, y'_2} \cdot (\mp \hat{a}_{y'}) dx' \quad (83)$$

where the upper sign (minus sign) and $y' = y'_1 = 0$ refers to the superscript A (path “A” in Figs. 2a,b) and the lower sign (plus sign) and $y' = y'_2$ (path “C” in Fig. 2b) refers to the superscript C. The limits of the integrals are numerically $x'_1 = -1$, $x'_2 = r' = 1$, $y'_1 = 0$ and $y'_2 = 2.212$. The integral over the vertical flat sections of the rectangular loop is given by

$$I^{B,D}(g, E_z) \equiv \int_{y'_1=0}^{y'_2} \left[E_z \left(\frac{\partial g}{\partial x'} \right) - g \left(\frac{\partial E_z}{\partial x'} \right) \right]_{x'=x'_2, x'_1} \cdot (\pm \hat{a}_{x'}) dy' \quad (84)$$

where the upper sign (plus sign) and $x' = x'_2$ (labeled “B”, Fig. 2b) refers to the superscript B and the lower sign (minus sign) and $x' = x'_1$ (labeled “D”, Fig. 2b) refers to the superscript D. The integral over the upper semicircular path (labeled “E” in Fig. 2a) is given by

$$I^E(g, E_z) \equiv \int_0^\pi \left[E_z \left(\cos \phi' \frac{\partial g}{\partial x'} + \sin \phi' \frac{\partial g}{\partial y'} \right) - g \left(\cos \phi' \frac{\partial E_z}{\partial x'} + \sin \phi' \frac{\partial E_z}{\partial y'} \right) \right]_{\rho'=r'=x'_1} r' d\phi' \quad (85)$$

Altogether

$$I^{REC}(g, E_z) \equiv I^A(g, E_z) + I^B(g, E_z) + I^C(g, E_z) + I^D(g, E_z) \quad (86)$$

$$I^{CIR}(g, E_z) \equiv I^A(g, E_z) + I^E(g, E_z) \quad (87)$$

In carrying out the $I^A(g, E_z)$ integral of Eq. (83) special care was required in calculating the integrals over the normal derivative ($\frac{\partial}{\partial n'} = -\frac{\partial}{\partial y'}$) of both the $H_0^{(2)}(k\rho)$ Hankel function (occurring in Eq. (44)) and g_ϕ^\pm (Eq. (50)) terms when y'_s is very small. The normal derivative Hankel function integral in $I^A(g, E_z)$ is

$$I_{Han} \equiv \int_{x'_1=-r'}^{x'_2=r'} \left[E_z \left(-\frac{\partial}{\partial y'} \left(\frac{j}{4} H_0^{(2)}(k\rho) \right) \right) \right]_{y'=0} dx' \quad (88)$$

where $\rho = [(x' - x'_s)^2 + (y' + y'_s)^2]^{1/2}$. It turns out in Eq. (88) that as $y'_s \rightarrow 0$ that

$$\begin{aligned} -\frac{\partial}{\partial y'} \left(\frac{j}{4} H_0^{(2)}(k\rho) \right) &= -\frac{\partial}{\partial y'} \left(\frac{j}{4\pi} \int_{-\infty}^{\infty} \frac{1}{k_y} \exp[-jk_x(x' - x'_s) - jk_y(y' + y'_s)] dk_x \right) \\ &= -\frac{j}{4\pi} \int_{-\infty}^{\infty} \frac{-jk_y}{k_y} \exp[-jk_x(x' - x'_s) - jk_y(y' + y'_s)] dk_x \\ &= \frac{-1}{4\pi} \int_{-\infty}^{\infty} \exp[-jk_x(x' - x'_s) - jk_y(y' + y'_s)] dk_x \quad (89) \end{aligned}$$

At $y' = 0$, $y'_s \rightarrow 0$, the last integral in Eq. (89) approaches

$$\frac{-1}{4\pi} \int_{-\infty}^{\infty} \exp[-jk_x(x' - x'_s)] dk_x = -\frac{1}{2} \delta[x' - x'_s] \quad (90)$$

Substitution of Eq. (90) in Eq. (88) gives

$$I_{Han} = -\frac{1}{2} E_z(x'_s, 0) \quad (91)$$

When evaluating the integral of Eq. (88) for values of y'_s very close to zero, one must either approximate the integral of Eq. (88) by Eq. (91) or perform a very careful, small-step integration about the point $x' = x'_s$ in Eq. (88) for accurate and correct integration results to occur for this case. Numerical experimentation may be needed in order to find the best choice to use.

The normal derivative g_ϕ^\pm integral term in $I^A(g, E_z)$ that needs care in evaluation is the exponential term $\pm X \exp[\mp jkX]/(X^2 + Y^2)$, $X = x' - x'_s$ which arises in $\left[\frac{dg_\phi^\pm}{dy'} \right]_{y'=0}$ of Eq. (50). This term approaches $\pm \exp[\mp jkX]/X$, as $Y = y' + y'_s \rightarrow 0$ (when $y' = 0$, $y'_s \rightarrow 0$) and thus the integral over this term is given by

$$\begin{aligned} &\lim_{y'_s \rightarrow 0} \int_{x'_1}^{x'_2} E_z(x', 0) \left[\frac{\pm X}{X^2 + Y^2} \right] \exp[\mp jkX] dx' \\ &= \int_{x'_1}^{x'_2} E_z(x', 0) \left[\frac{\pm 1}{x' - x'_s} \right] \exp[\mp jk(x' - x'_s)] dx' \end{aligned}$$

$$= \int_{x'_1 - x'_s}^{x'_2 - x'_s} \tilde{E}_z(X, 0) \left[\frac{\pm 1}{X} \right] \exp[\mp jkX] dX \quad (92)$$

where $\tilde{E}_z(X, 0) \equiv E_z(X + x'_s, 0)$. The principal value integral of Eq. (92) is carried out; by dividing the interval $x'_1 - x'_s \leq X \leq x'_2 - x'_s$ into symmetric and non symmetric intervals about the point $X = 0$ ($x' = x'_s$); rewriting $\tilde{E}_z(X, 0)$ as a sum of an even and odd function in the variable X ; substituting these odd and even functions into Eq. (92), and then evaluating the resulting integrals over both the symmetric and nonsymmetrical intervals to produce the final principal value integral. One notices in carrying out this procedure, that as $x'_s \rightarrow x'_1$ or $x'_s \rightarrow x'_2$ and $y'_s \rightarrow 0$, that the symmetrical interval in Eq. (92) approaches zero length and that the integral over the remaining non symmetric interval is, therefore in the limit stated, logarithmically divergent.

7. ALTERNATE INTEGRATION METHODS TO VALIDATE GREEN'S SECOND THEOREM

A useful property of using a rectangular path P' (Fig. 2b) and plane wave E_z as given in Eq. (73) to calculate $I(g, E_z)$ in Eq. (81) is the property that the spatial integration in Eq. (81) for each straight-line portion of the rectangular path P' can be performed in closed form before carrying out the k -space integral. Thus the entire numerical calculation of $I(g, E_z)$ in Eq. (81) can be reduced to summing the single, k -space integrals that result from the endpoint evaluation of the closed form spatial integrations of the straight-line portions of the rectangular path of P' . This is useful; (1) because it provides a very accurate way and alternate way to calculate the $I(g, E_z)$ integral than is specified in Eq. (81); (2) because it gives insight into how the $I^A(g, E_z)$ integral (the straight-line portion of the rectangular path evaluated at $y' = 0$) behaves when y'_s approaches zero (the difficulties in evaluating $I^A(g, E_z)$ when y'_s is small has been discussed earlier); and (3) because, as will be shown, the single k -space endpoint integrals that result from the closed form spatial integration, themselves, can be expressed in a rapidly convergent form (using the complex plane integration techniques described in Appendix B) and thus, this rapidly convergent form can give theoretical insight into how the integrals of Green's second theorem behave, for difficult integration situations that might occur (i.e., when the source point (x'_s, y'_s) is close to the endpoint $((x'_1, 0)$ or $(x'_2, 0))$ of a straight-line portion of the rectangular path as occurs for path segment "A" of Fig. 2b). In the following, for simplicity,

we will present the $I(g_I^-, E_z)$ k -space, endpoint integrals (Eq. (81) with g_I^- replacing g) corresponding to the negative invisible range only, as integration over any other k -space range is similar to this one. The g_I^- function which is defined by the k -space integral of Eq. (28) for $y'_s > 0$, $y' \geq 0$, is solution of the homogenous Helmholtz wave equation and thus satisfies Green's second theorem over the closed loops shown in Figs. 2a,b. We also note that for the numerical case of this paper, presented in Section 2, that there are no poles in the negative invisible range which define the g_I^- function.

For the negative invisible range, carrying out, in closed form, the straight-line integration, as discussed earlier, it is found

$$\begin{aligned} I^A(g_I^-, E_z) &= T_{H,2,1} - T_{H,1,1}, & I^B(g_I^-, E_z) &= T_{V,2,2} - T_{V,2,1}, \\ I^C(g_I^-, E_z) &= -(T_{H,2,2} - T_{H,1,2}), & I^D(g_I^-, E_z) &= -(T_{V,1,2} - T_{V,1,1}) \end{aligned} \quad (93)$$

where,

$$T_{H,p,q} = E_z(x'_p, y'_q) \int_0^\infty \Gamma^-(u) \Gamma_H^-(u) \exp[A_{p,q}] du \quad (94)$$

$$T_{V,p,q} = E_z(x'_p, y'_q) \int_0^\infty \Gamma^-(u) \Gamma_V^-(u) \exp[A_{p,q}] du \quad (95)$$

$$A_{p,q} = jk \cosh(u)(x'_p - x'_s) - k \sinh(u)(y'_q + y'_s)$$

$$\Gamma_H^-(u) = \frac{k \sinh(u) - jk_y}{jk \cosh(u) - jk_x} = \frac{N_H}{D_H}, \quad \Gamma_V^-(u) = \frac{jk \cosh(u) + jk_x}{-k \sinh(u) - jk_y} = \frac{N_V}{D_V}$$

where x'_p, y'_p ($(p, q) = (1, 2)$) have been defined in Eqs. (83), (84), where $N_{H,V}$ and $D_{H,V}$ denote the numerators and denominators of $\Gamma_H^-(u)$ and $\Gamma_V^-(u)$, where $\Gamma^-(u)$ is defined in Eq. (31). The subscripts H and V represent the horizontal and vertical parts of the rectangular path. Substituting Eqs. (94), (95) into Eq. (93) and grouping terms that have a common endpoint we find that Eq. (86) becomes

$$\begin{aligned} I^{REC}(g_I^-, E_z) &= [-T_{H,1,1} + T_{V,1,1}] + [T_{H,2,1} - T_{V,2,1}] \\ &\quad + [-T_{H,2,2} + T_{V,2,2}] + [-T_{V,1,2} + T_{H,1,2}] \end{aligned} \quad (96)$$

Each of the terms in square brackets may be shown to be zero. For example

$$T_{H,2,1} - T_{V,2,1} = E_z(x'_2, y'_1) \int_0^\infty \Gamma^-(u) (\Gamma_H^- - \Gamma_V^-) \exp(A_{2,1}) du \quad (97)$$

$$\Gamma_H^- - \Gamma_V^- = \frac{N_H D_V - N_V D_H}{D_H D_V} \quad (98)$$

After cancellation of like positive and negative terms, and using the facts that $k_x^2 + k_y^2 = k^2$ and $\cosh^2(u) - \sinh^2(u) = 1$, we find

$$N_H D_V - N_V D_H = -k^2 \sinh^2(u) - k_y^2 + k^2 \cosh^2(u) - k_x^2 = 0 \quad (99)$$

and thus Eq. (97) is zero as stated. The fact that $I^{REC}(g_I^-, E_z)$ of Eq. (96) is zero theoretically is not surprising since the plane wave $E_z(x', y')$ and the factor $\exp[+jk \cosh(u)(x' - x'_s) - k \sinh(u)(y' + y'_s)]$ in the invisible k -space integral integrand of Eq. (28) are both solutions of the wave equation (in x', y' coordinates) and thus should satisfy Green's second theorem for each value of u .

Very accurate formulas for the endpoint k -space integrals $T_{H,p,q}$ and $T_{V,p,q}$ of Eqs. (94), (95), may be obtained by adding and subtracting the constant

$$\lim_{u \rightarrow \infty} [\Gamma^-(u) \Gamma_H^-(u)] = \lim_{u \rightarrow \infty} [\Gamma^-(u) \Gamma_V^-(u)] = \frac{1}{4\pi j} \frac{\alpha - j}{\alpha + j} = \Gamma_\infty \quad (100)$$

to the integrands of Eqs. (94), (95) and evaluating the resulting integrals in the complex plane in exactly the same manner as the Green's functions of Eqs. (42)–(50) were analyzed in Appendix B. The $T_{H,p,q}$ and $T_{V,p,q}$ integrals for $(p, q) = (1, 2)$ and $R = H, V$ are given by

$$T_{R,p,q} = E_z(x'_p, y'_q) \left\{ \int_0^\infty [\Gamma^- \Gamma_R - \Gamma_\infty] \exp[A_{p,q}] du + \Gamma_\infty \int_0^\infty \exp[A_{p,q}] du \right\} \quad (101)$$

where

$$\int_0^\infty \exp[A_{p,q}] du = \frac{\pi}{2j} H_0^{(2)}(k\rho_{p,q}) - \frac{1}{j} \int_0^{\pi/2 + \phi_{p,q}} \exp[-jk\rho_{p,q} \cos u] du \quad (102)$$

where

$$\rho_{p,q} = [(x'_p - x'_s)^2 + (y'_q + y'_s)^2]^{1/2}, \quad \phi_{p,q} = \tan^{-1}[(x'_p - x'_s)/(y'_q + y'_s)]$$

The first integral converges since the factor $\Gamma^- \Gamma_R - \Gamma_\infty$ approaches zero as $u \rightarrow \infty$. Eqs. (101), (102) for $T_{H,p,q}$ and $T_{V,p,q}$ clearly show that for the case when the x'_s equals the endpoint x'_1 or x'_2 , when $y'_1 = 0$, and when $y'_s \rightarrow 0$, that both the endpoint k -space integrals $T_{H,p,q}$ and $T_{V,p,q}$ approach infinity logarithmically. This occurs because

the argument of the Hankel function $H_0^{(2)}(k\rho_{p,q})$ approaches zero ($k\rho_{p,q} \rightarrow 0$) for the case under consideration, and is well known, $H_0^{(2)}(k\rho_{p,q})$ is logarithmically divergent as its argument approaches zero.

It is interesting to note that in the case when the source point approaches the endpoint point of the rectangular path that, $I^{REC}(g_I^-, E_z)$ of Eq. (96) is still zero, even if the horizontal or vertical k -space endpoint integrals diverge. This is true because the horizontal and vertical endpoint integrals at each endpoint exactly cancel one another out. For example, it has already been shown in Eqs. (97)–(99) that for the right endpoint ($x'_2 = 1, y'_1 = 0$) of segment “A” in Fig. 2b, that $T_{H,2,1} - T_{V,2,1} = 0$ for all values of x'_s and $y'_s > 0$, including the case when $x'_s \rightarrow x'_2, y'_s \rightarrow y'_1 = 0$. Thus $T_{H,2,1}, T_{V,2,1}$ each diverge when $x'_s \rightarrow x'_2, y'_s \rightarrow y'_1 = 0$, but their term difference contribution $T_{H,2,1} - T_{V,2,1}$ to $I^{REC}(g_I^-, E_z)$ of Eq. (96) is zero. In other words this means that Green’s second theorem still holds in the sense that the two divergent terms from the endpoint of the horizontal path and the endpoint of the vertical path cancel. In applying a MoM solution as was done by Monzon in [2, 3], it can be expected that the any integrals over products of the k -space Green’s function of the system and over any expansion and testing functions used to implement the MoM solution of the system, will exhibit the same logarithmic behavior when $y'_s \rightarrow y'_1 = 0$ as has already been observed in Eq. (102) when a known plane wave solution $E_z(x', y')$ of Eq. (73) was used as a sample expansion function to evaluate the integrals of $I^{REC}(g_I^-, E_z)$ listed in Eqs. (96)–(102).

In Section 4 in Eq. (45) one of the terms making up the overall Green’s function g was the convergent, k -space integral g_c^\pm given by Eq. (45). The only difference between this function g_c^\pm and the k -space, negative invisible integral g_I^- of Eq. (28), is that g_c^\pm had the factor $\Gamma_{conv}^\pm(u)$ in the integrand (Eqs. (39), (45)) and g_I^- had the factor $\Gamma^-(u)$ (Eqs. (28), (31)). Thus when calculating the integrals of Green’s second theorem $I(g, E_z)$ of Eq. (81) over a rectangular path, the integrals involving the g_c^\pm terms, namely $I^{REC}(g_c^\pm, E_z)$, may be carried out in the same way as was the integral $I^{REC}(g_I^-, E_z)$ calculated in Eqs. (93)–(99). Carrying out integrals of $I^{REC}(g_c^\pm, E_z)$ spatially first, and then in k -space second for a rectangular loop might produce more accurate results than vice-versa because the spatially integral is being calculated exactly in closed form rather than approximately.

When in calculating the Green’s second theorem integrals $I(g, E_z)$ of Eq. (81), the Green’s function g is calculated in k -space first and then the spatial integrals of Green’s second theorem are done secondly

(this is the most typical way), the integration of $I(g, E_z)$, will then be referred to as being calculated by the *spatial* integration method. When Green's second theorem integrals (over a rectangular path) over the g_I^\pm and the g_c^\pm terms are calculated spatially first in closed form, and then the resulting k -space endpoint integrals (over a specified k -space integration range) are done secondly, these integrations will be referred to as being performed by the g_I *k-space endpoint* (using the $\Gamma^\pm(u)$ factor of Eq. (31)) and the g_c *k-space endpoint* integration methods (using the $\Gamma_{conv}^\pm(u)$ factor of Eq. (39)), respectively. Specifically the integration range to be used to present numerical example results for the g_I *k-space endpoint* integration method will be the negative invisible range. The integration range to be used to present numerical example results for the g_c *k-space endpoint* integration method will be taken to be the entire positive and negative invisible range, excluding the pole integration range defined in Section 5. When referring to an overall numerical result as being calculated by the g_I *k-space endpoint* or by the g_c *k-space endpoint* integration method, it is meant that the g_I^\pm or g_c^\pm function integrals contributing to the overall numerical result have had the g_I^\pm or g_c^\pm integrals in this overall result calculated by the just named methods.

8. GREEN'S FUNCTION ERROR ANALYSIS

We now present in Tables 1–3 to follow, a detailed error analysis of how well the homogeneous Green's function g and the individual terms making up g satisfy Green's second theorem as specified by Eq. (81). The closed loop path of integration and its dimensions used to calculate the error to be presented in Tables 1–3 is either the semicircular or rectangular paths shown in Figs. 2a and 2b respectively. In Table 4 a detailed error analysis of how well the Green's function $G = g_f + g$ satisfies the mixed-partial derivative boundary condition of Eq. (15) is also presented. In Tables 1–3 percent error results will be presented for two different source points, namely, $(x'_s = -0.799, y'_s = 9.9101 \times 10^{-10})$, $(x'_s = -0.799, y'_s = 9.9101 \times 10^{-2})$ and in Table 4 the boundary condition of Eq. (15) is tested over a very wide range of source points (x'_s, y'_s) .

The homogeneous Green's function g is given by $g = g_{VIS} + g_I^- + g_I^+$ where the function g_{VIS} (Eq. (32)) is a visible region integral and where the functions g_I^\pm (Eqs. (28), (36)) are the invisible region integrals of the system. The g_I^\pm functions themselves are expressed as a linear combination of the functions g_c^\pm, g_ϕ^\pm , and $H_0^{(2)}(k\rho)$ in Eq. (42); where the g_c^\pm function (Eq. (45)) represents an invisible region integral

Table 1. Percent error test of Green's second theorem on a closed path (Figs. 2a,b) using homogeneous Green's sub-functions and a plane wave $E_z(x', y')$.

Closed Path	y'_s value of source point ($x'_s = -0.799$)	N	Error (%) $E(g_{VIS})$	Error (%) $E(g_{c,Pole})$	Error (%) $E(g_c)$	Error (%) $E(g_\phi^-)$	Error (%) $E(g_\phi^+)$
SemiCir	9.9101×10^{-10}	100	5.84×10^{-2}	8.11×10^{-2}	2.02×10^{-2}	3.09×10^{-1}	3.50×10^{-1}
Rec	9.9101×10^{-10}	100	3.45×10^{-2}	1.61×10^{-1}	1.63×10^{-2}	2.84×10^{-1}	3.30×10^{-1}
SemiCi	9.9101×10^{-10}	300	6.48×10^{-3}	9.02×10^{-3}	2.33×10^{-2}	2.65×10^{-1}	3.15×10^{-1}
Rec	9.9101×10^{-10}	300	3.83×10^{-3}	1.78×10^{-2}	2.45×10^{-2}	2.63×10^{-1}	3.12×10^{-1}
SemiCir	9.9101×10^{-10}	1000	5.83×10^{-4}	8.12×10^{-4}	2.63×10^{-2}	4.93×10^{-4}	4.28×10^{-4}
Rec	9.9101×10^{-10}	1000	3.45×10^{-4}	1.61×10^{-3}	2.65×10^{-2}	2.45×10^{-4}	2.66×10^{-4}
SemiCir	9.9101×10^{-10}	2000	1.45×10^{-4}	2.03×10^{-4}	2.64×10^{-2}	1.78×10^{-4}	9.98×10^{-5}
Rec	9.9101×10^{-10}	2000	8.63×10^{-5}	4.02×10^{-4}	2.65×10^{-2}	1.64×10^{-4}	1.21×10^{-4}
SemiCir	9.9101×10^{-2}	100	5.96×10^{-2}	7.55×10^{-2}	2.66×10^{-2}	3.82×10^{-2}	4.61×10^{-2}
Rec	9.9101×10^{-2}	100	3.47×10^{-2}	1.55×10^{-1}	1.54×10^{-2}	2.82×10^{-2}	2.48×10^{-2}
SemiCir	9.9101×10^{-2}	300	6.62×10^{-3}	8.39×10^{-3}	7.36×10^{-3}	4.27×10^{-3}	5.14×10^{-3}
Rec	9.9101×10^{-2}	300	3.86×10^{-3}	1.72×10^{-2}	7.99×10^{-3}	3.16×10^{-3}	2.84×10^{-3}
SemiCir	9.9101×10^{-2}	2000	1.49×10^{-4}	1.88×10^{-4}	8.90×10^{-3}	1.12×10^{-4}	1.21×10^{-4}
Rec	9.9101×10^{-2}	2000	8.69×10^{-5}	3.88×10^{-4}	8.98×10^{-3}	1.22×10^{-4}	1.56×10^{-4}

over the rapidly, convergent spectral amplitude Γ_{conv}^\pm of Eq. (39) respectively; where g_ϕ^\pm (Eq. (48)) is a function which resulted from the complex plane-contour integration analysis of Appendix B; and where $H_0^{(2)}(k\rho)$ is an image Hankel function of the second kind which also resulted from the contour integration analysis of Appendix B. The $g_{c,Pole}$ function (defined in the paragraph after Eq. (64)) makes a partial contribution to the overall g_c^+ function for the numerical cases tested in this paper. An interesting and useful feature of the individual terms making up g , namely g_{VIS} , $g_{c,Pole}$, g_I^\pm , g_c^\pm , g_ϕ^\pm , and $H_0^{(2)}(k\rho)$ (these terms are given in Sections 3–5), is the fact that each term individually satisfies the homogeneous Helmholtz wave equation for $y'_s > 0$. Thus each term, which will be called a homogeneous Green's sub-function, can be individually inserted into the integrals of Eq. (81),

Table 2. Percent error test of Green's second theorem on a closed path (Figs. 2a,b) using the homogeneous Green's function g , an image Hankel function $H_0^{(2)}(k\rho)$ and a plane wave $E_z(x', y')$.

Closed Path	y'_s value of source point ($x'_s = -0.799$)	N	N_{Han}	Error (%) $E(H_0^{(2)}(k\rho))$	Error (%) $E(g)$ (g_c Ksp EndPt)	Error (%) $E(g)$ (spatial)
SemiCir (delta, $y' = 0$)	9.9101×10^{-10}	100	2,000	-	NA	9.527×10^{-2}
Rec (delta, $y' = 0$)	9.9101×10^{-10}	100	2,000	9.407×10^{-5}	7.807×10^{-2}	7.757×10^{-2}
SemiCir (delta, $y' = 0$)	9.9101×10^{-10}	100	10,000	-	NA	9.526×10^{-2}
Rec (delta, $y' = 0$)	9.9101×10^{-10}	100	10,000	2.805×10^{-5}	7.807×10^{-2}	7.757×10^{-2}
SemiCir (delta, $y' = 0$)	9.9101×10^{-10}	300	10,000	-	NA	6.365×10^{-2}
Rec (delta, $y' = 0$)	9.9101×10^{-10}	300	10,000	2.805×10^{-5}	6.201×10^{-2}	6.207×10^{-2}
SemiCir (delta, $y' = 0$)	9.9101×10^{-10}	1,000	10,000	-	NA	3.921×10^{-4}
Rec (delta, $y' = 0$)	9.9101×10^{-10}	1,000	10,000	2.805×10^{-5}	2.654×10^{-4}	2.329×10^{-4}
SemiCir (delta, $y' = 0$)	9.9101×10^{-10}	2,000	2,000	-	NA	1.521×10^{-4}
Rec (delta, $y' = 0$)	9.9101×10^{-10}	2,000	2,000	9.407×10^{-5}	1.280×10^{-4}	1.211×10^{-4}
SemiCir (no delta)	9.9101×10^{-2}	100	2,000	-	NA	7.692×10^{-2}
Rec (no delta)	9.9101×10^{-2}	100	2,000	1.399×10^{-4}	4.869×10^{-2}	4.354×10^{-2}
SemiCir (no delta)	9.9101×10^{-2}	300	10,000	-	NA	8.539×10^{-3}
Rec (no delta)	9.9101×10^{-2}	300	10,000	6.282×10^{-6}	5.373×10^{-3}	4.799×10^{-3}
SemiCir (no delta)	9.9101×10^{-2}	1,000	10,000	-	NA	7.780×10^{-4}
Rec (no delta)	9.9101×10^{-2}	1,000	10,000	6.282×10^{-6}	4.709×10^{-4}	4.198×10^{-4}
SemiCir (no delta)	9.9101×10^{-2}	2,000	2,000	-	NA	2.490×10^{-4}
Rec (no delta)	9.9101×10^{-2}	2,000	2,000	1.399×10^{-4}	2.046×10^{-4}	1.960×10^{-4}

Table 3. Segment integral values of Green's second theorem and percent error test for the homogeneous, negative-invisible, Green's subfunction g_I^- and a plane wave $E_z(x', y')$ as calculated by using the *spatial*, g_I and g_c *k-space*, *endpoint* integration methods.

Path Segment(s) (Figs. 2a,b)	y'_s value of source point ($x'_s = -0.799$)	$I^R(g_I^-, E_z)$ $R = A, BCD, \text{ or } E$ ($N = 2000$) (<i>spatial</i> or g_c <i>Ksp EndPt</i>)	$I_{KEP}^A(g_I^-, E_z)$ $= T_{H,2,1} - T_{H,1,1}$ (g_I <i>Ksp EndPt</i>)	Error (%) , $E_p(g_I^-)$ $I_p^{diff}(g_I^-, E_z) =$ $I^R(g_I^-, E_z) - (-1)^p I_{KEP}^A(g_I^-, E_z)$
Seg. "A" $y' = 0, p = 0$ (<i>delta</i>)	9.9101×10^{-10}	(0.1066415, -0.1731906) (<i>spatial</i>)	(0.1066414, -0.1731907) (g_I <i>Ksp EndPt</i>)	7.59×10^{-5}
	9.9101×10^{-10}	(0.1066415, -0.1731905) (g_c <i>Ksp EndPt</i>)		7.67×10^{-5}
Seg. "E" (SemiCir) $y' > 0, p = 1$ (<i>no delta</i>)	9.9101×10^{-10}	(-0.1066217, 0.1731855) (<i>spatial</i>)		1.00×10^{-2}
Segs. "BCD" (UpperRec) $y' > 0, p = 1$ (<i>no delta</i>)	9.9101×10^{-10}	(-0.1066219, 0.1731852) (<i>spatial</i>)		9.97×10^{-3}
	9.9101×10^{-10}	(-0.1066417, 0.1731905) (g_c <i>Ksp EndPt</i>)	1.63×10^{-4}	
Seg. "A" $y' = 0, p = 0$ (<i>no delta</i>)	9.9101×10^{-2}	(0.0890153, -0.1202950) (<i>spatial</i>)	(0.0890151, -0.1202951) (g_I <i>Ksp EndPt</i>)	1.57×10^{-4}
	9.9101×10^{-2}	(0.0890153, -0.1202950) (g_c <i>Ksp EndPt</i>)		1.56×10^{-4}
Seg. "E" (SemiCir) $y' > 0, p = 1$ (<i>no delta</i>)	9.9101×10^{-2}	(-0.0890092, 0.1202924) (<i>spatial</i>)		4.35×10^{-3}
Segs. "BCD" (UpperRec) $y' > 0, p = 1$ (<i>no delta</i>)	9.9101×10^{-2}	(-0.0890095, 0.1202924) (<i>spatial</i>)		4.19×10^{-3}
	9.9101×10^{-2}	(-0.0890154, 0.1202950) (g_c <i>Ksp EndPt</i>)	2.16×10^{-4}	

and thus the accuracy to which each of these terms individually satisfy Green's second theorem can be evaluated. This is very useful because it gives a very good idea of how accurately matrix elements from each of these terms may be calculated when instituting a Green's second theorem-integral equation, method of moments (MoM) analysis of an anisotropic scattering system, as was done by Monzon [2, 3, 13, 14, 16]. An error analysis showing how well these terms satisfy Green's second theorem will be presented in Tables 1–3.

In computing the error (Tables 1–3) associated with Green's second theorem integral $I(g, E_z)$ of Eq. (81), $I(g, E_z)$ was calculated by three different methods (described at the end of Section 7) which were called; (1) the *spatial* integration method, where the k -space integral was performed first and the spatial integral second (the usual method of Green's function calculation); (2) the g_c *k-space endpoint* method, where the g_c k -space endpoint integrals were performed after the spatial integration had been performed first in closed form (specified by Eqs. (93)–(99) with g_c^\pm replacing g_I^-); and (3) the g_I *k-space endpoint* method which is similar to the g_c *k-space endpoint* method and is defined in Eqs. (93)–(99). The k -space endpoint integral of the g_I *k-space endpoint* method (Eqs. (93)–(95)) was further manipulated to be computationally more accurate (Eqs. (100)–(102)) than the original k -space endpoint integral defined in Eqs. (93)–(95). We remind the reader (Section 7) that the integration range for numerical examples to be presented in this section for the g_c *k-space endpoint* method will be the entire invisible range except the pole integration range (Section 5), and for simplicity in presenting numerical results, the integration range for the g_I *k-space endpoint* method will be limited to just the negative invisible range. We further remind the reader that the g_c *k-space endpoint* and g_I *k-space endpoint* methods can only be carried out for the straight-line segments that arise when carrying out the Green's second theorem integrals of Eqs. (83)–(84).

The percentage error data for the homogeneous Green's function g and its associated Green's sub-functions to be presented in Tables 1 and 2 will be calculated by the formula

$$E(g) = \left\{ |I(g, E_z)| / |I^A(g, E_z)| \right\} \times 100.0 \quad (\%) \quad (103)$$

where; $I(g, E_z)$ is the closed path integral of Green's second theorem (Figs. 2a,b) given by Eq. (81); $I^A(g, E_z)$ is the flat $y' = 0$ straight-line segment integral given by Eq. (83) (Figs. 2a,b); $E_z = E_0 \exp[-jk_x x' - jk_y y']$, $E_0 = 1.0$ (V/m) is the testing incident plane wave Eq. (73) with $k_x = k \cos(\phi_0)$, $k_y = k \sin(\phi_0)$, $k = 3.0$, $\phi_0 = 36.0^\circ$; and g represents the homogeneous Green's functions given by Eqs. (22), (23). The numerical values used to calculate g are specified at the end

of Section 2. The error associated with the Green's sub-functions $g_{VIS}, g_I^\pm, g_c \equiv g_c^- + g_c^+, g_{c,Pole}, g_\phi^\pm$, and $H_0^{(2)}(k\rho)$ is calculated by substituting in place of g in Eq. (103) the individual Green's sub-function terms which were described earlier.

Table 1 displays the error data E (Eq. (103)) of the individual terms $g_{VIS}, g_{c,Pole}, g_c \equiv g_c^- + g_c^+, g_\phi^-$ and g_ϕ^+ of Sections 3–5 (Cols. 4–8, respectively) which are associated with the homogeneous Green's function g for a semicircular or rectangular path; when the source point ($x'_s = -0.799, y'_s = 9.9101 \times 10^{-10}$) was very close to the boundary $y' = 0$; when the source point was relatively far from the boundary $y' = 0$ ($x'_s = -0.799, y'_s = 9.9101 \times 10^{-2}$); and when the number of integration points in each upper segment was $N = 100, 300, 1,000$ or $2,000$ points. The *spatial* integration method was used to calculate the error displayed in Cols. 4–6. As can be seen from Table 1 the percentage error E for the terms $g_{VIS}, g_{c,Pole}, g_\phi^-,$ and g_ϕ^+ (Cols. 4,5,7,8 respectively) grows increasingly smaller as N increases, with overall values ranging from approximately 0.3% ($N = 100$) to 0.0001% ($N = 2000$). This shows that Green's second theorem integrals over these terms are converging rapidly and are giving very acceptable error results. We remind the reader that principal value integration spatially was used when integrating over the $dg_\phi^\pm/dy'|_{y'=0}$ term in the $I^A(g_\phi^\pm, E_z)$ Green's second theorem integral of Eq. (83). Despite the fact that principal value integration was used in these integrals, very convergent results were observed in Table 1.

In evaluating the percentage error $E(g_c)$ (Col. 6) in Table 1 one observes that for both of the source points tested ($x'_s = -0.799, y'_s = 9.9101 \times 10^{-10}$) and ($x'_s = -0.799, y'_s = 9.9101 \times 10^{-2}$) that the error stays approximately constant with increasing N having a maximum value of 0.0266%. It is not surprising that the error increases slightly as N increases for the ($x'_s = -0.799, y'_s = 9.9101 \times 10^{-10}$) case because the k -space integral for g_c and its derivatives (even including the fact that $\Gamma_{conv}^\pm(u)$ (Eq. (39)) in the integrand of the g_c integral is proportional to an exponential factor) is highly oscillatory in the x' and y' integration variables. Thus when $I(g_c, E_z)$ (Eq. (81)) is being integrated around a closed loop to test Green's second theorem, increasing the number of integration points, N , increases the random integration error (or integration "noise"), thus producing a higher integration error for larger N rather than a lower value one. For the $y'_s = 9.9101 \times 10^{-2}$ source point case, the error decreases slight with increasing N . This is not surprising either because the term $-k \sinh(u)Y = -k \sinh(u)(y' + y'_s)$ in the argument of the k -space exponential factors for g_c and its derivatives (Eqs. (45)–(47)) is relatively large in magnitude and thus these integrals converge very quickly, leading the $I(g_c, E_z)$ integral of

Eq. (81) to be less oscillatory when integrated. Thus the error, $E(g_c)$, for the $y'_s = 9.9101 \times 10^{-2}$ case, is less than in the $y'_s = 9.9101 \times 10^{-10}$ case. We remind the reader that principal value integration in k -space was carried out to form the $g_c \equiv g_c^- + g_c^+$ function. Overall, the error of 0.0266% for the g_c function for both cases tested is very acceptable.

Table 2 displays the error $E(g)$ (Eq. (103)) associated with the homogenous Green's function g formed by summing all of the Green's sub-functions together when calculated by the g_c k -space endpoint method (Col. 6) and also calculated by the *spatial* integration method (Col. 7). Also displayed in Table 2 (Col. 5) is the error $E(H_0^{(2)}(k\rho))$ associated with the "image" Hankel function $H_0^{(2)}(k\rho)$, $\rho = [(x' - x'_s)^2 + (y' - (-y'_s))^2]^{1/2}$. Cols. 1–3 of Table 2 are defined in the same way as were Cols. 1–3 in Table 1. Col. 4 lists the number, N_{Han} , of integration points per segment used to integrate the Green's second theorem $I(H_0^{(2)}(k\rho), E_z)$ of Eq. (81) around a closed path. The error term for $H_0^{(2)}(k\rho)$ has been included because it is an important term contributing to the homogeneous Green's function $g = g_{VIS} + g_I^- + g_I^+$ (Eq. (42)) and secondly because the Hankel function $H_0^{(2)}(k\rho)$ is extremely well known to satisfy Green's second theorem and thus the error induced by this term gives a good sense numerically of how well or how badly the other Green's sub-functions (i.e., $g_{VIS}, g_{c,Pole}, g_c \equiv g_c^- + g_c^+, g_\phi^-$ and g_ϕ^+) of the present analysis are satisfying Green's second theorem. (Please note that $H_0^{(2)}(k\rho)$ satisfies the homogeneous form of Green's second theorem and the homogeneous Helmholtz wave equation, because for $y'_s > 0$, the source point $(x'_s, -y'_s)$ of $H_0^{(2)}(k\rho)$ is an "image" source point which lies outside the closed contours of Figs. 2a,b being used to test Green's second theorem in the present analysis.)

In observing the error data $E(g)$ (Table 2) of Col. 6 (g_c k -space endpoint method) and Col. 7 (*spatial* method) for both the rectangular and semicircular paths of Figs. 2a,b, one observes that the percent error decreases rapidly for both methods as N increases from a value of approximately 0.1% ($N = 100$) to a value of approximately 0.0001% ($N = 2,000$). In comparing the error data $E(g)$ of Cols. 6 and 7 one further observes that remarkably close percentage error results occur by both methods for the rectangular closed path used and for both values of y'_s tested. This indicates that by calculating the homogeneous Green's function by the *spatial* method (that is in k -space first and then integrating over this Green's function spatially second (the usual method of Green's function calculation)), over whatever expansion function one might want to use (in this paper the plane

wave $E_0 \exp[-jk_x x' - jk_y y']$ (Eq. (73) was used as an example of a possible expansion function) will probably be a very acceptable way to impose a MoM algorithm. In observing the error of Cols. 6 and 7 for both the rectangular and semicircular paths, one also observes that the percent error decreases rapidly for both methods as N increases from a value of approximately 0.1% ($N = 100$) to a value of approximately 0.0001% ($N = 2,000$).

In viewing the Hankel function percent error data $E(H_0^{(2)}(k\rho))$ of Col. 5, Table 2, for $(x'_s = -0.799, y'_s = 9.9101 \times 10^{-10})$ and $(x'_s = -0.799, y'_s = 9.9101 \times 10^{-2})$, for $N_{Han} = 2,000$ and $N_{Han} = 10,000$, and for testing on the rectangular path of Fig. 2b, very accurate integration of Green's second theorem with maximum error being about $1.4 \times 10^{-4}\%$ is seen. Specifically it is observed for the $y'_s = 9.9101 \times 10^{-10}$ case that an increase of N_{Han} from $N_{Han} = 2,000$ to $N_{Han} = 10,000$ causes about a threefold decrease in the percent error (from approximately $1.0 \times 10^{-4}\%$ to $3.0 \times 10^{-5}\%$), whereas for the $y'_s = 9.9101 \times 10^{-2}$ case, an increase of N_{Han} from $N_{Han} = 2,000$ to $N_{Han} = 10,000$ causes about a twenty-fold decrease in the percent error (from approximately $1.4 \times 10^{-4}\%$ to $6.3 \times 10^{-6}\%$).

It's interesting to compare in Rows 10 and 18, the Hankel function percent error $E(H_0^{(2)}(k\rho))$ in Col. 5 with the homogeneous Green's function g percent error $E(g)$ in Cols. 6 and 7. In Rows 10 and 18, Col. 5-7 data was calculated using $N = N_{Han} = 2,000$, $y'_s = 9.9101 \times 10^{-10}$ (Row 10) and $y'_s = 9.9101 \times 10^{-2}$ (Row 18). It turns out that the percent errors for this case have approximately the same value ranging between 0.0001% and 0.0002%. This is interesting because it shows that for the same number of integration points, $N = N_{Han} = 2,000$, that the two functions $H_0^{(2)}(k\rho)$ and g satisfy Green's second theorem to about the same degree of accuracy for cases when the y'_s is very close to the $y' = 0$ boundary ($y'_s = 9.9101 \times 10^{-10}$) and relatively far from the boundary ($y'_s = 9.9101 \times 10^{-2}$). Because the Hankel function $H_0^{(2)}(k\rho)$ is extremely well known to satisfy Green's second theorem and is being calculated by an extremely efficient and accurate numerical procedure [27], this indicates that the homogeneous Green's function is also probably being calculated about as accurately as possible. Further evidence that is probably being calculated about as accurately as possible is the fact that two different integration methods (the g_c k -space endpoint method (Col. 6) and the spatial integration method (Col. 7)) used produced almost identical error results for the rectangular path of Fig. 2b, as may be seen by comparing Col. 6 to Col. 7.

One further observation that may be made about Table 2 for

$N = 100$ (Rows 1–4) is that an increase in N_{Han} from $N_{Han} = 2,000$ to (Rows 1,2) to $N_{Han} = 10,000$ (Rows 3,4) may no improvement in the percent error $E(g)$ that was seen. For this reason Rows 9,10,17 and 18 ($N = 2,000$) were calculated for $N_{Han} = 2,000$.

In concluding the discussion of Table 2 we remind the reader that a delta function approximation was used for the calculation of the integrals for the data shown in Cols. 6–8, Rows 1–10 because direct integration of the $\partial H_0^{(2)}/\partial y'|_{y'=0}$ term (which arises for small values of y'_s , $y'_s = 9.9101 \times 10^{-10}$), is a very difficult and inaccurate one, because of the singular nature of $\partial H_0^{(2)}/\partial y'|_{y'=0}$, when $\rho = [(x' - x'_s) + (y' + y'_s)^2]^{1/2}$ is near zero. Overall Table 2 shows that the total homogeneous function is being calculated accurately to a high degree of accuracy.

Table 3 displays the percent error data that results for the negative invisible range when all three integration methods (*spatial*, *g_c k -space endpoint*, and *g_I k -space endpoint* methods) are used to integrate the integrals of Green's second theorem. The purpose of the analysis is to further cross check the numerical error results of Tables 1 and 2. It is felt that this analysis is important because, as discussed earlier, the Green's sub-function $g_c \equiv g_c^- + g_c^+$ turned out to be highly oscillatory after integration in k -space in the x', y' variables when integrated over a closed loop (Eq. (81)) to test Green's second theorem. Specifically, it was observed in Table 1, Col. 6 that an increase in the number of integration points N didn't reduce the error ($E(g_c)$) in satisfying Green's second theorem but actually increased it slightly. For this reason it is useful to study in Table 3, as a representative example, the calculation of the k -space and spatial Green's second theorem integrals associated with the g_I^- term (Eq. (42)) since one of the terms which contributes to this term is the Green's sub-function term g_c^- of Eq. (45).

Col. 1, Table 3 lists the segment that the integrals of Green's second theorem are being evaluated for (segment "A" (Figs. 2a,b), upper semicircle "E" (Figs. 2a), or upper rectangle "BCD" (Fig. 2b)) and Col. 2 lists the y'_s value of source point used ($y'_s = 9.9101 \times 10^{-10}$ or $y'_s = 9.9101 \times 10^{-2}$). The percent error in Table 3 calculated by the formula,

$$E_p(g_I^-) \equiv \left\{ \left| I_p^{diff}(g_I^-, E_z) \right| / \left| I_{KEP}^A(g_I^-, E_z) \right| \right\} \times 100.0 \quad (\%) \quad (104)$$

where $I_p^{diff}(g_I^-, E_z) \equiv I^R(g_I^-, E_z) - (-1)^p I_{KEP}^A(g_I^-, E_z)$, $p = 0, 1$; where $R = "A"$ ($I^A(g_I^-, E_z)$ integral over flat line segment, $y' = 0$, Figs. 2a,b, Eq. (83)); where $R = "BCD"$ (sum of $I^B(g_I^-, E_z)$, $I^C(g_I^-, E_z)$, and $I^D(g_I^-, E_z)$ integrals over upper

rectangular section of Fig. 2b, $y' > 0$ Eqs. (83), (84)); where $R =$ “E” ($I^E(g_I^-, E_z)$ integral over upper semicircular section, Fig. 2a, $y' > 0$, Eq. (85)); and where $I_{KEP}^A(g_I^-, E_z)$ is the integral value of segment “A” as calculated by the g_I k -space endpoint method ($I_{KEP}^A(g_I^-, E_z) \equiv T_{H,2,1} - T_{H,1,1}$, Eq. (93), and $T_{H,2,1}, T_{H,1,1}$, are calculated by Eqs. (101), (102)). In Table 3 the numerical values of $I^R(g_I^-, E_z)$ are listed in Col. 3, the numerical values of $I_{KEP}^A(g_I^-, E_z)$ are listed in Col. 4, and the error of Eq. (104) is listed in Col. 5. The value $p = 0$ is used in Rows 1,2,6,7 (Cols. 3,5) because difference error between Cols. 3 and 4 is being calculated in Col. 5, whereas in Rows 3–5, 8–10 (Cols. 3,5), the value $p = 1$ is used because sum error of adding Cols. 3 and 4 is being calculated in Col. 5. In Rows 1,2, Col. 3, because the source point ($x'_s = -0.799$, $y'_s = 9.9101 \times 10^{-10}$) was very close to $y' = 0$, a delta function approximation was needed to integrate over the $\partial H_0^{(2)}(k\rho)/\partial y'|_{y'=0}$ term when calculating $I^A(g_I^-, E_z)$ by using either the spatial or g_c k -space endpoint methods.

In observing the percent error data $E_0(g_I^-)$ of Col. 5, Rows 1,2 one notices that about $0.76 \times 10^{-4}\%$ error occurred in Rows 1,2 (segment “A” (Figs. 2a,b), $y'_s = 9.9101 \times 10^{-10}$) and in Rows 6,7 of Col. 5 (segment “A” (Figs. 2a,b), $y'_s = 9.9101 \times 10^{-2}$) it was about $1.6 \times 10^{-4}\%$. This indicates that the *spatial*, g_c k -space endpoint and g_I k -space endpoint integration methods for calculating the negative invisible integrals for the $y' = 0$ segment “A” of Figs. 2a,b are producing virtually identical numerical results to one another. The g_I k -space endpoint integration method as specified by Eqs. (93)–(102) is very numerically independent of the *spatial* or g_c k -space endpoint integration methods because in the g_I k -space endpoint integration method, the full k -space endpoint integral is performed after the closed form spatial integral is calculated as detailed in Eqs. (93)–(102).

The error $E_1(g_I^-)$ of Col. 5, Row 3 (upper semi-circle “E” (Figs. 2a), $y'_s = 9.9101 \times 10^{-10}$) and the error of Row 4 (upper rectangle “BCD” (Fig. 2b), $y'_s = 9.9101 \times 10^{-10}$) were both calculated by the *spatial* integration method and despite the difference in path shapes (semicircle as opposed to upper rectangle), both errors were about $1.0 \times 10^{-2}\%$ as can be seen from the Table 3. This is about one hundred times larger than that shown in Rows 1 and 2. The error $E_1(g_I^-)$ of Col. 5, Row 5 (upper rectangle “BCD” (Fig. 2b), $y'_s = 9.9101 \times 10^{-10}$) was calculated by the g_c k -space endpoint method and the error was $1.6 \times 10^{-4}\%$, which is only about twice as large as the error calculated in Rows 1,2 and is about sixty times smaller than that of Rows 3,4, Col. 5, which was calculated by the *spatial* integration method. The g_c k -space endpoint method clearly has done a much better job calculating

the Green's theorem integrals for the negative invisible region over the upper rectangular path ("BCD" (Fig. 2b)), than did the *spatial* integration method for the same path. The error $E_0(g_I^-)$ of Rows 1,2, Col. 5 was $0.76 \times 10^{-4}\%$, which was not significantly different than the error $E_1(g_I^-)$ of Row 5, Col. 5 which was $1.6 \times 10^{-4}\%$, even though Green's second theorem integrals were calculated over a large, upper rectangular path for Row 5. In observing the data for $y'_s = 9.9101 \times 10^{-2}$ which is lower half of Table 3, the identical trend as was observed for the upper half of the table, namely that on the upper semi-circular and rectangular paths, much better integration results occurred for the g_c *k-space endpoint* integration method than the *spatial* integration method.

Table 4 displays the percent error as calculated by the formula

$$E_{BC} = \left\{ \left| \left(\alpha \frac{\partial G}{\partial x'} + \frac{\partial G}{\partial y'} \right) \Big|_{y'=0} \right| / \left| \frac{\partial G}{\partial y'} \Big|_{y'=0} \right| \right\} \times 100.0 (\%) \quad (105)$$

when the mixed-partial derivative boundary condition of the overall Green's function $G = g_f + g$ is evaluated at the boundary $y' = 0$ over a wide range of different source point locations (x'_s, y'_s) . Cols. 1 and 2 list the x'_s and y'_s source point locations used, Col. 3 lists the value of the Green's function $G = g_f + g$ at the boundary, Col. 4 lists the value of the normal derivative of $G = g_f + g$ at the boundary, Col. 5 lists the value of the mixed-partial derivative boundary condition at the boundary $y' = 0$, and Col. 6 lists the percent error using Eq. (105). As can be seen from Cols. 5 and 6, the Green's function $G = g_f + g$ is satisfying the mixed-partial derivative boundary condition of Eq. (15) to a high degree of accuracy for values of the source point very close to the boundary observation point (Row 1) and very far way from it (Row 9). The maximum percent error for the values tested was $1.26 \times 10^{-4} (\%)$, which occurred when the source point is far away from the boundary observation point. The fact that the mixed-partial derivative boundary condition is satisfied for a wide range of values shows that the Green's $G = g_f + g$ and its associated derivatives are converging to the correct value very well.

9. NUMERICAL PLOTS

Figs. 4–6 display the mixed-partial derivative $(\alpha \frac{\partial}{\partial x'} + \frac{\partial}{\partial y'})$ of the Green's function G , the free space Green's function g_f and the homogeneous function g , respectively; when the source point is taken to be $x'_s = 0$, $y'_s = 1.0 \times 10^{-2}$; when the other parameters are the same as those used to generate the data of Tables 1–3 (listed in

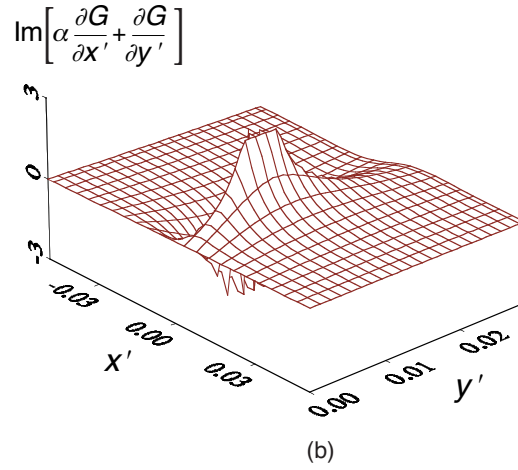
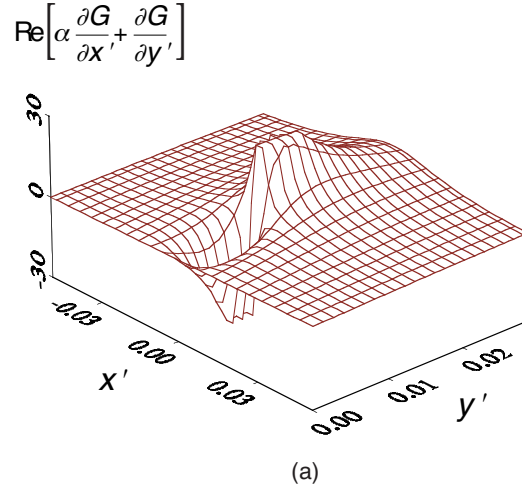


Figure 4. The real and imaginary parts of the mixed-partial derivative Green's function, $\alpha \frac{\partial G}{\partial x'} + \frac{\partial G}{\partial y'}$, $G = g_f + g$, is displayed when the source point is $(x'_s = 0, y'_s = 1.0 \times 10^{-2})$ and when the anisotropic material parameters listed in the Fig. 2 caption and Section 2 are used. The parameter α was $\alpha = 0.0 + j0.1$. The boundary condition $\left(\alpha \frac{\partial G}{\partial x'} + \frac{\partial G}{\partial y'}\right) \Big|_{y'=0} = 0$ is seen to be satisfied at $y' = 0$, PMC boundary.

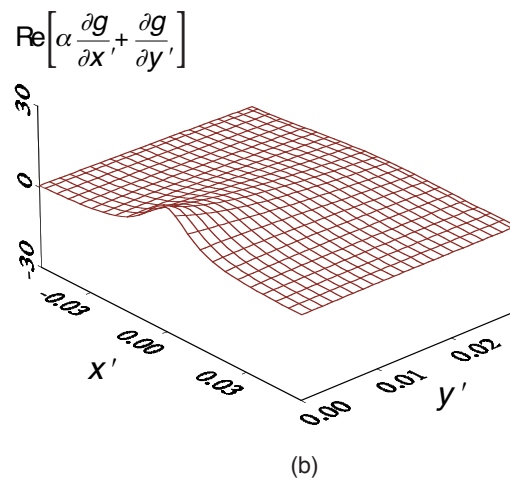
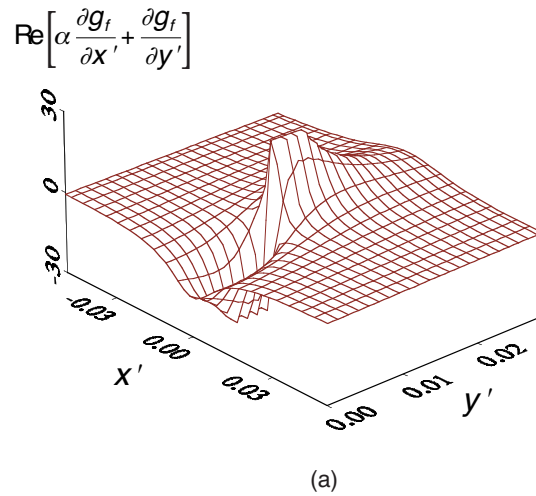


Figure 5. The real part of the mixed-partial derivative free space (Fig. 5a) and homogeneous Green's functions (Fig. 5b) are shown respectively for the same parameters as listed in Figs. 2,4 captions and Section 2. The expected behavior on the $y' = 0$ line of Figs. 5a and 5b, that the plotted functions are almost exact negatives of each other, is seen to hold. The mixed-partial derivative free space (Fig. 5a) and homogeneous Green's functions (Fig. 5b) clearly show significantly different field variation over the x', y' region plotted.

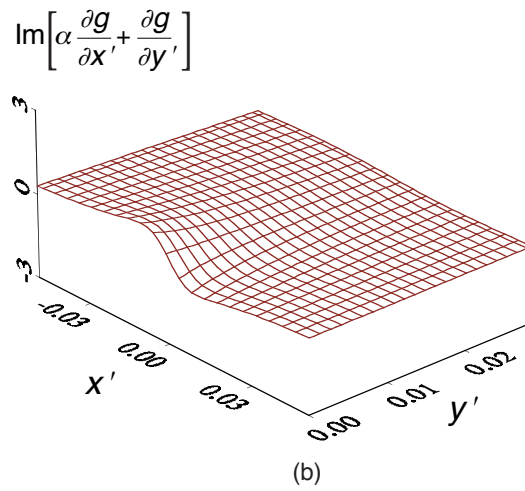
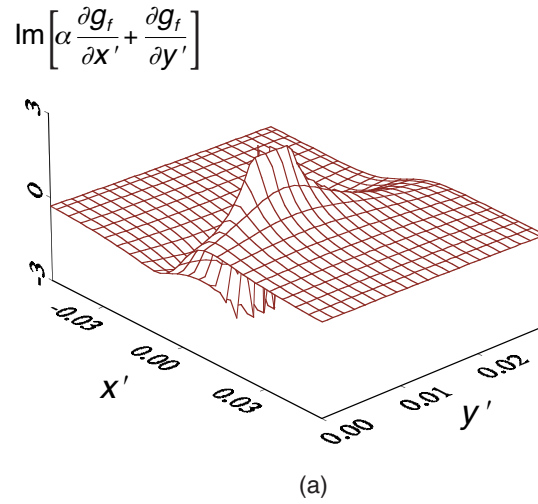


Figure 6. The imaginary part of the mixed-partial derivative free space (Fig. 6a) and homogeneous Green's functions (Fig. 6b) are shown respectively for the same parameters as in Fig. 5. The same comments made in Fig. 5 apply to Fig. 6.

Table 4. Percent error test of the mixed-partial derivative boundary condition for the system Green's function $G = g_f + g$.

x'_s	y'_s	$G _{y'=0}$ ($G = g_f + g$)	Approx. value of $\frac{\partial G}{\partial y'} _{y'=0}$ or $-\alpha \frac{\partial G}{\partial x'} _{y'=0}$	$\left(\alpha \frac{\partial G}{\partial x'} + \frac{\partial G}{\partial y'}\right) _{y'=0}$	Error(%) $E_{bc}(G)$
-0.0001	9.9101×10^{-10}	$(-2.64 \times 10^0,$ $5.05 \times 10^{-1})$	$(2.95 \times 10^{-4},$ $-3.21 \times 10^2)$	$(1.95 \times 10^{-7},$ $1.78 \times 10^{-14})$	6.10×10^{-8}
0.0001	9.9101×10^{-10}	$(-2.64 \times 10^0,$ $4.04 \times 10^{-1})$	$(3.32 \times 10^{-4},$ $3.21 \times 10^2)$	$(1.95 \times 10^{-7},$ $-1.78 \times 10^{-14})$	6.10×10^{-8}
0.799	9.9101×10^{-10}	$(2.56 \times 10^{-1},$ $7.08 \times 10^{-2})$	$(5.85 \times 10^{-2},$ $-1.68 \times 10^{-2})$	$(-1.43 \times 10^{-7},$ $-3.72 \times 10^{-10})$	2.35×10^{-4}
5.0	9.9101×10^{-10}	$(1.01 \times 10^{-1},$ $5.87 \times 10^{-2})$	$(1.25 \times 10^{-2},$ $-7.87 \times 10^{-3})$	$(-1.47 \times 10^{-7},$ $-1.30 \times 10^{-9})$	1.00×10^{-3}
-0.01	9.9101×10^{-2}	$(-4.06 \times 10^{-1},$ $4.46 \times 10^{-1})$	$(2.61 \times 10^{-2},$ $-3.31 \times 10^{-2})$	$(1.52 \times 10^{-7},$ $1.49 \times 10^{-9})$	3.59×10^{-4}
0.01	9.9101×10^{-2}	$(-4.06 \times 10^{-1},$ $4.40 \times 10^{-1})$	$(2.98 \times 10^{-2},$ $3.68 \times 10^{-2})$	$(1.51 \times 10^{-7},$ $-2.04 \times 10^{-18})$	3.19×10^{-4}
-0.799	1.0	$(-1.49 \times 10^{-2},$ $-1.78 \times 10^{-1})$	$(1.00 \times 10^{-2},$ $3.24 \times 10^{-2})$	$(-1.20 \times 10^{-7},$ $4.24 \times 10^{-8})$	3.72×10^{-4}
0.799	1.0	$(6.09 \times 10^{-2},$ $-1.68 \times 10^{-1})$	$(-6.24 \times 10^{-3},$ $-4.48 \times 10^{-2})$	$(-1.20 \times 10^{-7},$ $-4.02 \times 10^{-8})$	2.79×10^{-4}
5.0	5.0	$(9.17 \times 10^{-2},$ $1.70 \times 10^{-2})$	$(1.59 \times 10^{-2},$ $-1.49 \times 10^{-3})$	$(-8.27 \times 10^{-8},$ $-1.85 \times 10^{-7})$	1.26×10^{-3}

Sections 2–7); and when the observation points are varied over the range $-5.0 \times 10^{-2} \leq x' \leq 5.0 \times 10^{-2}$, $0 \leq y' \leq 3.0 \times 10^{-2}$. The y'_s value of the source point used to make the plots was intermediate between the values $y'_s = 9.9101 \times 10^{-10}$ (very close to the boundary $y' = 0$) and $y'_s = 9.9101 \times 10^{-2}$ (relatively far from the $y' = 0$ boundary) which were used in error analysis of Tables 1–3. As can be seen from Figs. 4a and 4b, the real and imaginary parts of the mixed-partial derivative Green's function, $\alpha \frac{\partial G}{\partial x'} + \frac{\partial G}{\partial y'}$, evaluated at the PMC boundary, $y' = 0$, equals zero which shows that the Green's function is overall meeting proper boundary conditions. In Figs. 4a and 4b one also clearly sees the large magnitude value of the mixed-partial derivative Green's function, $\alpha \frac{\partial G}{\partial x'} + \frac{\partial G}{\partial y'}$, in the x', y' region near to the source point ($x'_s = 0$, $y'_s = 1.0 \times 10^{-2}$).

Figs. 5a and 5b show, respectively, the real part of the free

space and homogeneous mixed-partial derivative Green's functions that make up the overall Green's function, namely $\text{Re}\left[\alpha\frac{\partial g_f}{\partial x'} + \frac{\partial g_f}{\partial y'}\right]$ and $\text{Re}\left[\alpha\frac{\partial g}{\partial x'} + \frac{\partial g}{\partial y'}\right]$ and Figs. 6a and 6b show the imaginary parts of these functions, namely, $\text{Im}\left[\alpha\frac{\partial g_f}{\partial x'} + \frac{\partial g_f}{\partial y'}\right]$ and $\text{Im}\left[\alpha\frac{\partial g}{\partial x'} + \frac{\partial g}{\partial y'}\right]$. In viewing both Figs. 5 and 6, one clearly observes the expected behavior that the $y' = 0$ line of Fig. 5a and Fig. 5b are almost exact negatives of each other and that the $y' = 0$ line of Fig. 6a and Fig. 6b are also almost exact negatives of each other. This behavior is of course expected and necessary to occur if the sum of the functions on the $y' = 0$ line in Figs. 5a,b and the $y' = 0$ line in Figs. 6a,b, respectively, are to sum together to zero to meet the overall mixed-partial derivative boundary condition on the $y' = 0$ line shown in Fig. 1.

A very interesting feature of the plots of Figs. 5 and 6 is the extremely different shape that the free space $(\alpha\frac{\partial g_f}{\partial x'} + \frac{\partial g_f}{\partial y'})$ and homogeneous mixed-partial derivative Green's function $(\alpha\frac{\partial g}{\partial x'} + \frac{\partial g}{\partial y'})$ have as y' increases away from the boundary at $y' = 0$. As mentioned earlier, the free space mixed-partial derivative Green's and the mixed-partial derivative homogeneous Green's function (both real and imaginary parts), near the line $y' = 0$, are almost exact negatives of one another. On a line $x' = 0$, as y' increases away from the boundary toward values near the source point values ($x'_s = 0$, $y'_s = 1.0 \times 10^{-2}$), the free space mixed-partial derivative Green's function shows a large effect of the source point (i.e., a large magnitude and discontinuous variation), whereas the homogeneous mixed-partial derivative Greens function varies very gently as y' increases away from the boundary. This behavior is very expected since the free space mixed-partial derivative Greens function is proportional to derivatives of the Hankel function of the second kind, which is singular at the source point, whereas the homogeneous mixed-partial derivative Green's function is composed of the derivatives of four functions, namely; the Hankel function $H_0^{(2)}(k\rho)$, $\rho = [X^2 + Y^2]^{1/2}$, $g_{VIS}(X, Y)$, the $g_\phi^\pm(X, Y)$ and the convergent k -space $g_c(X, Y)$ function ($X = x' - x'_s$, $Y = y' + y'_s$) and all of these functions are well behaved and nonsingular in the region $y' \geq 0$ with $y'_s > 0$. Thus the sum of these homogeneous derivative functions vary slowly as y' varies away from the boundary on a line $x' = 0$, in contrast to the rapid variation of the free space derivative Green's function on this same line. Evidently the terms of the homogeneous Green's function are acting in such a way as to meet the boundary condition in as smooth and gentle a way as possible.

10. SUMMARY AND CONCLUSIONS

The Green's function excited by an electric line source in a magnetic permeable, anisotropic $\underline{\underline{\mu}}$ medium (called herein TM^z polarization) in the presence of a perfect magnetic conductor ground plane, for the non-image theory case, has been derived. The Green's function for the case dual to present one (called herein TE^z polarization) may be obtained from the present solution by using duality as specified by [2, Eq. (2)]. Through the use of a novel, linear coordinate transformation, Maxwell's, anisotropic equations were reduced to a scalar Helmholtz wave equation from which the Green's function of the TM^z system could be obtained. The coordinate transformation was a modification of the one used by Monzon [2, 3] who studied the TE^z case dual to the present one when a magnetic line source excited the Green's function of the system; (1) in infinite, unbounded, homogeneous anisotropic space; and (2) in the presence of an electric perfect conductor plane, for the anisotropic case when $\tilde{\epsilon}_{xy} = \tilde{\epsilon}_{yx} = 0$ and thus when ordinary image theory could be used to define the Green's function of the system. The novel modified linear, coordinate transformation introduced herein, namely $\tilde{x}' = (\sigma_P/\tau)\tilde{x} + \sigma_M\tilde{y}$, $\tilde{y}' = \tilde{y}$ (Eqs. (6a-d), called the "primed" coordinate system), was ideally suited to the present PMC ground plane problem because the vertical transformed \tilde{y}' coordinate equaled the original \tilde{y} coordinate and thus the $\tilde{y} = 0$, PMC boundary in the original coordinate system (Fig. 1a) remained at the same location as the original boundary (Fig. 1b), thus facilitating and simplifying boundary matching of EM field equations. The present author also feels the present modified, coordinate transformation Eqs. (6a-d) is useful because all horizontal lines parallel to the $\tilde{y} = 0$, PMC boundary remain unchanged in the transformed coordinate system and thus any change in the shape of, for example, a scattering object, from the original coordinate system to the transformed coordinate system occurs in only the lateral direction from the relation $\tilde{x}' = (\sigma_P/\tau)\tilde{x} + \sigma_M\tilde{y}$. This is useful because it is much easier to interpret the scattering geometry and to interpret numerical results in the primed (transformed) coordinate system when only a lateral change in the \tilde{x}, \tilde{x}' , coordinates has occurred as opposed to changes in both the \tilde{x}, \tilde{x}' and \tilde{y}, \tilde{y}' coordinates. Figs. 2a,b (in normalized coordinates $x = \tilde{k}_f\tilde{x}$, $x' = \tilde{k}_f\tilde{x}'$, etc.) shows examples of the x, x' , lateral change that occurs in the shape of a possible scattering object using the linear transformation defined by Eqs. (6a-d).

The present author feels the transformation will also be very useful for the defining, in general, the Green's function of multi-layer, anisotropic systems [6]. It will be useful because, again, in

the transformation $\tilde{y}' = \tilde{y}$, horizontal lines remain unchanged in position in the primed and unprimed coordinate systems, and this will thus greatly simplify boundary matching at each layer. The multi-layer, spectral domain, transmission line ladder integral approach developed very recently by [11] for isotropic layers (called by [11] the Spectral Integral Method (SIM)) can be directly applied to finding the Green's function of a multi-layer, anisotropic system. This may be accomplished by using the transformation of Eqs. (6a–d) to reduce Maxwell's equations in each anisotropic layer to a primed-coordinate, Helmholtz wave equation from which the EM fields in each layer may be found. In implementing such an algorithm, it is expected of course that a different and possibly more complicated set of boundary conditions might arise in boundary matching at each $\tilde{y}' = \tilde{y}$ layer boundary due to the anisotropic nature of the boundary layers and the linear transformation of Eqs. (6a–d).

It was found in Section 3 of the paper, that the imposition of the EM boundary condition on the Green's function that the tangential magnetic field of the Green's function expressed in the normalized, primed coordinate system Eqs. (6a–d), (8) vanish at the $\tilde{y}' = \tilde{y} = 0$ PMC boundary led to the mixed-partial derivative boundary condition given by Eq. (15), namely that $\left[\alpha \frac{\partial G}{\partial x'} + \frac{\partial G}{\partial y'}\right] \Big|_{y'=0} = 0$, $\alpha \equiv \alpha_{TM}$, $G \equiv G_{TM} \equiv E_z$ where G is assumed excited by an electric line source. For the TE^z -PEC ground plane problem dual to the present one, the mixed-partial derivative boundary condition was given $\left[\alpha_{TE} \frac{\partial G_{TE}}{\partial x'} + \frac{\partial G_{TE}}{\partial y'}\right] \Big|_{y'=0} = 0$, where $G_{TE} \equiv H_z$, α_{TE} was specified in the text just after Eq. (12), and where $G_{TE} \equiv H_z$ is assumed excited by a magnetic line source. An interesting feature of the TE^z -PEC case was the fact that the coefficient α_{TE} turned out to be the same as the first of two coefficients $S_1 \frac{dl_v}{dl}$ and $S_2 \frac{dl_v}{dl}$ derived by Monzon [2, 3]. The coefficients $S_1 \frac{dl_v}{dl}$ and $S_2 \frac{dl_v}{dl}$ were used in [2, 3] to express primed-coordinate, normal derivatives in terms of tangential EM fields which were expressed in the original coordinates of the system. The author was not able to justify why the coefficients α_{TE} and $S_1 \frac{dl_v}{dl}$ of [2, 3] just happened to be identical even though they served different purposes here and in [2, 3]. An interesting question is whether the two coefficients α_{TE} and $S_1 \frac{dl_v}{dl}$ were the same because it was a coincidence or are they the same because of a more fundamental EM property of the anisotropic system.

The Green's function $G = g_f + g$ for the TM^z -PMC ground plane case, meeting the mixed-partial derivative boundary condition $\left[\alpha \frac{\partial G}{\partial x'} + \frac{\partial G}{\partial y'}\right] \Big|_{y'=0} = 0$, $\alpha \equiv \alpha_{TM}$ in the primed coordinate system was

determined; (1) by expanding, in a k -space, Fourier integral of known spectral amplitude, the incident EM field of the exciting line source (this EM field was called a “free space” Green’s functions g_f herein); (2) by expanding the EM field scattered by the incident line source in a k -space, Fourier integral of unknown spectral amplitude (this EM field was called a “homogeneous” Green’s function g herein); (3) by substituting the sum of the just described incident and scattered EM fields into the mixed-partial derivative boundary condition (Eq. (15)) of the system; and (4) from this equation, determining the unknown spectral amplitude of the scattered EM field and thus the Green’s function $G = g_f + g$ of the system. The EM field scattered by the incident line source was called a homogeneous Green’s function because it satisfied in the primed coordinate system, a homogeneous Helmholtz wave equation. Because the integrand of the k -space Fourier integral of the homogeneous Green’s function corresponded to an infinite set of propagating and evanescent plane waves traveling away from the PMC boundary (in the primed coordinate system) the homogeneous Green’s function of the system was also referred to as the “imperfect image” Green’s function of the system because the EM fields associated with this Green’s function appear to be due to an imperfect image source located in the region $y' < 0$ below the $y' = 0$ PMC plane.

In calculating the Green’s function developed herein, a contribution of the paper was the conversion of the slowly convergent infinite k -space integrals defining the Green’s function into a rapidly convergent form through the use of contour integration in the complex plane as detailed in Appendix B. The slowly convergent k -space integrals were expressed as a linear combination of an “image” Hankel function $H_0^{(2)}(k\rho)$, a finite range, integral which was called the g_ϕ^\pm Green’s sub-function, and an exponentially convergent, infinite k -space integral which was called the g_c^\pm Green’s sub-function. Eqs. (42)–(50) specify these functions and their partial derivatives. It was found that the normal derivative of the “image” Hankel function $H_0^{(2)}(k\rho)$ when evaluated at the PMC surface lead to Dirac delta like behavior when the source point (x'_s, y'_s) was very close to the PMC boundary. It was also found that principal value integration was required to properly evaluate integrals over the normal derivative of the g_ϕ^\pm Green’s function when these integrals were evaluated at the PMC $y' = 0$ surface when the source point (x'_s, y'_s) was very close to the PMC boundary, that is, when $y'_s \rightarrow 0$.

One of the important contributions made by Monzon [2, 3, 12–16] was the use of Green’s second theorem to formulate an integral equation from which the EM scattering from homogenous, anisotropic material objects could be studied. A similar integral equation method

SIM for isotropic materials layers was implemented by [11]. These methods involved expanding the unknown EM fields of the system in a series of functions, substituting this series and the Green's functions of the system into the closed loop integrals (taken over the boundary of the scattering object) of Green's second theorem, and from these integrals after application of an appropriate testing or enforcement method, forming a matrix equation from which the unknowns of the system may be determined.

When applying the methods of [2, 3, 11–16] to the present problem, an important question that arises is how accurately are the matrix elements of the system being calculated. For this reason, herein, this question has been partially answered by; (1) substituting a known EM solution of Maxwell's anisotropic equations meeting boundary conditions and the Green's functions derived herein into Green's second theorem integrals as defined in Sec 6; (2) evaluating these integrals over some given closed path; and (3) introducing an appropriate error function to see how well Green's second theorem was satisfied. The testing of the Green's function developed in this paper in Green's second theorem is important to perform because the calculation of the homogeneous portion of the Green's function required numerical techniques (such as; k -space integration over an infinite spectral range; k -space integration over a pole; approximation of some spatial integrals by Dirac delta functions; and principal value integration of some divergent spatial integrals) which potentially could be numerically very error prone and thus lead to incorrect matrix elements and incorrect numerical results. Overall it is felt that if a known EM solution and the Green's functions developed herein could satisfy Green's second theorem to a high degree of accuracy, then hopefully, the same Green's function could be used to calculate correct matrix elements for a scattering problem involving unknown EM fields. A further comment concerning the testing of the homogeneous Green's function in Green's second theorem, is the interesting and useful fact that the individual terms making up the homogeneous Green's function g , namely g_{VIS} , $g_{c,Pole}$, g_I^\pm , g_c^\pm , g_ϕ^\pm , and $H_0^{(2)}(k\rho)$ (given in Sections 3–5) each individually satisfy the homogeneous wave equation for $y'_s > 0$. This is very useful because it gives a very good idea of how accurately matrix elements from each of these terms may be calculated when instituting a Green's second theorem MoM solution algorithm.

In this paper to test Green's second theorem, the known EM solution chosen for testing was the sum of an incident and its reflected plane wave (expressed in primed coordinates, Eq. (72)) and the closed loop paths chosen for testing were the rectangular and semicircular closed loop paths shown in Figs. 2a,b. Because the free space Green's

function was very well known to individually satisfy Green's second theorem, testing of only the homogeneous Green's function was carried out. Also because the incident and reflected plane waves making up the known EM solution, each individually satisfy Green's second theorem over a closed loop, it was felt that error testing of the incident plane wave alone in Green's second theorem was sufficient to obtain an accurate estimate of the error associated with the Green's functions which were derived herein.

Tables 1 and 2 presented extensive error testing of Green's second theorem; using the homogeneous Green's sub-functions g_{VIS} , g_{Pole} , $g_c \equiv g_c^+ + g_c^-$ and g_ϕ^\pm (Table 1); using the homogeneous Green's function g (Table 2); and using the "image" Hankel function $H_0^{(2)}(k\rho)$ (Table 2). In Tables 1 and 2, Green's second theorem was observed to hold to a high degree of accuracy as discussed in detail in Section 8 for the terms tested. Table 3 presented extensive error testing of the Green's second theorem integral $I(g_I^-, E_z)$ (Eq. (81) with g_I^- substituted for g) where the Green's sub-function g_I^- was defined in Eq. (28). The integral $I(g_I^-, E_z)$ was calculated by three different integration methods; which were called the *spatial*, the g_c *k-space endpoint* and the g_I *k-space endpoint* integration methods. The first method involved calculating $I(g_I^-, E_z)$ in *k-space* first and then spatially second (the most usual way to calculate Green's functions), and the second and third methods calculated $I(g_I^-, E_z)$ spatially first in closed form and then in *k-space* second. The second and third methods were calculated only over the rectangular path of Fig. 2b, as only a straight-line path segment could be integrated spatially in closed form, whereas the first method, the *spatial* method, could be used to calculate $I(g_I^-, E_z)$ for both the rectangular and semicircular paths of Figs. 2a,b. In Table 3 Green's second theorem was shown to hold using the g_I^- Green's sub-function to a high degree of accuracy.

In Table 3 the author feels that the third method, the g_I *k-space endpoint* method, was the best and most direct method of the three integration methods to calculate, test and evaluate $I(g_I^-, E_z)$ over a closed rectangular loop because the *k-space*, endpoint integrals making up the third method were transformed into a rapidly convergent form involving a Hankel function (Eqs. (100)–(102) and Appendix B) which could be evaluated accurately. The author also feels that the third method was very independent of the first and second methods because the invisible *k-space* integrals of the first and second methods are changed into a rapidly convergent form before the spatial and *k-space* integrals are calculated, whereas in the third method, the closed form spatial integrals are done first, without alteration, and then the *k-*

space integrals are evaluated. The independence of the third method is useful since it provides an independent, cross check of the first and second method numerical results.

An interesting feature of the rapidly convergent form of the third method, as expressed in Eqs. (101), (102), is that the Hankel function term contained in these equations, showed precisely and analytically in closed form, the logarithmic divergence that will occur when the source point (x'_s, y'_s) approaches an endpoint $(x'_1, y'_1 = 0)$ or $(x'_2, y'_1 = 0)$ of the rectangular path integral which is located on the PMC boundary. Eqs. (101), (102) were the result of carrying out the integrals of Green's second theorem $I(g_I^-, E_z)$ (Eq. (81) with g_I^- substituted for g) when $E_z = E_0 \exp(-jk_x x' - jk_y y')$ was taken to be the known EM field plane wave solution of the system. The logarithmic divergence of the Hankel function term $H_0^{(2)}(k\rho_{p,q})$ contributing to $I(g_I^-, E_z)$ in Eqs. (101), (102) occurred when $x'_s \rightarrow x'_p$, $p = 1, 2$, $y'_s \rightarrow y'_1 = 0$, $\rho_{p,1} = [(x'_p - x'_s)^2 + (y'_1 + y'_s)^2]^{1/2} \rightarrow 0$ and thus the Hankel function term $H_0^{(2)}(k\rho_{p,1})$ approached $j\infty$ (as $\rho_{p,1} \rightarrow 0$, $H_0^{(2)}(k\rho_{p,1}) \propto -j \ln(k\rho_{p,1}) \rightarrow j\infty$). Knowledge of this behavior of $I(g_I^-, E_z)$ (and therefore for $I(g, E_z)$, since $g = g_{VIS} + g_I^- + g_I^+$) is very valuable because it shows exactly the type of divergence that will occur when an unknown EM field is being solved for when applying the Monzon's [2, 3] MoM Green's second theorem integral equation formulation to a problem where a scattering object is located on top of the PMC ground plane.

An interesting result of the error analysis presented in Table 3 was that much more accurate integration results were determined by using the g_c and g_I *k-space endpoint* methods (second and third integration methods, respectively) than by using the *spatial* integration method to calculate the integrals of $I(g_I^-, E_z)$. (The *spatial* method was used to calculate the integrals of $I(g_I^-, E_z)$ over the semicircular and rectangular paths of Figs. 2a,b, respectively, whereas the g_c and g_I *k-space endpoint* methods calculated the integrals of $I(g_I^-, E_z)$ only over the rectangular path of Fig. 2b.) This is shown by the error $E_1(g_I^-)$ displayed in Table 3 (Cols. 2,3,5; Rows 3-5, 8-10). As discussed in detail in Section 8, the improved accuracy for the second and third integration methods occurred for both the cases when the source point was both relatively close to and far away from the PMC plane. This indicates that when calculating MoM matrix elements, that it might be useful to try to implement the second and third integration methods as opposed to using the spatial method. This would probably cause more analytical and numerical work because it would be necessary to divide the integration path into a path made up of many straight line

segments for which the second and third methods could be applied (approximating the original shape of a scattering object), but might also produce better overall numerical results.

Table 4 presented error results that showed, over a very wide range of source point locations, the degree to which the mixed-partial derivative boundary condition of Eq. (15) was satisfied by the overall Green's function $G = g_f + g$ which has been developed herein. As can be seen from Table 4 the maximum error was $1.26 \times 10^{-3}\%$ (last row of Table 4) which occurred for a source point located extremely far away from where the boundary condition was tested. For most other source point values tested, the error was much less than $1.26 \times 10^{-3}\%$.

The fact that overall the boundary condition was satisfied to a high degree of accuracy in Table 4 is a very good cross check and indication that the homogeneous Green's developed herein are being calculated correctly. This follows because the mixed-partial derivative boundary condition requires mathematically that $\left[\alpha \frac{\partial G}{\partial x'} + \frac{\partial G}{\partial y'} \right] \Big|_{y'=0} = 0$, or that

$$\left[\alpha \frac{\partial g}{\partial x'} + \frac{\partial g}{\partial y'} \right] \Big|_{y'=0} = - \left[\alpha \frac{\partial g_f}{\partial x'} + \frac{\partial g_f}{\partial y'} \right] \Big|_{y'=0} \quad (106)$$

where $g_f = \frac{j}{4} H_0^{(2)}(k|\bar{\rho}' - \bar{\rho}'_s|)$. Thus it would be numerically difficult, over the wide range of different source points that were tested, for the complicated k -space integrals making up the homogeneous Green's function g being differentiated on the left hand side of Eq. (106), to almost exactly equal the mixed-partial derivative, free space, Hankel (calculated by [27]) Green's function term on the right hand side of Eq. (106) (as displayed in Table 4) unless the homogeneous Green's function g was being calculated correctly. We remind the reader that one of the complicated k -space integrals making up the homogeneous Green's function g required a principal value integration over a pole (Eqs. (53)–(64)) and this is an integration that can be worrisome because it involves adding oppositely signed, divergent integrals whose infinities hopefully cancel out correctly.

Figs. 4–6 display plots of the mixed-partial derivatives of the total, free space and homogeneous Green's functions. In Figs. 4a and 4b the real and imaginary parts of $\alpha \frac{\partial G}{\partial x'} + \frac{\partial G}{\partial y'}$ ($G = g_f + g$), respectively, was displayed, and the mixed-partial derivative boundary condition of Eq. (15) was seen to hold to a high degree of accuracy at $y = y' = 0$ the PMC boundary as expected. Figs. 5a,b displayed, respectively, the real part of $\alpha \frac{\partial g_f}{\partial x'} + \frac{\partial g_f}{\partial y'}$ and $\alpha \frac{\partial g}{\partial x'} + \frac{\partial g}{\partial y'}$, and Figs. 6a,b displayed the imaginary parts of the same functions as Figs. 5a,b. In viewing both Figs. 5 and 6, overall, it is very clearly seen that the

functions $\alpha \frac{\partial g_f}{\partial x'} + \frac{\partial g_f}{\partial y'}$ and $\alpha \frac{\partial g}{\partial x'} + \frac{\partial g}{\partial y'}$ were almost exact negatives of each other when evaluated at $y' = 0$, the PMC boundary, as required to meet mixed-partial derivative boundary conditions Eq. (106). A very interesting feature displayed in both Figs. 5 and 6, is the clear difference in behavior of free space Green's mixed-partial derivative function (Figs. 5a, 6a) as opposed to the behavior of the homogeneous Green's mixed-partial derivative function (Figs. 5b, 6b). The free space Green's mixed-partial derivative function (Figs. 5a, 6a) varies very rapidly on a line $x' = 0$ as the observation point moves away from the $y' = 0$, PMC boundary toward the source point, whereas the homogeneous Green's mixed-partial derivative function (Figs. 5b, 6b) on the same $x' = 0$ line, decreases very slowly and smoothly away from the $y' = 0$, PMC boundary. It appears that the homogeneous Green's derivative function (Figs. 5b, 6b) is varying in as minimal a way as possible to meet the boundary conditions of the system.

In conclusion the Green's function for an anisotropic half-space TM^z -PMC system has been developed and extensively numerically tested. The results may be applied to the half-space TE^z -PEC case dual to the present one. Future work will be devoted to use the Green's function to study scattering from anisotropic objects located above a perfect magnetic conductor ground plane using the MoM integral equation method developed by Monzon [2, 3, 12–16]. This work may be validated using the Rigorous Coupled Wave Analysis (RCWA) algorithm of [19, 28]. Future work will also be applied to study the Green's functions of anisotropic metamaterials when adjacent to a perfect conductor ground plane as discussed in the Introduction. Future work will also focus on applying the theory developed in this paper to multi-layer anisotropic systems as was done in [6, 11].

APPENDIX A.

The purpose of the present appendix is to verify that the transformation as defined by Eqs. (6a–d) reduces the mixed-derivative PDE of Eq. (4) to the wave equation form Eq. (7). Let the first three terms of Eq. (4) be

$$T \equiv \tilde{\mu}_{xx} \frac{\partial^2 E_z}{\partial \tilde{x}^2} + \tilde{\mu}_{yy} \frac{\partial^2 E_z}{\partial \tilde{y}^2} + [\tilde{\mu}_{xy} + \tilde{\mu}_{yx}] \frac{\partial^2 E_z}{\partial \tilde{x} \partial \tilde{y}} \quad (\text{A1})$$

Using Eqs. (6c,d) in Eq. (A1) we find that the \tilde{x} and \tilde{y} derivatives of E_z in the transformed variables \tilde{x}' and \tilde{y}' are given by

$$\frac{\partial E_z}{\partial \tilde{x}} = \frac{\partial E_z}{\partial \tilde{x}'} \frac{\partial \tilde{x}'}{\partial \tilde{x}} + \frac{\partial E_z}{\partial \tilde{y}'} \frac{\partial \tilde{y}'}{\partial \tilde{x}} = \frac{\partial E_z}{\partial \tilde{x}'} \frac{\sigma_P}{\tau} \quad (\text{A2})$$

$$\frac{\partial E_z}{\partial \tilde{y}} = \frac{\partial E_z}{\partial \tilde{x}'} \frac{\partial \tilde{x}'}{\partial \tilde{y}} + \frac{\partial E_z}{\partial \tilde{y}'} \frac{\partial \tilde{y}'}{\partial \tilde{y}} = \frac{\partial E_z}{\partial \tilde{x}'} \sigma_M + \frac{\partial E_z}{\partial \tilde{y}'} \quad (\text{A3})$$

since $\frac{\partial \tilde{y}'}{\partial \tilde{x}} = \frac{\partial \tilde{y}}{\partial \tilde{x}} = 0$, $\frac{\partial \tilde{x}'}{\partial \tilde{y}} = \frac{\partial}{\partial \tilde{y}} \left[\frac{\sigma_P}{\tau} \tilde{x} + \sigma_M \tilde{y} \right] = \sigma_M$ and $\frac{\partial \tilde{x}}{\partial \tilde{y}} = 0$. Following a similar change of variable analysis, the second order derivatives $\frac{\partial^2 E_z}{\partial \tilde{x}^2}$, $\frac{\partial^2 E_z}{\partial \tilde{y}^2}$ and $\frac{\partial^2 E_z}{\partial \tilde{x} \partial \tilde{y}}$ may be found. After algebra T of Eq. (A1) is found in the transformed coordinates \tilde{x}' and \tilde{y}' to be

$$T = c_{xx} \frac{\partial^2 E_z}{\partial \tilde{x}'^2} + c_{xy} \frac{\partial^2 E_z}{\partial \tilde{x}' \partial \tilde{y}'} + \tilde{\mu}_{yy} \frac{\partial^2 E_z}{\partial \tilde{y}'^2} \quad (\text{A4})$$

$$c_{xx} = \frac{1}{\tau^2} \left[\tilde{\mu}_{xx} \sigma_P^2 + \tilde{\mu}_{yy} \sigma_M^2 \tau^2 + (\tilde{\mu}_{xy} + \tilde{\mu}_{yx}) \sigma_P \sigma_M \tau \right] \quad (\text{A5})$$

$$c_{xy} = \frac{1}{\tau^2} \left[\tilde{\mu}_{yy} (2\sigma_M \tau^2) + (\tilde{\mu}_{xy} + \tilde{\mu}_{yx}) \sigma_P \tau \right] \quad (\text{A6})$$

Noticing from Eqs. (6a-d) that $\sigma_P = \frac{2}{\sigma_1 \sigma_2}$, $\sigma_M = \frac{-(\tilde{\mu}_{xy} + \tilde{\mu}_{yx})}{\sigma_1 \sigma_2 \sqrt{\tilde{\mu}_{xx} \tilde{\mu}_{yy}}}$,

$$\sigma_1^2 \sigma_2^2 = 4 - \frac{(\tilde{\mu}_{xy} + \tilde{\mu}_{yx})^2}{\tilde{\mu}_{xx} \tilde{\mu}_{yy}}, \quad (\text{A7})$$

$\sigma_P \sigma_M = \frac{1}{\sigma_1^2 \sigma_2^2} \left[\frac{-2(\tilde{\mu}_{xy} + \tilde{\mu}_{yx})}{\sqrt{\tilde{\mu}_{xx} \tilde{\mu}_{yy}}} \right]$, $\tau = \sqrt{\frac{\tilde{\mu}_{xx}}{\tilde{\mu}_{yy}}}$, we find that c_{xx} simplifies to or

$$\begin{aligned} c_{xx} &= \frac{1}{\tau^2} \left[\tilde{\mu}_{xx} \frac{4}{\sigma_1^2 \sigma_2^2} + \tilde{\mu}_{yy} \frac{1}{\sigma_1^2 \sigma_2^2} \frac{(\tilde{\mu}_{xy} + \tilde{\mu}_{yx})^2}{\tilde{\mu}_{xx} \tilde{\mu}_{yy}} \frac{\tilde{\mu}_{xx}}{\tilde{\mu}_{yy}} \right. \\ &\quad \left. + (\tilde{\mu}_{xy} + \tilde{\mu}_{yx}) \frac{1}{\sigma_1^2 \sigma_2^2} \left[\frac{-2(\tilde{\mu}_{xy} + \tilde{\mu}_{yx})}{\sqrt{\tilde{\mu}_{xx} \tilde{\mu}_{yy}}} \right] \sqrt{\frac{\tilde{\mu}_{xx}}{\tilde{\mu}_{yy}}} \right] \end{aligned}$$

or

$$\begin{aligned} c_{xx} &= \frac{1}{\tau^2 \sigma_1^2 \sigma_2^2} \left[4\tilde{\mu}_{xx} - \frac{(\tilde{\mu}_{xy} + \tilde{\mu}_{yx})^2}{\tilde{\mu}_{yy}} \right] \\ &= \frac{\tilde{\mu}_{yy}}{\tilde{\mu}_{xx}} \frac{\tilde{\mu}_{xx}}{\sigma_1^2 \sigma_2^2} \left[4 - \frac{(\tilde{\mu}_{xy} + \tilde{\mu}_{yx})^2}{\tilde{\mu}_{xx} \tilde{\mu}_{yy}} \right] = \tilde{\mu}_{yy} \quad (\text{A8}) \end{aligned}$$

where $\tau^2 = \frac{\tilde{\mu}_{xx}}{\tilde{\mu}_{yy}}$ and Eq. (A7) have been used to determine the last part of Eq. (A8). The quantity c_{xy} simplifies to

$$\begin{aligned} c_{xy} &= \frac{1}{\tau^2} \left[\tilde{\mu}_{yy} 2 \left\{ \frac{1}{\sigma_1 \sigma_2} \left[\frac{-2(\tilde{\mu}_{xy} + \tilde{\mu}_{yx})}{\sqrt{\tilde{\mu}_{xx} \tilde{\mu}_{yy}}} \right] \frac{\tilde{\mu}_{xx}}{\tilde{\mu}_{yy}} \right\} + (\tilde{\mu}_{xy} + \tilde{\mu}_{yx}) \left[\frac{2}{\sigma_1 \sigma_2} \right] \sqrt{\frac{\tilde{\mu}_{xx}}{\tilde{\mu}_{yy}}} \right] \\ &= 0 \quad (\text{A9}) \end{aligned}$$

Thus

$$T = \tilde{\mu}_{yy} \frac{\partial^2 E_z}{\partial \tilde{x}^2} + \tilde{\mu}_{yy} \frac{\partial^2 E_z}{\partial \tilde{y}^2} \quad (\text{A10})$$

and the wave equation given by Eq. (7) results when T is substituted in Eq. (4) and $\tilde{\mu}_{yy}$ is divided out from the resulting equation.

APPENDIX B.

We are interested in showing the detailed steps used in evaluating the integral I^- given by Eq. (40), namely

$$I^- = \int_0^\infty \exp[k\rho\psi^-] du = \int_0^\infty \exp[-jk\rho \cos(\pi/2 + \phi + ju)] du \quad (\text{B1})$$

We are also interested in presenting numerically efficient formulas to calculate the I^- and I^+ integrals of Eq. (40). To start the analysis of Eq. (B1), it is useful to make the change of variables $w = \pi/2 + \phi + ju$. Doing so, it is found; that $du = w/j$; that when $u = 0$, $w = \pi/2 + \phi$; that when $u = \infty$, $w = \pi/2 + \phi + j\infty$; and that with this change of variable, the integral I^- becomes

$$I^- = \frac{1}{j} \int_{\pi/2+\phi}^{\pi/2+\phi+j\infty} \exp[-jk\rho \cos w] dw \quad (\text{B2})$$

The path of integration is the right leg of the rectangular contour C shown in Fig. 3. We note that since $\phi = \tan^{-1}(X/Y)$, $Y > 0$ and $-\infty < X < \infty$, we see that $-\pi/2 < \phi < \pi/2$.

It is now useful to consider, over the closed, rectangular contour path C shown in Fig. 3, the integral

$$\oint_C I dw = \int_{\pi/2+\phi}^{\pi/2+\phi+j\infty} I dw + \int_{\pi/2+\phi+j\infty}^{\delta+j\infty} I dw + \int_{\delta+j\infty}^0 I dw + \int_0^{\pi/2+\phi} I dw = 0 \quad (\text{B3})$$

where

$$I = \frac{1}{j} \exp[-jk\rho \cos w] \quad (\text{B4})$$

and where $\delta \rightarrow 0$. Letting $I_\infty^- = \int_{\pi/2+\phi+j\infty}^{\delta+j\infty} I dw$, $I_H^- = \int_{\delta+j\infty}^0 I dw$ and $I_\phi^- = \int_0^{\pi/2+\phi} I dw$, we have that Eq. (B3) is

$$\oint_C I dw = I^- + I_\infty^- + I_H^- + I_\phi^- = 0 \quad (\text{B5})$$

The integral $\oint_C I dw$ defined by Eqs. (B3), (B4) is zero according to the Cauchy-Goursat theorem because the function $I = \frac{1}{j} \exp[-jk\rho \cos w]$ is analytic inside the contour C in the complex w plane [21, pg. 488]. We will now proceed to evaluate the separate integrals I_∞^- , I_H^- and I_ϕ^- in Eq. (B5) and from this find I^- .

Proceeding, we first note that I_∞^- is zero because the integrand $I = \frac{1}{j} \exp[-jk\rho \cos w]$ approaches zero as $w_i \rightarrow \infty$. This follows because

$$\cos(w_r + jw_i) = \cos w_r \cosh(w_i) - j \sin w_r \sinh(w_i) \quad (\text{B6})$$

which therefore means,

$$\begin{aligned} \exp[-jk\rho \cos w] &= \exp[-jk\rho \cos w_r \cosh(w_i)] \\ &\quad \times \exp[(-jk\rho)(-j \sin w_r \sinh(w_i))] \end{aligned} \quad (\text{B7})$$

$$\begin{aligned} I &= \frac{1}{j} \exp[-jk\rho \cos w] \\ &= \frac{1}{j} \exp[-jk\rho \cos w_r \cosh(w_i)] \exp[-k\rho \sin w_r \sinh(w_i)] \end{aligned} \quad (\text{B8})$$

On the horizontal top path of Fig. 3 we have, $0 < \sin w_r$ since $0 < w_r < \pi$, and since $0 < k\rho$, we find $k\rho \sin w_r \sinh(w_i) \rightarrow \infty$ as $w_i \rightarrow \infty$. This means in Eq. (B8) that the factor $\exp[-k\rho \sin w_r \sinh(w_i)] \rightarrow 0$ as $w_i \rightarrow \infty$, which thus means I of Eq. (B8) approaches zero as $w_i \rightarrow \infty$, which is what was to be shown.

The I_H^- integral with $\delta \rightarrow 0$ may be evaluated by using the result from Felson and Marcuvitz [21, pg. 488] that

$$H_0^{(2)}(k\rho) = \frac{1}{\pi} \int_{-\delta-j\infty}^{\delta+j\infty} \exp[-jk\rho \cos w] dw = I_{neg} + I_{pos} \quad (\text{B9})$$

where $\delta \rightarrow 0$, where the path of integration is vertical w_i axis of Fig. 3 and where $I_{pos} \equiv \frac{1}{\pi} \int_0^{\delta+j\infty} \exp[-jk\rho \cos w] dw$ and $I_{neg} \equiv \frac{1}{\pi} \int_{-\delta-j\infty}^0 \exp[-jk\rho \cos w] dw$. If in the integral I_{neg} : we change variables with $w' = -w$; note that $\cos w = \cos(-w') = \cos(w')$; note that when $w = 0$, $w' = 0$; and note that when $w = -\delta - j\infty$, $w' = \delta + j\infty$, we find, after reversing limits and the negative sign of the differential, (namely $dw' = -dw$), that $I_{neg} = I_{pos}$. Thus we find

$$H_0^{(2)}(k\rho) = \frac{2}{\pi} \int_0^{\delta+j\infty} \exp[-jk\rho \cos w] dw \quad (\text{B10})$$

or after reversing upper and lower integration limits and reversing sign

$$H_0^{(2)}(k\rho) = \frac{-2j}{\pi} \left[\frac{1}{j} \int_{\delta+j\infty}^0 \exp[-jk\rho \cos w] dw \right] = \frac{-2j}{\pi} I_H^- \quad (\text{B11})$$

$$I_H^- = \frac{-\pi}{2j} H_0^{(2)}(k\rho) \quad (\text{B12})$$

Alternatively, if the integral representations Abramowitz and Stegun [25, pg. 360, Eq. (9.1.23)]

$$Y_0(k\rho) = \frac{-2}{\pi} \int_0^\infty \cos[k\rho \cosh(w_i)] dw_i \quad (\text{B13})$$

$$J_0(k\rho) = \frac{2}{\pi} \int_0^\infty \sin[k\rho \cosh(w_i)] dw_i \quad (\text{B14})$$

are substituted into the linear combination $H_0^{(2)}(k\rho) = J_0(k\rho) - jY_0(k\rho)$, if Euler's formula is used to combine the resulting integrals into an exponential integral, and if a change of integration variables is made, Eq. (B10) will also result and again the I_H^- is evaluated by Eq. (B12).

The contour path for the I_ϕ^- integral of Eq. (B5) is the lower leg of the rectangle shown in Fig. 3 and is given by $w = w_r + j0$. Letting $u \equiv w_r$ and defining a new function

$$g_\phi^- \equiv \int_0^{\pi/2+\phi} \exp[-jk\rho \cos u] du = jI_\phi^- \quad (\text{B15})$$

we have $I_\phi^- = \int_0^{\pi/2+\phi} I dw = \frac{1}{j} g_\phi^-$. Combining results, we find after substitution of $I_\phi^- = \frac{1}{j} g_\phi^-$, $I_\infty^- = 0$ and $I_H^- = \frac{-\pi}{2j} H_0^{(2)}(k\rho)$ into Eq. (B5) that

$$\oint_C I dw = 0 = I^- + 0 + \left[-\frac{\pi}{2j} H_0^{(2)}(k\rho) \right] + \frac{1}{j} g_\phi^- \quad (\text{B16})$$

Thus

$$I^- = \frac{\pi}{2j} H_0^{(2)}(k\rho) - \frac{1}{j} g_\phi^- \quad (\text{B17})$$

An analysis similar to that made for the I^- integral shows that the I^+ integral defined in Eq. (40) is given by

$$I^+ = \frac{\pi}{2j} H_0^{(2)}(k\rho) - \frac{1}{j} g_\phi^+ \quad (\text{B18})$$

where

$$g_{\phi}^{+} = \int_0^{\pi/2-\phi} \exp[-jk\rho \cos u] du \quad (\text{B19})$$

A useful formula for calculating g_{ϕ}^{\pm} numerically is given by

$$g_{\phi}^{-} = \begin{cases} g_{\phi}, & -\pi/2 < \phi < 0 \\ \pi J_0(k\rho) - g_{\phi}^{*}, & 0 < \phi < \pi/2 \end{cases} \quad (\text{B20})$$

$$g_{\phi}^{+} = \begin{cases} \pi J_0(k\rho) - g_{\phi}^{*}, & -\pi/2 < \phi < 0 \\ g_{\phi}, & 0 < \phi < \pi/2 \end{cases} \quad (\text{B21})$$

where

$$g_{\phi} = \int_0^{\pi/2-|\phi|} \exp[-jk\rho \cos u] du \quad (\text{B22})$$

The above formulas were derived using the integral $\int_0^{\pi} \exp[-jk\rho \cos u] du = \pi J_0(k\rho)$ as given by Abramowitz and Stegun [25, pg. 360, Eq. (9.1.21)]. The above formulas are useful because they allow g_{ϕ}^{\pm} to be computed in terms of the integral g_{ϕ} , which thus provides the smallest numerical integration range ($0 \leq u \leq \pi/2 - |\phi|$) for which to compute g_{ϕ}^{\pm} and this thus provides the best integration accuracy.

REFERENCES

1. Monzon, J. C. and N. J. Damaskos, "Two-dimensional scattering by a homogeneous anisotropic rod," *IEEE Transactions on Antennas and Propagation*, Vol. 34, No. 10, 1243–1249, Oct. 1986.
2. Monzon, J. C., "On a surface integral representation for homogeneous anisotropic regions: two-dimensional case," *IEEE Transactions on Antennas and Propagation*, Vol. 36, No. 10, 1401–1406, Oct. 1988.
3. Monzon, J. C., "The equivalence principle for two-dimensional anisotropies," *IEEE Transactions on Antennas and Propagation*, Vol. 39, No. 12, 1781–1784, Dec. 1991.
4. Shul'ga, S. N., "Scattering of electromagnetic wave by an inhomogeneous anisotropic inclusion immersed in anisotropic half-space," *Journal of Communications Technology and Electronics*, Vol. 43, No. 10, 1086–1090, Oct. 1998.
5. Shul'ga, S. N., "Two-dimensional problem of scattering of a wave beam by the anisotropic half-space with an anisotropic inclusion,"

- Optics and Spectroscopy, Physical and Quantum Optics*, Vol. 87, No. 3, 465–471, Sept. 1999.
6. Zhuk, N. P., S. N. Shul'ga, and A. G. Yarovoi, "Two-dimensional scattering of electromagnetic waves from a permeable inclusion in an anisotropic medium," *Technical Physics*, Vol. 43, No. 1, 75–79, Jan. 1998.
 7. Zhuck, N. P. and A. G. Yarovoy, "Two-dimensional scattering from a inhomogeneous dielectric cylinder embedded in a stratified medium: case of TM polarization," *IEEE Transactions on Antennas and Propagation*, Vol. 42, No. 1, 16–21, Jan. 1994.
 8. Goryushko, D. N., A. V. Malyuskin, S. N. Shulga, and A. A. Shmat'ko, "Wavetrains scattering by anisotropic composite absorbing layer with metal-dielectric substrate," *2002 12th Int. Conference "Microwave & Telecommunications Technology," (CriMiCo'2002)*, 439–440, Sevastopol, Crimea, Ukraine, Sept. 9–13, 2002.
 9. Malyuskin, A. V., D. N. Goryushko, A. A. Shmat'ko, and S. N. Shulga, "Scattering of a wave beam by an inhomogeneous anisotropic chiral layer," *MMET'02 Proceedings, Kiev, Ukraine, IX-th International Conference on Mathematical Methods in Electromagnetic Theory*, 566–568, 2002.
 10. Malyuskin, A. V., M. P. Perepechai, and S. N. Shulga, "Effective electromagnetic parameters of strongly fluctuating statistically layered bianisotropic medium," *MMET'2000 Proceedings, Kharkov, Ukraine, VIII-th International Conference on Mathematical Methods in Electromagnetic Theory*, 361–363, 2000.
 11. Simsek, E., J. Liu, and Q. H. Liu, "A spectral integral method (SIM) for layered media," *IEEE Transactions on Antennas and Propagation*, Vol. 54, No. 6, 1742–1749, June 2006.
 12. Monzon, J. C., "On the application of the Sommerfeld representation in a two-dimensional rotationally invariant anisotropic medium," *IEEE Transactions on Antennas and Propagation*, Vol. 38, No. 7, 1028–1034, July 1990.
 13. Monzon, J. C., "Two-dimensional Green's functions for a rotationally invariant anisotropic medium," *IEEE Transactions on Antennas and Propagation*, Vol. 38, No. 5, 616–624, May 1990.
 14. Monzon, J. C., "Two-dimensional surface integral representations for a rotationally invariant anisotropic medium: applications to scattering," *IEEE Transactions on Antennas and Propagation*, Vol. 39, No. 1, 108–111, Jan. 1991.
 15. Monzon, J. C., "Three-dimensional field expansion in the most general rotationally symmetric anisotropic material: application

- to scattering by a sphere," *IEEE Transactions on Antennas and Propagation*, Vol. 37, No. 6, 728–735, June 1989.
16. Monzon, J. C., "Radiation and scattering in homogeneous general biisotropic regions," *IEEE Transactions on Antennas and Propagation*, Vol. 38, No. 2, 227–235, Feb. 1990.
 17. Ren, W., "Contributions to the electromagnetic wave theory of bounded homogeneous anisotropic media," *Physical Review E*, Vol. 47, No. 1, 664–673, Jan. 1993.
 18. Lindell, I. V., A. H. Sihvola, S. A. Tretyakov, and A. J. Viitanen, *Electromagnetic Waves in Chiral and Bi-isotropic Media*, Artech House, Boston, London, 1994.
 19. Jarem, J. M. and P. P. Banerjee, *Computational Methods for Electromagnetic and Optical Systems*, Marcel Dekker, Inc., July 2000.
 20. Shulga, S. N. and O. V. Bagatskaya, "Analysis of a waveguide T-junction with a 2D scatterer in the interaction region via Green's theorem approach," *International Conference on Antenna Theory and Techniques, September 9–12, 2003*, 785–788, Sevastopol, Ukraine, 2003.
 21. Felson, L. B. and N. Marcuvitz, *Radiation and Scattering of Waves*, Prentice-Hall, Inc., Englewood Cliffs, New Jersey, 1973.
 22. Pendr, J. B. and D. R. Smith, "The quest for the superlens," *Scientific American*, Vol. 295, No. 1, 60–67, July 2006.
 23. Itoh, T. and A. A. Oliner (eds.), *IEEE Trans. on Microwave Theory and Techniques, IETMAB*, Special Issue on Metamaterial Structures, Phenomena, and Applications, Vol. 53, No. 4, 1413–1417, April 2005.
 24. Engheta, N. and R. W. Ziolkowski, "A positive future for double-negative metamaterials," *IEEE Trans. on Microwave Theory and Techniques, IETMAB*, Special Issue on Metamaterial Structures, Phenomena, and Applications, Vol. 53, No. 4, 1535–1556, April 2005.
 25. Abramowitz, M. and I. A. Stegun, *Handbook of Mathematical Functions*, Dover Publications, Inc., New York, 1972.
 26. Ishimaru, A., *Electromagnetic Wave Propagation, Radiation, and Scattering*, Prentice Hall, Englewood Cliffs, N.J., 1991.
 27. Visual Numerics, Inc., "Bessel functions," (Bessel function subroutines BSJS/DBSJS and BSYS/DBSYS), Chap. 6: Bessel Functions, IMSL MATH/LIBRARY Special Functions, 103–106, July 2006.

28. Jarem, J. M., "Rigorous coupled wave theory of anisotropic, azimuthally-inhomogeneous cylindrical systems," *Progress In Electromagnetics Research*, PIER 19, 109–127, 1998.
<http://ceta.mit.edu/PIER/pier19/04.971031p.Jarem.pdf>